ABSTRACT

SHARMA, ABHINAV. Development and Validation of an Integrated Modeling Approach to Reconstruct the Propagation of Fluvial Sediment Pulses After Dam Removals. (Under the direction of Dr. Celso Castro-Bolinaga).

In the last 30 years, over 1,500 dams have been removed as part of river restoration efforts in the United States. This trend is expected to continue in the future due to aging infrastructure, high rehabilitation costs, and the impacts of climate change on the severity of hydrologic events. However, only less than 10% of past dam removals have been closely monitored and documented, severely limiting quantitative and predictive understanding of river response. As a result, there is a pressing need to develop innovative approaches that allow to reconstruct the propagation of past fluvial sediment pulses and expand scientific knowledge on how these sediment-supply disturbances impact rivers. Such knowledge will enable presenting a realistic picture of the pros and cons of the dam removal practice to stakeholders, decision makers, and the general public. In this dissertation, an integrated modeling approach that couples machine learning, remote sensing, numerical modeling, and parameter optimization was developed to reconstruct the propagation of fluvial sediment pulses generated after past dam removals. The performance of the modeling approach was critically assessed using the well-documented case of the Elwha River dam removals, which took place in Washington state between 2011 and 2014, becoming the largest dam removal in the United States to date. The following specific research objectives were pursued when developing and validating the integrated modeling approach: (1) to create a modeling framework for simulating turbidity as a proxy for suspended sediment transport using remote sensing and machine learning for data-rich and data-scarce regions; (2) to construct and validate a simplified physics-based hydro-

morphodynamic numerical model solely based on remote sensing and publicly available data; and (3) to reconstruct the upstream sediment supply time-series associated with fluvial sediment pulses by using an inverse modeling framework, a simplified hydro-morphodynamic model, and turbidity-based suspended sediment concentrations. In Objective 1, turbidity was predicted using different machine learning algorithms and different predictor combinations based on reflectance values obtained from USGS Landsat imagery. Results showed that for the Elwha River dam removals, maximum accuracy was yielded by the Random Forest algorithm with a combination of reflectance band ratios and a novel Soil Delivery Index (SDI) as predictor variables. As part of Objective 2, a simplified process-based one-dimensional (1D) hydro-morphodynamic numerical model was created for a 2.6 km long reach of the lower Elwha River. Longitudinal river channel attributes such as width, sinuosity, and slope were extracted using publicly available remote sensing data, which were aggregated into four distinct sections by using the e-divisive non-parametric multivariate approach. Results showed that the simplified numerical model successfully simulated the hydraulics, suspended sediment concentration, and channel bed evolution from 2015 to 2017. Lastly, in Objective 3, an inverse modeling approach using Markov Chain Monte Carlo (MCMC) sampling was applied with the simplified 1D hydro-morphodynamic numerical model and turbidity-based suspended sediment concentrations to reconstruct the upstream sediment supply that followed the dam removals between 2012 and 2017 in a 2.6 km long reach of the lower Elwha River. The reconstructed upstream suspended sediment concentration was found to vary from 194 mg/l to 97 mg/l during this period, and the optimized numerical model successfully reconstructed the initial phase of the sediment pulse from 2012 to 2014, but model accuracy decreased post 2014 and continued to decrease till 2017. The results were constrained by the availability of cloud-free USGS Landsat imagery, upstream

water flow rate, and the range of turbidity-based suspended sediment concentrations along the study reach. Overall, the proposed methodology was successful in reconstructing the sediment pulses generated after dam removal. The accuracy of the optimized model was impacted by the quantity and quality of measured and remote sensing data that was used as input data, and the simplifications made to the numerical model in terms of dimensionality and channel geometry. However, the applicability of the proposed methodology is not only limited to dam removals but could be used for any sediment pulse scenario in any geographical location.

Development and Validation of an Integrated Modeling Approach to Reconstruct the Propagation of Fluvial Sediment Pulses After Dam Removals

by
Abhinav Sharma

A dissertation submitted to the Graduate Faculty of
North Carolina State University
in partial fulfillment of the
requirements for the degree of
Doctor of Philosophy

Biological and Agricultural Engineering

Raleigh, North Carolina
2023

APPROVED BY:

_____	_____
Dr. Celso Castro – Bolinaga Committee Chair	Dr. Natalie Nelson
_____	_____
Dr. Lucie Guertault	Dr. Dan Obenour

DEDICATION

To my sister and mother

ACKNOWLEDGMENTS

First and foremost, I would like to express my deepest appreciation and heartfelt gratitude towards my PhD mentor, Dr. Celso Castro – Bolinaga. It is with great joy and humility that I acknowledge his invaluable contributions as a consistent source of inspiration, guidance, and unwavering support throughout my doctoral journey. His passion for research and dedication to advancing the boundaries of knowledge have been instrumental in shaping my intellectual growth. Through our weekly discussions, he consistently encouraged me to think critically, and explore innovative approaches to solving complex problems. I am thankful for the time and effort you invested in mentoring me throughout my PhD at NCSU.

Next, I would like to express my sincere appreciation to three esteemed individuals, Dr. Natalie Nelson, Dr. Lucie Guertault, and Dr. Dan Obenour, for their invaluable contributions as members of my PhD committee. Your willingness to answer my questions, provide thoughtful insights, and engage in stimulating discussions have broadened my horizons and shaped my research approach. I am truly grateful for the sincerity and time you dedicated to supporting my professional progress.

Additionally, I would like to thank my departmental colleagues Dr. Lise Montefiore and Dr. Piyush Pandey for their invaluable assistance in navigating my computer programming learning journey. Their explanations, advice, and patient troubleshooting were immensely appreciated. I am also deeply grateful to my Research group (Alexis Swanson, Emily Darr, Rebecca Hatley, Swarna Choudhary, Zach Little), Writing group (Megan Carr, Rifat Hasan), and social circle (Andrew Hillman, Arun Bawa, Hemanth Dakshinamurthy, Hemendra Kumar, Jagdeep Sidhu, Navdeep Dhillon, Piyush Patil, Sonal Garg, Suraiya Akter, Sushant Mehan) for their indispensable roles in my doctoral success.

On a personal level, I extend my heartfelt thanks to my sister and my mother. Your love, support, and teachings have been the foundation on which I have built my academic journey. Thank you Didi for teaching me the significance of cultivating a positive mindset, helping me to accept and face uncomfortable moments with grace and resilience. Thank you Mom, for being my pillar of strength and a guiding light throughout my academic pursuits. Your strength and determination have always been a constant source of inspiration, teaching me the importance of trusting the process and persevering with silent determined efforts. The sheer understanding of having both of you present in my life made all the difference in achieving this goal.

TABLE OF CONTENTS

LIST OF TABLES

LIST OF FIGURES

1 INTRODUCTION

1.1 Problem Description

Dam Removal for River Restoration: Current Outlook and Future Directions.

Dam removal is increasingly being recognized as a valuable practice for restoring rivers and promoting sustainable water management approaches across the globe (Ding et al., 2019; Duda & Bellmore, 2022). The practice seeks to remove dams that pose environmental and/or safety concerns due to aging infrastructure and climate change, as well as those that are no longer useful due to changing energy needs (S. Sharma et al., 2019; Vahedifard et al., 2021). In the United States, estimates from the National Inventory of Dams (NID) indicate over 91,000 dams in existence (Graf, 1999), many of which are aging (average age of 61 years) and require maintenance or removal.

The rate of dam removals in the United States has been increasing in recent years, with a total of 442 dams removed between 2017 and 2021 alone, where the average operational age was 86 years (American Rivers, 2023). To date, the removal of the Elwha and Glines Canyon Dams on the Elwha River in Washington, USA, is the largest removal project and one of the most significant river restoration projects. It began in 2011 and was completed successfully in 2014, allowing for the restoration of natural fish habitats and ecosystem functions (East et al., 2015; Konrad, 2009; Magirl et al., 2015; Warrick et al., 2015). However, the removal of the Elwha River dams released 10.5 million tons of sediment generating channel-bed aggradation of around 32ha in the estuary section of the lower Elwha River. In some cases, dam removals have been a viable solution to address safety concerns, as demonstrated by the removal of the Teton Dam in Idaho, USA, following its catastrophic failure in 1976 (Seed & Duncan, 1987; Solava & Delatte, 2003).

Although the majority of dam removals have taken place in the Northeast region of the United States, followed by the Pacific Northwest and the Southeast regions, many more dams still need to be removed, highlighting that dam removal will continue to be a challenge in the foreseeable future (Duda & Bellmore, 2022; O'Connor et al., 2015). For instance, the removal project targeting four dams on the Klamath River in California began in 2023 and is intended to be completed in 2024. More importantly, it would replace the Elwha River dam removals as the largest dam removal project in the United States (Blumm & Illowsky, 2022), releasing an estimated 6 to 14 million tons of fine reservoir sediment (C. W. Anderson et al., 2019).

Europe has emerged as another region where the practice has gained some traction, with dam removals being carried out for environmental reasons, safety concerns, and a shift to other forms of renewable energy (Belletti et al., 2020; Hommes, 2022). In contrast, dam removals in Asia and Africa are fewer and mostly limited to small or outdated dams, with significant challenges to their removal due to their importance in providing water supply, flood control, and hydropower generation. However, there is growing recognition in these regions of the importance of balancing the benefits of water infrastructure with the protection of environmental and social values while promoting sustainable water management practices (Chen et al., 2016; Noda et al., 2018; Young & Ishiga, 2014). In South America, the rate of dam removals and river restoration efforts is generally slower than in other regions due to the prevalence of large hydroelectric dams, and the political and economic challenges associated with their removal. However, there have been some notable examples of dam operation optimization aimed at balancing tradeoffs between hydropower generation and ecological diversity (O'Hanley et al., 2020).

The future of dam removal as a river restoration practice is an area of active research and debate, with an increasing number of studies exploring the benefits and challenges of this practice and the factors influencing their success (Ding et al., 2019). To develop effective restoration strategies, it is essential to study the downstream impacts of dam removals for minimizing the potential negative effects on downstream ecosystems. This is particularly important given that dam removals are associated with the generation of fluvial sediment pulses, which suddenly increase the supply of loose sediment to downstream reaches (East et al., 2015). Additionally, it is important to consider the potential socio-economic impacts of dam removals, such as changes to benefits like hydropower, irrigation, and flood control that can affect downstream communities (Fox et al., 2022; Leisher et al., 2022). Finally, dam removals are subject to legal and regulatory frameworks, and understanding their downstream impacts is crucial to ensuring compliance with these frameworks and avoiding legal disputes (Hilbert-Wolf & Gerlak, 2022; Hommes, 2022).

Impact of Fluvial Sediment Pulses Following Dam Removals: Importance of Monitoring and Modeling to Improve Understanding of River Response.

Fluvial sediment pulses following dam removals affect the physical, chemical, and biological characteristics of rivers, including increased turbidity, reduced light penetration,

altered temperature and oxygen levels, and changes to the shape and structure of the river channel (Castro-Bolinaga et al., 2020; Collins et al., 2017). Previous researchers have shown that the occurrence of sediment pulses is associated with high suspended sediment concentrations (SSC), hyperconcentrated flows, significant channel-bed aggradation and degradation, and severe bank failure (Castro-Bolinaga et al., 2020; East et al., 2015; Foley et al., 2017; Konrad, 2009; Palu & Julien, 2019; Wilcox et al., 2014). Benda et al. (2004) found that a fluvial sediment pulse caused a significant increase in fine sediment in the channel-bed, reducing the quality of habitat for fish and other aquatic organisms, and altered the geomorphology of the river by changing flow patterns. Fluvial sediment pulses can also significantly impact water quality by increasing suspended sediment and turbidity, which reduces light penetration and alters temperature and dissolved oxygen levels, negatively impacting aquatic organisms (Aspray et al., 2017; Bilotta & Brazier, 2008; Foley et al., 2015, 2017).

Existing methods for monitoring sediment transport dynamics in rivers include utilizing sensor-based point measurements of water quality and morphology of the channel bed and banks, as well as spatially continuous remote sensing approaches like Lidar and aerial imagery scanning (Leopold et al., 1964; Sehgal et al., 2022; Syvitski et al., 2000). Physics-based numerical models have also been widely used to supplement measured data and simulate sediment transport dynamics following dam removals (Castro-Bolinaga et al., 2020; Cui et al., 2006, 2019; Konrad, 2009; Palu & Julien, 2019). However, the development and overall applicability of numerical models are contingent upon the availability of input data, including channel geometrical features such as shape, depth, width, as well as the characteristics of channel-bed sediment.

In the case of dam removals, understanding the relationship between upstream sediment supply and downstream river response is crucial. However, such an understanding is severely limited by the lack of monitored data, which are only available for less than 10% of dams that have been removed in the United States (Foley et al., 2017; Bellmore et al., 2017). As a result, it is difficult to make informed suggestions to the stakeholders, decision makers, and the general public regarding the pros and cons of this practice for river restoration (Duda & Bellmore, 2022). Therefore, there is a pressing need to develop innovative approaches that allow to reconstruct past fluvial sediment pulses and expand scientific knowledge on how these sediment-supply disturbances impact rivers. Integrating remote sensing as part of such innovative approaches has the potential to dramatically increase data availability, including for example that required to

construct and validate physics-based hydro-morphodynamic numerical models that simulate fluvial sediment pulse propagation (e.g., Castro-Bolinaga et al., 2020).

Role of Remote Sensing in Improving Monitoring and Modeling of Fluvial Sediment Pulses:

In order to reconstruct fluvial sediment pulses generated by dam removals, spatiotemporal sediment transport dynamics, and morphological evolution of the channel must be quantified. Herein, remote sensing due to its ability to provide spatial and temporal information on sediment dynamics in riverine and coastal areas presents an opportunity (Gupta et al., 2013; Long & Pavelsky, 2013; Strick et al., 2019; Tarolli & Mudd, 2020). Previous studies have demonstrated the effectiveness of remote sensing techniques in monitoring suspended sediment concentrations and turbidity in water bodies (Chen et al., 2007; Dethier et al., 2020; Umar et al., 2018; Wang & Lu, 2010). For instance, Zhang et al. (2014) used remote sensing data to monitor suspended sediment concentrations in the Yellow River in China. The study employed a combination of USGS Landsat 8 and Moderate Resolution Imaging Spectroradiometer (MODIS) data to estimate the spatial and temporal variations in sediment concentration. In addition to monitoring suspended sediment concentrations and turbidity, remote sensing can also be used to study changes in the morphology of river channels and coastal areas. For example, Khan et al. (2022) used satellite imagery to map changes in the morphology of the Ganges-Brahmaputra delta in Bangladesh over a period of 25 years. The study found that remote sensing can provide valuable information on the changes in river channels and deltaic features. Another study by Ji et al. (2022) used remote sensing data such as ADCP and aerial imagery data to identify sediment sources and sinks in the Yellow River basin in China.

Remote sensing is a powerful tool for studying sediment transport in riverine and coastal areas. In recent years, its applications have been expanding with the development of new sensors and data processing techniques. For example, the NASA Surface Water and Ocean Topography (SWOT) mission will add spatial detail to different hydrological variables such as discharge, and may aid in reconstruction of sediment pulses using a high-fidelity model setup. In addition, NASA-ISRO (Indian Space Research Organization) SAR (Synthetic Aperture Radar) mission may provide an additional utility to focus on groundwater and surface water bodies alike, and present an opportunity to understand river-floodplain exchanges post a dam removal (Kellogg et al., 2020). Also, optical satellite imagery being made available publicly with spatial resolution

less than 1m such as WorldView3 may aid in detailed monitoring of river corridors around the globe for smaller scale dam removal projects (Longbotham et al., 2015).

1.2 Overarching Goal and Specific Research Objectives

The overarching goal of this study was to develop a novel modeling approach to reconstruct the propagation of past fluvial sediment pulses following dam removals by integrating remote sensing, machine learning, and numerical modeling. To achieve this goal, the following specific research objectives were pursued:

a) To create a modeling framework for simulating turbidity as a proxy for suspended sediment transport using remote sensing and machine learning for data-rich and data-scarce regions.
b) To construct and validate a simplified physics-based hydro-morphodynamic numerical model solely based on remote sensing and publicly available data.
c) To reconstruct sediment supply time-series following fluvial sediment pulses using an inverse modeling framework.

The performance of the integrated modeling approach was critically assessed using data from the well-documented case of the Elwha River dam removals in Washington, USA. The connection among the three specific research objectives is shown in Figure 1. The first objective focused on developing a framework to simulate point-scale turbidity across Washington using remote sensing and machine learning. The second objective focused on utilizing remote sensing and publicly available data to construct and validate a simplified one-dimensional (1D) hydro-morphodynamic numerical model of a reach of the lower Elwha River. Finally, the third objective focused on inverse modeling the upstream sediment supply time-series associated with the fluvial sediment pulse that followed the Elwha River dam removals by coupling turbidity-based suspended sediment concentrations from the first objective with the simplified 1D numerical model developed in the second objective.

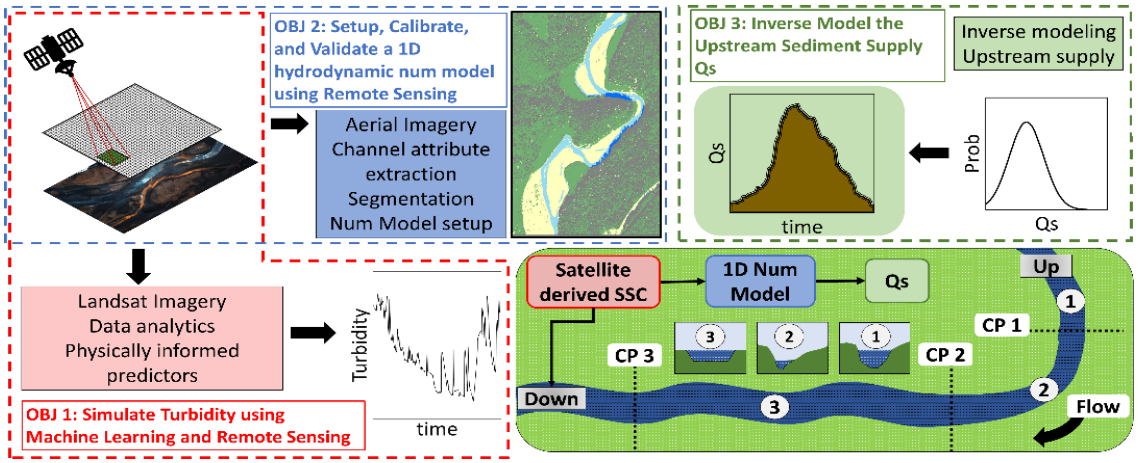

Figure 1.1 Overview of the integrated modeling approach to reconstruct the propagation of past fluvial sediment pulses, showing contribution and connectivity of each specific research objective toward accomplishing the overarching goal.

1.3 Organization of Dissertation

This dissertation consists of three self-contained chapters that will be submitted for publication in scholarly journals. Chapter 2 will be submitted to the International Journal of Sediment Research, Chapter3 will be submitted to Earth Surface Processes and Landforms, and Chapter 4 will be submitted to Journal of Hydrology. Together, these chapters highlight strengths and limitations of the integrated modeling approach, providing a framework that can be used to reconstruct past fluvial sediment pulses and expand scientific knowledge on how these sediment-supply disturbances impact rivers.

Chapter 2 - Abhinav Sharma, Celso Castro-Bolinaga, Natalie Nelson, "Simulating Sediment Pulses using Remote Sensing and Machine Learning: Development of a Modeling Framework Applicable to Data Rich and Scarce Regions" submitted to *International Journal of Sediment Research*

Chapter 3 - Abhinav Sharma, Celso Castro-Bolinaga, Lucie Guertault, "Construction and Validation of Hydro-Morphodynamic Models for data-scarce regions using remote sensing*"* in preparation for submission to *Earth Surface Processes and Landforms*

Chapter 4 - Abhinav Sharma, Celso Castro-Bolinaga, Daniel Obenour, "Developing an inverse modeling framework for simulating upstream sediment supply time series for a dam removal scenario using numerical modeling, remote sensing, and uncertainty analysis*"* in preparation for submission to *Journal of Hydrology*

1.4 References:

Aspray, K. L., Holden, J., Ledger, M. E., Mainstone, C. P., & Brown, L. E. (2017). Organic sediment pulses impact rivers across multiple levels of ecological organization. *Ecohydrology*, *10*(6), e1855.

Belletti, B., Garcia de Leaniz, C., Jones, J., Bizzi, S., Börger, L., Segura, G., Castelletti, A., Van de Bund, W., Aarestrup, K., & Barry, J. (2020). More than one million barriers fragment Europe's rivers. *Nature*, *588*(7838), 436–441.

Benda, L. E. E., Poff, N. L., Miller, D., Dunne, T., Reeves, G., Pess, G., & Pollock, M. (2004). The network dynamics hypothesis: how channel networks structure riverine habitats. *BioScience*, *54*(5), 413–427.

Bilotta, G. S., & Brazier, R. E. (2008). Understanding the influence of suspended solids on water quality and aquatic biota. *Water Research*, *42*(12), 2849–2861.

Castro-Bolinaga, C. F., Diplas, P., & Bodnar, R. J. (2020). Modeling Hydro-Morphodynamic Processes During the Propagation of Fluvial Sediment Pulses: A Physics-Based Framework. *Journal of Geophysical Research: Earth Surface*, *125*(12), e2020JF005722.

Chen, J., Shi, H., Sivakumar, B., & Peart, M. R. (2016). Population, water, food, energy and dams. *Renewable and Sustainable Energy Reviews*, *56*, 18–28.

Collins, M. J., Snyder, N. P., Boardman, G., Banks, W. S. L., Andrews, M., Baker, M. E., Conlon, M., Gellis, A., McClain, S., & Miller, A. (2017). Channel response to sediment release: insights from a paired analysis of dam removal. *Earth Surface Processes and Landforms*, *42*(11), 1636–1651.

Cui, Y., Collins, M. J., Andrews, M., Boardman, G. C., Wooster, J. K., Melchior, M., & McClain, S. (2019). Comparing 1-D sediment transport modeling with field observations: Simkins Dam removal case study. *International Journal of River Basin Management*, *17*(2), 185–197.

Cui, Y., Parker, G., Braudrick, C., Dietrich, W. E., & Cluer, B. (2006). Dam removal express assessment models (DREAM). Part 1: model development and validation. *Journal of Hydraulic Research*, *44*(3), 291–307.

Ding, L., Chen, L., Ding, C., & Tao, J. (2019). Global trends in dam removal and related research: A systematic review based on associated datasets and bibliometric analysis. *Chinese Geographical Science*, *29*, 1–12.

Duda, J. J., & Bellmore, J. R. (2022). Dam Removal and River Restoration. *Encyclopedia of Inland Waters, Eds K. Tockner and T. Mehner (Oxford, UK: Elsevier Ltd). Doi*, *10*.

East, A. E., Pess, G. R., Bountry, J. A., Magirl, C. S., Ritchie, A. C., Logan, J. B., Randle, T. J., Mastin, M. C., Minear, J. T., & Duda, J. J. (2015). Large-scale dam removal on the Elwha River, Washington, USA: River channel and floodplain geomorphic change. *Geomorphology*, *228*, 765–786.

Ferguson, R. I., Church, M., Rennie, C. D., & Venditti, J. G. (2015). Reconstructing a sediment pulse: Modeling the effect of placer mining on Fraser River, Canada. *Journal of Geophysical Research: Earth Surface*, *120*(7), 1436–1454.

Foley, M. M., Duda, J. J., Beirne, M. M., Paradis, R., Ritchie, A., & Warrick, J. A. (2015). Rapid water quality change in the E lwha R iver estuary complex during dam removal. *Limnology and Oceanography*, *60*(5), 1719–1732.

Foley, M. M., Magilligan, F. J., Torgersen, C. E., Major, J. J., Anderson, C. W., Connolly, P. J., Wieferich, D., Shafroth, P. B., Evans, J. E., & Infante, D. (2017). Landscape context and the biophysical response of rivers to dam removal in the United States. *PloS One*, *12*(7), e0180107.

Guertault, L., Camenen, B., Paquier, A., & Peteuil, C. (2018). A one-dimensional process-based approach to study reservoir sediment dynamics during management operations. *Earth Surface Processes and Landforms*, *43*(2), 373–386.

Guertault, L., Camenen, B., Peteuil, C., Paquier, A., & Faure, J. B. (2016). One-dimensional modeling of suspended sediment dynamics in dam reservoirs. *Journal of Hydraulic Engineering*, *142*(10), 4016033.

Gupta, N., Atkinson, P. M., & Carling, P. A. (2013). Decadal length changes in the fluvial planform of the River Ganga: bringing a mega-river to life with Landsat archives. *Remote Sensing Letters*, *4*(1), 1–9.

Hansen, H. H., Bergman, E., Cowx, I. G., Lind, L., Pauna, V. H., & Willis, K. A. (2022). Resilient rivers and connected marine systems: a review of mutual sustainability opportunities. *Global Sustainability*, 1–71.

Hommes, L. (2022). The Ageing of Infrastructure and Ideologies: Contestations Around Dam Removal in Spain. *Water Alternatives*, *15*(3), 592–613.

Iverson, R. M., George, D. L., Allstadt, K., Reid, M. E., Collins, B. D., Vallance, J. W.,

Schilling, S. P., Godt, J. W., Cannon, C. M., & Magirl, C. S. (2015). Landslide mobility and hazards: implications of the 2014 Oso disaster. *Earth and Planetary Science Letters*, *412*, 197–208.

Ji, H., Chen, S., Pan, S., Xu, C., Tian, Y., Li, P., Liu, Q., & Chen, L. (2022). Fluvial sediment source to sink transfer at the Yellow River Delta: Quantifications, causes, and environmental impacts. *Journal of Hydrology*, *608*, 127622.

Khan, N. S., Roy, S. K., Mazumder, M. T. R., Talukdar, S., & Mallick, J. (2022). Assessing the long-term planform dynamics of Ganges–Jamuna confluence with the aid of remote sensing and GIS. *Natural Hazards*, *114*(1), 883–906.

Kondolf, G. M., Gao, Y., Annandale, G. W., Morris, G. L., Jiang, E., Zhang, J., Cao, Y., Carling, P., Fu, K., & Guo, Q. (2014). Sustainable sediment management in reservoirs and regulated rivers: Experiences from five continents. *Earth's Future*, *2*(5), 256–280.

Konrad, C. P. (2009). Simulating the recovery of suspended sediment transport and river-bed stability in response to dam removal on the Elwha River, Washington. *Ecological Engineering*, *35*(7), 1104–1115.

Leopold, L. B., Wolman, M. G., & Miller, J. P. (1964). Fluvial processes in geomorphology WH Freeman and Co. *San Francisco 522pp*.

Long, C. M., & Pavelsky, T. M. (2013). Remote sensing of suspended sediment concentration and hydrologic connectivity in a complex wetland environment. *Remote Sensing of Environment*, *129*, 197–209.

Magirl, C. S., Hilldale, R. C., Curran, C. A., Duda, J. J., Straub, T. D., Domanski, M., & Foreman, J. R. (2015). Large-scale dam removal on the Elwha River, Washington, USA: Fluvial sediment load. *Geomorphology*, *246*, 669–686.

Noda, K., Hamada, J., Kimura, M., & Oki, K. (2018). Debates over dam removal in Japan. *Water and Environment Journal*, *32*(3), 446–452.

O'Connor, J. E., Duda, J. J., & Grant, G. E. (2015). 1000 dams down and counting. *Science*, *348*(6234), 496–497.

Palu, M. C., & Julien, P. Y. (2019). Modeling the sediment load of the Doce River after the Fundão tailings dam collapse, Brazil. *Journal of Hydraulic Engineering*, *145*(5), 5019002.

Rivers, A. (2023). *American Rivers Dam Removal Database*. https://doi.org/10.6084/m9.figshare.5234068.v10

Seed, H. B., & Duncan, J. M. (1987). The failure of Teton dam. *Engineering Geology*, *24*(1–4), 173–205.

Sehgal, D., Martinez-Carreras, N., Hissler, C., Bense, V., & Hoitink, T. A. J. F. (2022). *Influence of riverine suspended sediment carbon content and particle size on turbidity*. Copernicus Meetings.

Solava, S., & Delatte, N. (2003). Lessons from the Failure of the Teton Dam. In *Forensic Engineering (2003)* (pp. 178–189).

Strick, R. J. P., Ashworth, P. J., Sambrook Smith, G. H., Nicholas, A. P., Best, J. L., Lane, S. N., Parsons, D. R., Simpson, C. J., Unsworth, C. A., & Dale, J. (2019). Quantification of bedform dynamics and bedload sediment flux in sandy braided rivers from airborne and satellite imagery. *Earth Surface Processes and Landforms*, *44*(4), 953–972.

Syvitski, J. P., Morehead, M. D., Bahr, D. B., & Mulder, T. (2000). Estimating fluvial sediment transport: the rating parameters. *Water Resources Research*, *36*(9), 2747–2760.

Tarolli, P., & Mudd, S. M. (2020). *Remote Sensing of Geomorphology* (Vol. 23). Elsevier.

Warrick, J. A., Bountry, J. A., East, A. E., Magirl, C. S., Randle, T. J., Gelfenbaum, G., Ritchie, A. C., Pess, G. R., Leung, V., & Duda, J. J. (2015). Large-scale dam removal on the Elwha River, Washington, USA: Source-to-sink sediment budget and synthesis. *Geomorphology*, *246*, 729–750.

Young, S. M., & Ishiga, H. (2014). Environmental change of the fluvial-estuary system in relation to Arase Dam removal of the Yatsushiro tidal flat, SW Kyushu, Japan. *Environmental Earth Sciences*, *72*, 2301–2314.

Zhang, M., Dong, Q., Cui, T., Xue, C., & Zhang, S. (2014). Suspended sediment monitoring and assessment for Yellow River estuary from Landsat TM and ETM+ imagery. *Remote Sensing of Environment*, *146*, 136–147.

2 SIMULATING SEDIMENT PULSES USING REMOTE SENSING AND MACHINE LEARNING: DEVELOPMENT OF A MODELING FRAMEWORK APPLICABLE TO DATA RICH AND SCARCE REGIONS

2.1 Abstract:

Sediment Pulses pose a significant threat to the overall ecological health of river systems. Nonetheless, the scarcity of monitored and published data underscores the importance of devising innovative methods for understanding and measuring how river systems react to the introduction of sediments across the fluvial domain. The objective of this study was to create a modeling framework based on reflectance turbidity that can be applied in regions with both limited and abundant data. Various combinations of predictor variables, training algorithms, and input data availability scenarios were examined to comprehend the factors influencing turbidity prediction on a regional scale. The results indicated that, for Washington state, the Random Forest algorithm, utilizing a combination of band ratios and Sediment Delivery Index (SDI) as predictors, produced the most accurate outcomes (Data rich: NSE = 0.54, RSR = 0.68, Data Scarce: NSE = 0.47, RSR = 0.73). However, when tested on three locations in Washington experiencing sediment pulses, the reflectance-based turbidity prediction model consistently underestimated the peak high and peak low turbidity levels for the Elwha River. The model also exhibited consistent inaccuracies in predicting the initial phase of sediment pulses following the Oso Landslide. Nevertheless, promising results were observed for the Toutle River, downstream to the St. Mt. Helens Volcanic eruption site. Overall, the inclusion of SDI in the model enhanced its efficiency and transferability. By enabling the reconstruction of fluvial sediment pulses in data-scarce regions following dam removals, this integrated approach contributes to advancing our understanding of how rivers respond quantitatively and predictively to these disturbances in sediment supply.

2.2 Introduction:

The sudden release of loose sediment into streams and rivers due to natural or anthropogenic factors leads to the generation of fluvial sediment pulses. Some of the main drivers of sediment pulses include landslides (Iverson, 2015), wildfires (Murphy et al., 2019; Reneau et al., 2007), flooding (A. Nelson & Dubé, 2016), dam removals (Wilcox et al., 2014), and volcanic eruptions (Major et al., 2016). Previous researchers have shown that the occurrence

of sediment pulses is associated with high Suspended Sediment Concentrations (SSC), hyperconcentrated flows, significant channel-bed aggradation and degradation, and severe bank failure (Castro-Bolinaga et al., 2020; East et al., 2015; Foley et al., 2017; Konrad, 2009; Palu & Julien, 2019; Wilcox et al., 2014).

Specifically in the United States (US), the most common driver of fluvial sediment pulses is dam removal (Foley et al., 2017). However, less than 10% of the removals have documented data or published research on the downstream river response (Bellmore et al., 2017). In part, such a gap exists because the deployment of dense monitoring networks of sensors capable of measuring sediment transport dynamics can be both logistically and economically expensive, and thus unrealistic. This gap has further resulted in limited understanding of how fluvial sediment pulses propagate across river corridors following dam removals. With dam removal gaining traction as a river restoration strategy, it is critical to improve monitoring and document river responses as more dam removals are anticipated in coming years (Duda & Bellmore, 2022).

Because it can be readily measured using optical instruments, turbidity has been widely used as a proxy to estimate SSC (Bright & Mager, 2020; East et al., 2015; Ritchie et al., 2018; Rymszewicz et al., 2017), making it a practical target metric for capturing sediment dynamics following dam removal. By definition, turbidity is the measure of the light attenuation properties of water and is measured as the scattering coefficient of light in water (Kirk, 1994). However, most turbidity data are recorded using sensors or cameras set up at a discrete location (e.g., US Geological Survey gauges) and in some cases are associated with limitations to the temporal resolution as well.

Recently, satellite data has emerged as a key tool to substantially increase the spatial extent and temporal coverage of turbidity data. Using remote sensing for development of prediction models to simulate turbidity relies on the fact that turbid water reflects electromagnetic radiation differently than pure water (Jensen, 2009). Previous researchers have determined turbidity to be dependent on sediment size, shape, and color (Bright et al., 2020; Kabir & Ahmari, 2020). The nature of the sediment reaching river networks depends on upland erosion processes, which are further impacted by soil availability and the structural hydrological connectivity in the watershed (Borselli et al., 2008). It therefore becomes imperative to account for such processes during the development and application of remote sensing-based turbidity prediction models. One way is to develop predictor variables reflecting relevant factors that

affect turbidity across the river system under study. Previous researchers have developed reflectance-based turbidity or SSC models by including band ratios, watershed lithology, and sediment color as predictors (Bright & Mager, 2020; Dethier et al., 2020; Long & Pavelsky, 2013). However, most of the models were developed for sites with significant amounts of measured data using classical statistical methods. Few studies have tested a method for informing transferability of turbidity prediction models across space (Dethier et al., 2020; Long & Pavelsky, 2013). The latter is important because it enables predictions in data-scarce regions.

The overarching goal of this study was to develop a reflectance-based modeling framework to predict turbidity during the propagation of fluvial sediment pulses, while testing the applicability of different machine learning algorithms and physically informed predictors for maximizing accuracy and transferability. The specific objectives of this study were to: (1) develop a reflectance – turbidity modeling framework to maximize the accuracy in estimating turbidity for data rich regions, (2) develop model predictors informing model transferability for a data scarce region; and (3) evaluate reflectance-turbidity prediction accuracy for three sites in Washington state that experienced sediment pulses in the past, the Elwha Dam removals, Oso Landslide, and the St. Mt. Helens volcanic eruption. We focus on using satellite data from the Landsat missions in particular (Landsat 5, 7, and 8), as they have collected data since 1984 and maintained consistency in spectral and spatial resolution. Landsat holds a distinct advantage over other satellite programs such as Sentinel in the context of long-term environmental monitoring, primarily due to its extensive operational history.

2.3 Study Area:

Rivers across Washington state, US, were selected to develop and test the reflectance - turbidity modeling framework. In addition to having diverse hydro-climatological conditions, Washington has the highest density of monitored fluvial sediment pulses in the US, including those generated after dam removals including (Elwha and Glines Canyon Dam (Castro-Bolinaga et al., 2020; East et al., 2015; Foley et al., 2015; Gelfenbaum et al., 2015; Konrad, 2009; Magirl et al., 2015; Randle et al., 2015; Ritchie et al., 2018; Warrick et al., 2015), Condit Dam (Wilcox et al., 2014), landslides including the Oso Landslide (Iverson et al., 2015; Iverson & George, 2016), and volcanic eruptions including the Mt. St. Helens case (Major, 2004; Major et al., 2000). Washington is divided into two different physiographic and climatic zones by the Cascade

Range (Figure 1). Rivers in the western part account for a third of the state and drain into Puget Sound, the Strait of Juan de Fuca, or the Pacific Ocean. Rivers in the eastern part drain predominantly into the Columbia River. Most rivers across the state have mountain headwaters. The climate in the western region is relatively warmer than in the eastern region with wet winters and dry summers. The western region receives over 1,000 cm rainfall annually compared to around 15 cm in and around the desert region, east of the Cascade Range (Schermerhorn, 1967). This results in a variety of hydrological flow regimes, which are further impacted by the presence of multiple dams across the state. To account for maximum spatial and temporal coverage, 20 US Geological Survey (USGS) gauge stations with measured turbidity data and average channel width larger than 30m (Landsat pixel size) were selected for the study. The locations were dispersed across the state, in 10 different watersheds (Figure 2.1). Inclusion of multiple watersheds with diverse hydro-climatology allowed for a more critical exploration into the transferability aspect of turbidity modeling for the data based approach by matching a donor catchment with a test catchment using hydrological regionalization (Choubin et al., 2019; Guo et al., 2021).

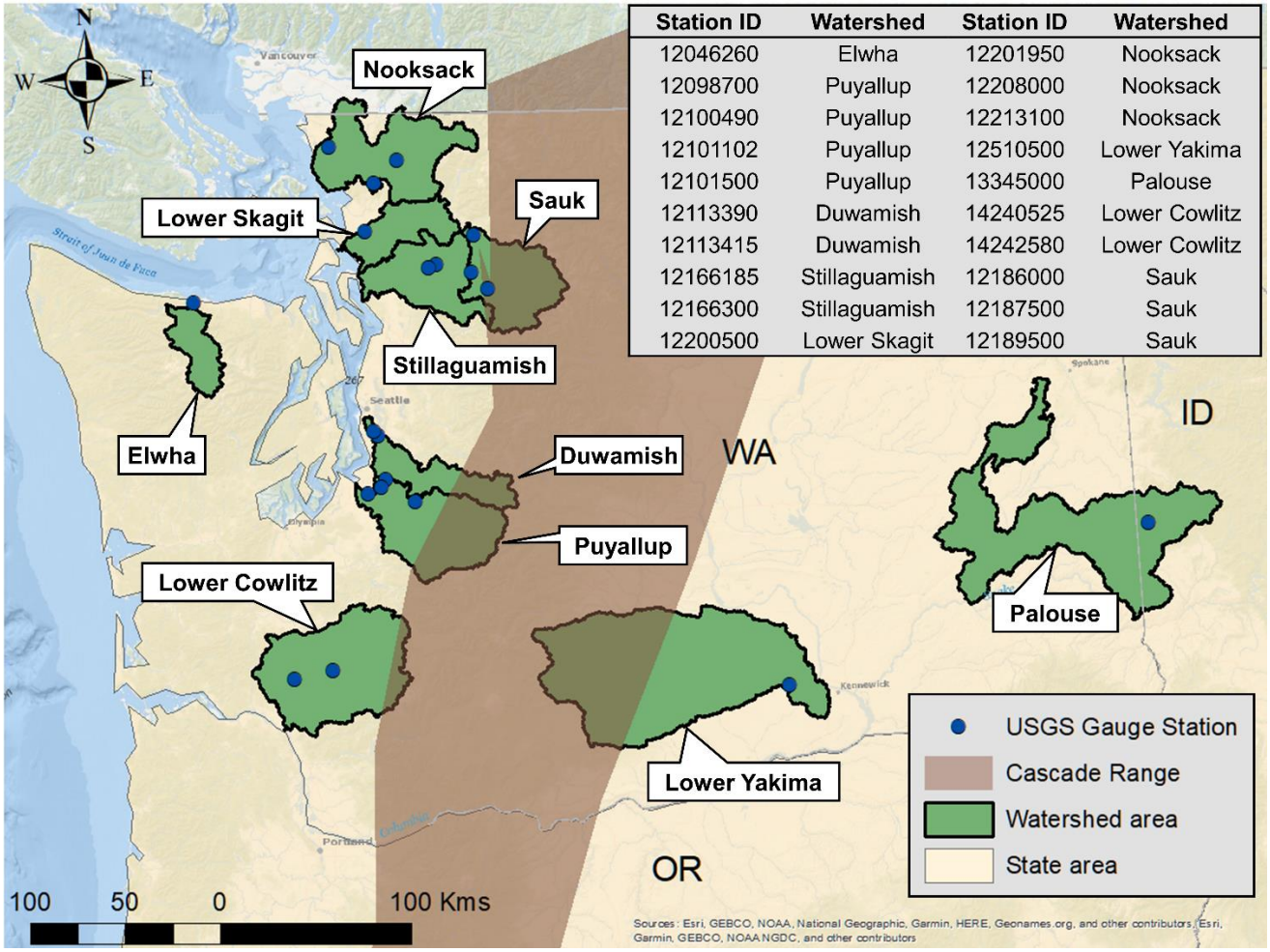

Station ID	Watershed	Station ID	Watershed
12046260	Elwha	12201950	Nooksack
12098700	Puyallup	12208000	Nooksack
12100490	Puyallup	12213100	Nooksack
12101102	Puyallup	12510500	Lower Yakima
12101500	Puyallup	13345000	Palouse
12113390	Duwamish	14240525	Lower Cowlitz
12113415	Duwamish	14242580	Lower Cowlitz
12166185	Stillaguamish	12186000	Sauk
12166300	Stillaguamish	12187500	Sauk
12200500	Lower Skagit	12189500	Sauk

Figure 2.1 Study area (Above) consisting multple USGS Gauge stations (Solid point) located within the different watersheds across the state of Washington separated by the Cascade range (brown) into two different hydrclimatological zones.

2.4 Data:

2.4.1 Turbidity:

Daily turbidity FNU (Formazin Nephelometric Unit) data from 2000 to 2020 were evaluated for each of the 20 United States Geological Survey (USGS) stations (Table 2.1). To reduce skew in measured data and ease the exploration of functional relationship between the dependent and independent variable, the available turbidity per station was log transformed, similar to suggestions by previous researchers (Francke et al., 2008; Helsel & Hirsch, 2002; Jastram et al., 2010; Rasmussen et al., 2009).

2.4.2 Reflectance:

Remotely sensed data from multiple Landsat sensors, namely Landsat 5, 7, and 8, were utilized (Lauer et al., 1997; Vermote et al., 2016). These sensors captured images of the Earth's surface for different wavelengths falling under the optical and near infrared zones of the electromagnetic spectrum, termed as spectral bands, allowing for the extraction of valuable information about different features and phenomena. The spatial resolution of the Landsat data was 30m (except thermal band not used in the study), with a revisit time of around 16 days, conditional on cloud cover. Further, spectral bands in the red, green, blue, and Near Infrared (NIR) spectrum of the water leaving reflectance were used for this study. The data were accessed from Google's Earth Engine platform, as were functions for masking cloud and non-water pixels. Non-water pixels were removed to focus the analysis specifically on the water areas of interest. After the non-water pixels were masked, the Surface Reflectance (SR) values were extracted for each cloud-free water pixel coinciding with each USGS station location (Table 2.1). By extracting the SR values, a dataset with reflectance values for each water pixel of interest was obtained. Next, band ratios were derived by dividing the values of one spectral band by another, resulting in new derived values. This was based on suggestions from previous research on satellite imagery-based turbidity modeling, where band ratios were used to reduce random noise caused by illumination and background (Dekker & Peters, 1993; Gitelson et al., 2008; Lindell et al., 1999; Long & Pavelsky, 2013; Song et al., 2011).

Table 2.1 List of the USGS stations used in the study with associated Landsat 5, 7, or 8 data quantity.

Station ID	Location	Watershed	Data	Start Date	End Date
12046260	Elwha River near Port Angeles	Elwha	96	6/26/2011	8/20/2019
12098700	White River near Buckley	Puyallup	57	7/27/2010	9/16/2020
12100490	White River near Auburn	Puyallup	137	7/26/2010	8/30/2020
12101102	White River at Dieringer	Puyallup	63	7/27/2016	12/4/2020
12101500	Puyallup River at Puyallup	Puyallup	49	7/8/2012	9/11/2015
12113390	Duwamish River at Tukwila	Duwamish	21	1/18/2014	2/21/2020
12113415	Duwamish River at Duwamish	Duwamish	8	8/17/2015	9/20/2016
12166185	Nf Stillaguamish River near Oso	Stillaguamish	34	11/21/2015	10/8/2019
12166300	Nf Stillaguamish River near Oso	Stillaguamish	11	5/11/2014	11/11/2014
12186000	White Chuck River near Darrington	Sauk	24	3/20/2013	6/7/2015
12187500	Sauk River at Darrington	Sauk	19	7/8/2012	11/30/2015
12189500	Sauk River near Sauk	Sauk	38	9/24/2011	10/2/2020
12200500	Skagit River Near Mount Vernon	Lower Skagit	5	9/20/2016	9/7/2017
12201950	Anderson Creek Near Bellingham	Nooksack	3	7/13/2014	8/7/2014
12208000	Mf Nooksack River near Deming	Nooksack	84	3/7/2014	11/19/2020
12213100	Nooksack River at Ferndale	Nooksack	111	2/6/2012	11/19/2020
12510500	Yakima River at Kiona	Lower Yakima	9	4/26/2005	6/11/2007
13345000	Palouse River near Potlatch	Palouse	18	12/12/2018	12/25/2020
14240525	Nf Toutle River near Kid Valley	Lower Cowlitz	93	5/8/2010	12/5/2020
14242580	Toutle River near Silver Lake	Lower Cowlitz	39	4/14/2010	7/27/2013

2.4.3 Elevation and Soil:

For the reflectance-based turbidity modeling framework, a combination of soil data from the STATSGO (Web Soil Survey) (Schwarz & Alexander, 1995) dataset and elevation data from the 30m National Elevation Dataset (NED) (Gesch et al., 2002) were utilized. These data were used to develop physically informed predictors for the modeling framework. STATSGO dataset was employed to extract soil properties (% sand, % silt, % clay, % soil Organic Carbon) for upslope drainage area for each USGS gauge station location. NED provided detailed information about the elevation of the Earth's surface. Elevation is important in understanding the topography and landscape characteristics, which influence various environmental processes, including water flow, its accumulation, and distribution. These factors were considered as key indicators representing the behavior of water movement across the watershed, its interaction with soils, upland erosional processes, and connection of the eroded soil to each location across the river network.

2.4.4 Sediment Delivery Index (SDI):

From the context of correlating reflectance with an optical property of water such as turbidity, it is critical to analyze pixel color with its subsequent attributes. These attributes are hue, saturation, and brightness (Ibraheem et al., 2012; O'Callaghan et al., 1982; Robertson & O'Callaghan, 1988; Wen & Chou, 2004). Hue refers to one of the primary attributes of color perception. It describes the property of color that distinguishes it as red, blue, green, or any other specific color. Saturation refers to the intensity or purity of a color. It represents how vibrant or vivid a color appears. Brightness refers to the perceived intensity or level of lightness in a color. It represents how light or dark a color appears. Brightness is determined by the amount of light reflected or emitted by an object or surface (Ibraheem et al., 2012).

In this study, a physically informed predictor, the Sediment Delivery Index (SDI), accounting for soil availability and hydrological connectivity across the watershed was derived to improve the correlation between pixel color and measured turbidity. Physically, SDI quantifies the degree of connection of each soil fraction (Sand, Silt, and Clay) to river pixels on the network relative to its availability. It uses upslope structural hydrological connectivity and variability in soil texture to determine how distinct soil fractions vary in their capacity to travel across the landscape and reach designated nodes along the river network (e.g., USGS gauge station locations used for the study). The areal availability of different soil fractions (sand, silt,

and clay), and the Soil Organic Carbon (SOC) estimates from the top 15 cm of soil from STASGO were extracted for each watershed in the study area. Next, the Index of Connectivity (Ic), developed by Borselli et al. (2008) was computed for different watersheds in the study region using the NED, based on the process developed by Cavalli et al. (2013) and Crema & Cavalli (2018). Ic was developed to explore the potential connection between hillslopes and downslope sinks. Mathematically, it can be represented using a ratio between potential for downward routing due to upslope catchment area (D_{up}) using elevation to the downslope sinking potential (D_{dn}) evaluated using the downslope path characteristics such as path length, terrain roughness, and gradient along the path (Equation 2.1).

$$I_c = \log_{10}\left(\frac{D_{up}}{D_{dn}}\right) = \frac{W*S*\sqrt{A}}{\sum_i \frac{d_i}{W_i*S_i}} \quad \text{(Equation 2.1)}$$

Where W = weighting factor of the upslope contributing area, S = Average slope of the upslope contributing area (m/m), A = upslope contributing area (m^2), di = length of the i^{th} cell along the downslope path (m), Wi = weighing factor of the i^{th} cell, Si = slope of the i^{th} cell (m/m).

Finally, SDI for each soil fraction was estimated for different USGS gauge station locations specified in Table 2.1 utilizing STATSGO, Ic and the upslope drainage area and used as predictor variables (Equation 2.2). Mathematically, SDI was calculated as the ratio of Ic-based soil properties (Sc; i.e., the degree of hydrologic connectivity) to availability-based soil properties (Sa; i.e., the soil available for the connection), considering the upslope drainage area for each water pixel in the watershed as:

$$SDI_{Sf} = \frac{Sc}{Sa} = \frac{\frac{\sum_i I_{ci}* P_{ci}}{\sum_i I_{ci}}}{\frac{\sum_i A_i* P_{ci}}{\sum_i A_i}} \quad \text{(Equation 2.2)}$$

where, Ic = Standardized Index of Connectivity (Ic) of each soil fraction of the upslope drainage area standardized from 0-1 across the watersheds, Sf = Soil fraction such as sand, silt, clay, and SOC, Pc = soil fraction percentages (sand, silt, clay, and SOC) per soil type across the drainage basin from STATSGO, A = Area of each soil fraction, and *i* represents the total number of soil type present across the upslope drainage area from STATSGO data.

In theory, SDI value ranges from zero to Inf. For example, an SDI value of zero for the clay fraction indicates no connection between upslope clay pixels and the river network. In contrast, an SDI value greater than one for the clay fraction represents a scenario where pixels associated with higher percentage of clay content are more connected to the river network than those characterized by having lower percentages of clay content. Consistently, an SDI value less than one implies that pixels associated with higher percentage of clay content are less connected to the river network than those characterized by having lower percentages of clay content. Therefore, an SDI of one for the clay fraction means that a proportionality exists between the soil fraction availability percentages content percentage and the connectivity to the river network of upslope clay pixels.

2.5 Modeling:

2.5.1 Conceptual Framework:

Theoretically, a model can be used for either understanding a system, prediction of a system variable, or developing control for a system (Haefner, 2005). According to Levins (1966), regardless of the model setup or framework, it is impossible to maximize realism, generality, and precision altogether in model predictions for any natural system. To ensure both transferability and accuracy in turbidity predictions, a regional scale model should encompass the spatiotemporal variability for all three components. In this study, a two-step framework was proposed to finalize a reflectance-turbidity prediction model. Development of a reflectance turbidity model was a two-step process. The first step considered the input data available for model development, and second considered factors affecting model efficiency and transferability such as training algorithm, and quality and quantity of predictor variables (Figure 2.2). The subsequent sections of the study discuss different scenarios of input data, training algorithms, and selected predictor variables.

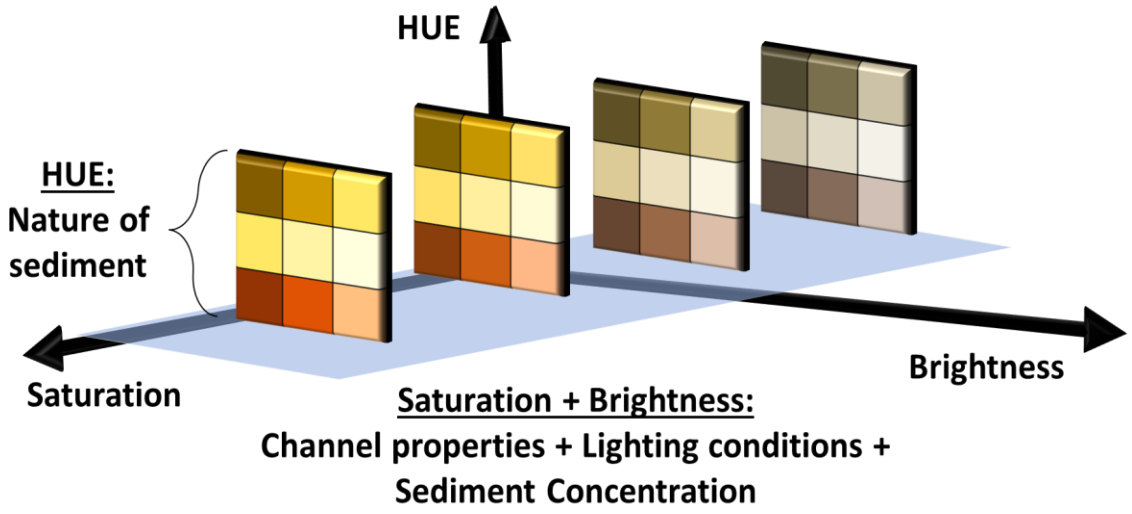

Figure 2.2 Pixel color perspective using Hue, Saturation, and Brightness aided in the developing the conceptual framework for simulating turbidity using reflectance on a regional scale.

2.5.2 Cross Validation:

Two different data models were tested as part of the reflectance-turbidity model framework (Figure 2.3). The first model involved training the model to all data from data-rich regions, while the second model was developed for application in a data-scarce region. Each model is characterized by a distinct method utilized for splitting data into training and testing subsets.

In the data-rich model, the objective was to maximize accuracy and generate predictions suitable for spatial interpolation and/or temporal prediction. To achieve this, all data across all sites were considered, and divided into training and testing subsets with a random split using a one split method and a 50-50,, 60-40, 70-30 and 80-20 split.

On the contrary, in the data-scarce model, the aim of the prediction model was to maximize the transferability of the model while still maintaining reasonable accuracy. An example of such a scenario would be making predictions in an ungauged watershed, using the concept of regionalization to establish similarities via SDI between a gauged donor location and an ungauged test location. Previous researchers across the globe have used different regionalization methods to promote prediction of different hydrological variables and model parameters at ungauged locations for different process based models (Choubin et al., 2019; Hsu & Huang, 2017; Piman & Babel, 2013; Pugliese et al., 2016; Razavi & Coulibaly, 2016; T.

Smith et al., 2014; Steinschneider et al., 2015; Swain & Patra, 2017; Tegegne & Kim, 2018; Van Liew & Mittelstet, 2018; Y. Zhang et al., 2018). To determine which locations had comparable characteristics and could thus be paired in model training/testing, a location-based split based on SDI values for each soil fraction was employed to divide the entire dataset into training and testing datasets. Herein, locations pertaining to the mean, max, and minimum SDI values across the regional distribution for each soil fraction were selected for model training. The rest were part of the model testing subset. The location-based approach to model training and testing mimics a scenario in which the model is applied to a data-scarce site for which turbidity observations would not be available for model training. The utilization of SDI to guide the location-based split in the context of the data-scarce scenario based on the premise that similarity between two or more locations can be expressed using spatial proximity, physical properties, and/or regression (Guo et al., 2021). SDI values representing a process or property of a system can therefore be used to identify two or more locations that are similar, and guide the selection of a donor location (model training), and test location.

Finally, prediction models for the data rich and data scarce scenarios were used to predict turbidity for different locations across the study area that experienced a historical sediment disturbance. So, three stations experiencing Dam removals, volcanic eruption, and landslide (USGS 12046260, USGS 14242580, USGS 12166300) were selected respectively for model testing while the rest were used for model training.

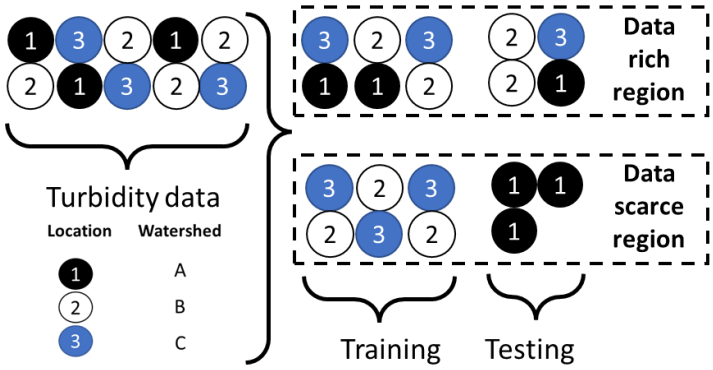

Figure 2.3 A random data split was used to depict a data rich scenario, where a subset of data from all locations across the study area was used to train the model algorithm. On the other hand, a location-based split was performed to denote prediction for an ungauged location based on SDI informed predictors that accounted for similarity in the soil properties and hydrological connectivity of upslope drainage area to each location on the river network.

2.5.3 Training algorithms:

In theory, a variable (response) can be estimated using a prediction model based on multiple input variables (predictors). The primary objective of such a model is to estimate the functional form that establishes the relationship between the response and the predictors. In classical methods such as linear regression, this functional form is assumed, and various approaches are employed to fit the model to the available data. However, these methods are not suitable for regional applications, as they assume a single function can adequately capture the functional relationships between the response and predictors across multiple points spread throughout space. On the other hand, non-parametric methods aim to estimate the functional form that best fits the data without making explicit assumptions about its shape. Unlike classical approaches, which tend to have lower variance due to their functional assumptions, machine learning algorithms such as random forest (Breiman, 2001), Support Vector Machine (SVM) (Hearst et al., 1998), and Artificial Neural Networks (ANN) (McCulloch & Pitts, 1943; Rojas, 2013) have the capacity to capture complex relationships between the response and predictors (Olden et al., 2008). However, they may introduce higher bias during model prediction due to their ability to closely match, and overfit, patterns in training data (Olden et al., 2008). In this study, three machine learning algorithms were tested to train the regional-scale functional relationship between the response and predictors. The purpose was to explore and evaluate different approaches that could accurately capture the complex dynamics within the dataset. The specific algorithms tested were linear regression, random forest, SVM, and Artificial Neural Networks (ANN). By comparing and analyzing the results from these algorithms, the most suitable training algorithm that effectively captured the relationship between the response and predictors in the regional context was identified.

2.5.4 Predictor Combinations:

Next, the impact of two sets of predictor variables on the accuracy of turbidity predictions was evaluated. The first combination included individual Landsat bands and band ratios as predictors, based on suggestions made by previous researchers (Bright & Mager, 2020; Long & Pavelsky, 2013). These predictors were selected due to their relevance in capturing important spectral characteristics related to turbidity and light luminance. Band ratios derived from the red, green, blue, and NIR bands such as red/green, red/blue, red/NIR, green/blue, green/NIR, blue/NIR, and NIR/red/blue were used as predictor variables to evaluate and predict

turbidity. The second combination of predictors focused on adding SDI values for sand, silt, clay, and SOC for each of the 20 USGS gauge stations selected for the study.

2.5.5 Application and Performance Metrics:

Overall, prediction models for two different input data scenarios, four training algorithms, and two combinations of predictor variables were set up and optimized to simulate turbidity, resulting in 40 models being evaluated in total. Next, performance metrics were used to finalize a suitable training algorithm, and predictor variable combination for the data rich and data scarce scenarios respectively.

At each step in the framework, model performance was evaluated using two statistical indices, namely, Ratio of Root Mean Squared Error of prediction data to the Standard Deviation of observations (RSR) (Moriasi et al., 2007) and Nash-Sutcliffe Efficiency (NSE) (Nash & Sutcliffe, 1970) as follows:

$$\mathrm{RSR} = \frac{\mathrm{RMSE}}{\mathrm{STDEV_{obs}}} = \left[\frac{\sqrt{\sum_{i=1}^{n}\left(Y_i^{obs} - Y_i^{sim}\right)^2}}{\sqrt{\sum_{i=1}^{n}\left(Y_i^{obs} - Y^{mean}\right)^2}}\right] \qquad \text{(Equation 2.3)}$$

$$\mathrm{NSE} = 1 - \left[\frac{\sum_{i=1}^{n}\left(Y_i^{obs} - Y_i^{sim}\right)^2}{\sum_{i=1}^{n}\left(Y_i^{obs} - Y^{mean}\right)^2}\right] \qquad \text{(Equation 2.4)}$$

Where, Y_i^{obs} = value of the i^{th} observation, Y_i^{sim}= value of the i^{th} simulated value, and Y^{mean}= mean of the observed values.

2.6 Results:

2.6.1 Data rich region:

Out of the 17024 USGS based measured turbidity data available, 919 discrete data points were available with coinciding satellite overpass dates. The ratio between total data and Landsat associated data was around 18, similar to the revisit time which is around 16 days. Figure 4 shows an overall agreement in statistical distributions of turbidity data across the different USGS gauge station locations supporting the use of Landsat based predictions through time in absence of measured data on a coarser time step.

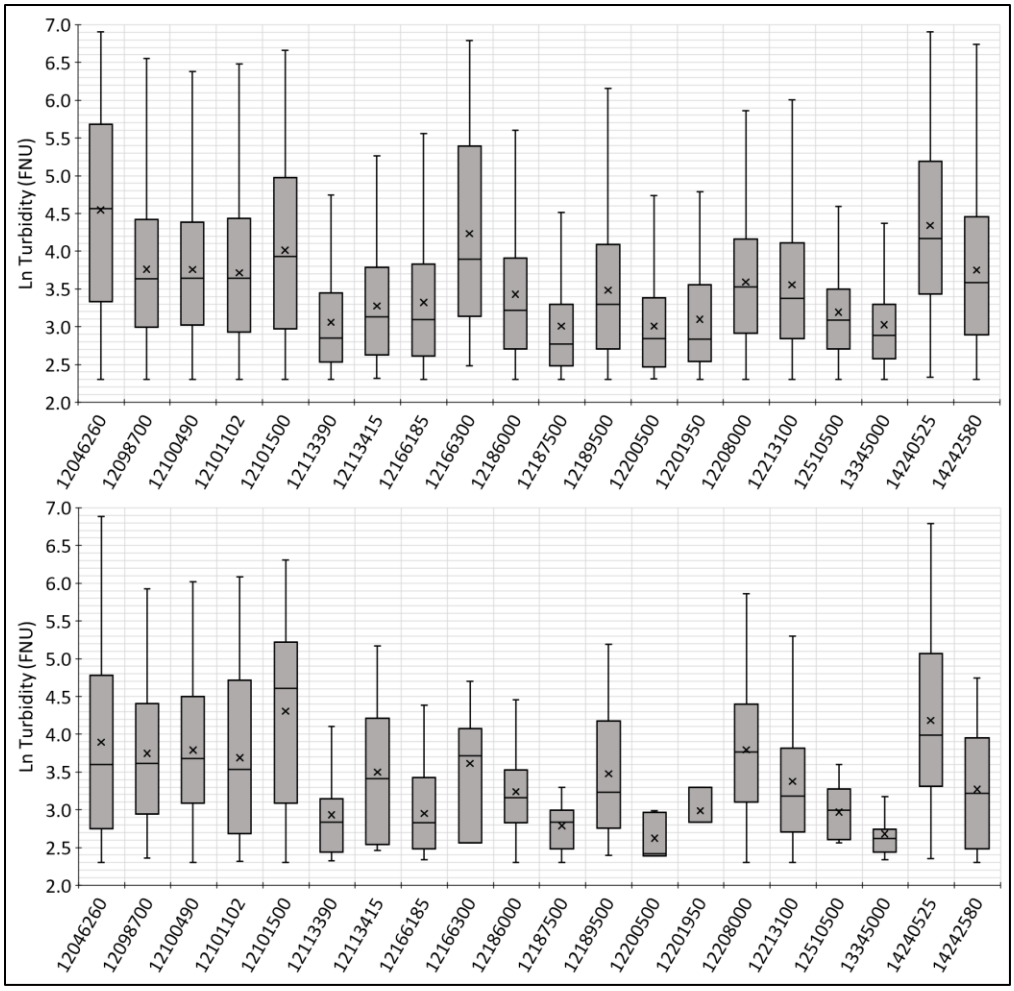

Figure 2.4 Boxplots representing the total measured turbidity data across different USGS Gauge stations in Washington in (above), and those coinciding with Landsat 5, 7, and 8 coverage (below).

Next, different training-testing splits such as 50-50, 60-40, 70-30, 80-20 were explored, and it was found that a split of 70% for training and 30% for testing, as well as a split of 80% for training and 20% for testing, yielded the most accurate results (Table 2.2).

Table 2.2 NSE and RSR values for prediction models under different algorithms, sets of predictor variables, and two different data partitions.

Data Partition		70% Training		30% Testing		80% Training		20% Testing	
Algorithm	**Predictors**	**NSE**	**RSR**	**NSE**	**RSR**	**NSE**	**RSR**	**NSE**	**RSR**
Linear	**Band_ratios**	0.19	0.9	0.27	0.85	0.2	0.91	0.26	0.86
	SDI	0.21	0.89	0.3	0.83	0.24	0.87	0.25	0.86
ANN	**Band_ratios**	0.28	0.85	0.29	0.84	0.22	0.88	0.14	0.93
	SDI	0.11	0.94	0.1	0.95	0.39	0.78	0.26	0.85
SVM	**Band_ratios**	0.35	0.8	***0.36***	***0.8***	0.4	0.77	0.3	0.84
	SDI	0.65	0.59	***0.54***	***0.68***	0.67	0.57	0.42	0.76
RF	**Band_ratios**	0.87	0.35	0.37	0.79	0.88	0.35	***0.33***	***0.82***
	SDI	0.9	0.31	0.51	0.7	0.91	0.29	***0.47***	***0.73***

For the 70-30 split, the SVM algorithm exhibited the highest efficiency (NSEtest = 0.54, RSRtest = 0.68). On the other hand, the random forest algorithm performed well for the 80-20 split (NSEtest = 0.47, RSRtest = 0.73). These findings highlight the dependence of different algorithms on the specific training data size and partition. Furthermore, the inclusion of physically informed SDI values as predictors for different soil fractions proved to enhance the model's efficiency. This observation held true for each of the algorithms and across each data partition. Notably, incorporating SDI as predictors alongside reflectance band ratios resulted in a substantial increase in test NSE. Specifically, there was an average increase of 45% in test NSE for SVM (0.36 vs 0.54) and a 40% increase for the random forest algorithm (0.33 vs 0.47) (Table 2.2). Results also revealed that the choice of algorithm influenced the model's accuracy in predicting turbidity across different ranges. SVM exhibited better performance in predicting lower and mid turbidity (ranging from 2 to 5 log transformed FNU), while the random forest algorithm excelled in predicting higher turbidity values (ranging from 5 to 7 log transformed FNU). These findings indicate the variability in model performance based on the range of turbidity used for training the algorithms.

Results demonstrate the importance of training algorithm selection, the size of the training dataset, and the inclusion of physically relevant predictors in improving the accuracy of turbidity predictions. By leveraging SDI and considering reflectance band ratios, the model achieved notable enhancements in accuracy. These findings provide valuable insights for developing effective models for turbidity prediction, highlighting the need to consider specific algorithm characteristics and data partitioning strategies based on the desired range of turbidity values.

2.6.2 Data scarce region:

The SDI values exhibited variability across the study area for each soil fraction. The highest variability was observed for the clay fraction, ranging from 0.8 to 2.0, where the mean (1.4) was higher than the median (1.1) and represented a positive skew in the data distribution. This was followed by the silt fraction, where SDI ranged from 0.8 to 1.7, and the mean (1.2) was lower than median (1.4) and signified a negative skew in the distribution. In contrast, the sand fraction showed minimal variability, ranging from 0.9 to 1.1, and the mean and median were also relatively close (Figure 2.5). Results showed that for the study region, area under the clay fraction was more connected to river network, followed by silt, and then sand. Different factors including the availability, and variability in the range and data distribution of SDI were considered while implementing the data split between training and testing datasets under the data scarce scenario using multiple locations across the region. The goal was to ensure that the test dataset was a subset of the training dataset and both had a similar turbidity signature. This approach constrained the applicability of the model to ungauged locations based on the similarity of SDI values between the training and test locations.

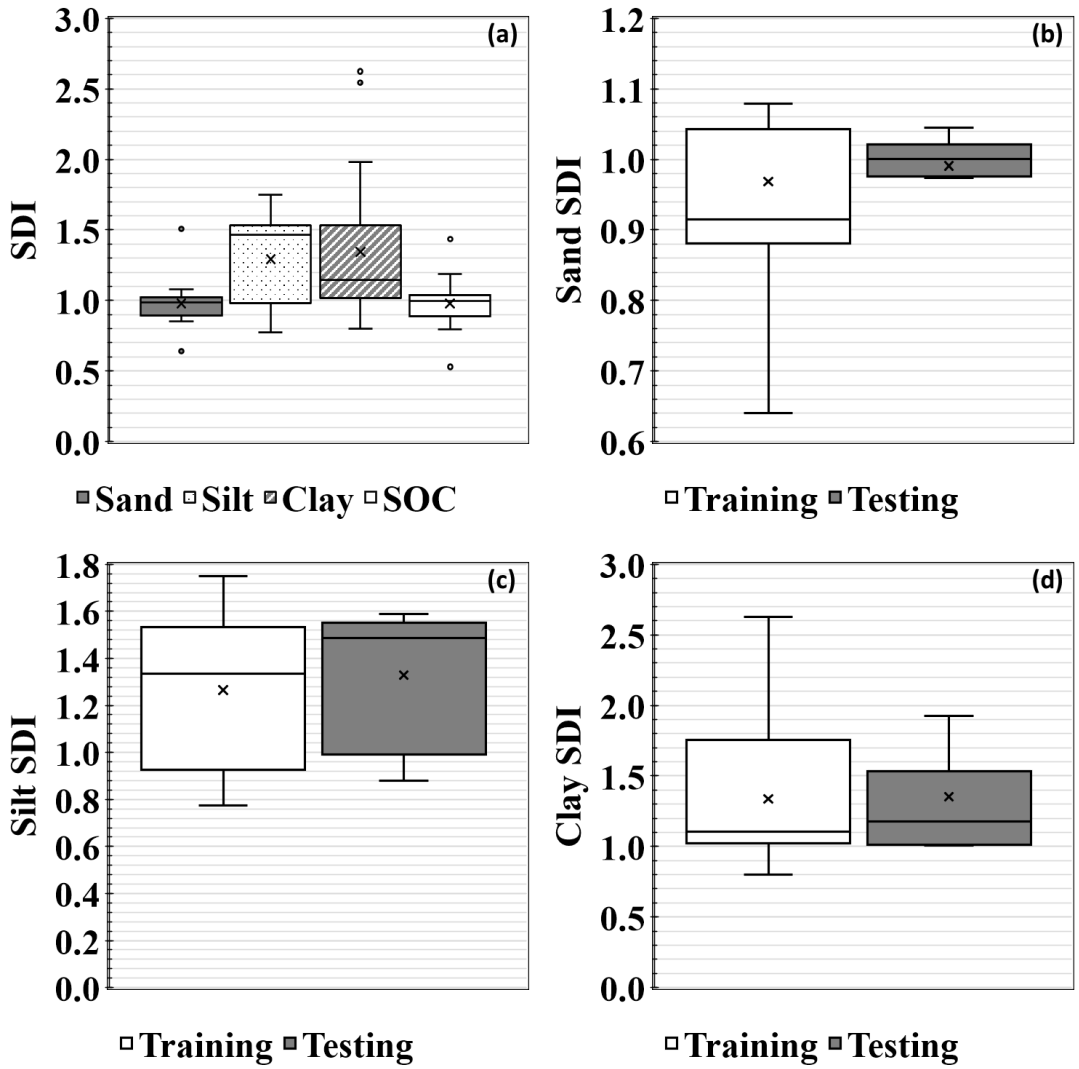

Figure 2.5 Boxplots showing the overall distribution of SDI values throughout the 20 USGS gage stations (a), along with the distribution for each soil fraction under model training and testing for the data scarce scenario (b), (c), (d).

Results showed that the training dataset consisted of 12 locations with 513 data points, while the testing dataset included 8 locations with 406 data points. This resulted in a data partition of 55% for training and 45% for testing, guided by SDI values. However, it was observed that the model accuracy for the data scarce scenario was lower compared to the data rich scenario with the same data partition (Data rich: NSEtest = 0.5, RSRtest = 0.6, Data scarce: NSEtest = 0.46, RSRtest = 0.7). Across different training algorithms and predictor combinations, the Random Forest algorithm demonstrated the highest accuracy during the model testing phase, with a test NSE of 0.46 and a test RSR of 0.73. SVM followed closely with an NSE of 0.33 and

an RSR of 0.82 (Table 3). The inclusion of SDI values for each soil fraction as predictors had varying impacts on the model efficiency across different algorithms. In the case of the SVM prediction model, incorporating SDI values led to a decrease in model efficiency during testing (NSE of 0.33 compared to 0.25, RSR of 0.82 compared to 0.86). Conversely, for the Random Forest algorithm, the inclusion of SDI values resulted in a minimal increase in efficiency during testing (NSE of 0.42 compared to 0.46, RSR of 0.76 compared to 0.73). Overall, the results indicated that the Random Forest algorithm outperformed SVM in predicting turbidity across low, mid, and high ranges. Furthermore, the findings suggested that SDI could effectively guide the selection process of donor and test locations, promoting the transferability of the model across different spatial contexts, but had minimal effect on model accuracy as compared to the band ratios only predictor combination.

Table 2.3 NSE and RSR values for prediction models under different algorithms, sets of predictor variables for the data scarce scenario.

Algorithms	**Predictors**	**Training**		**Testing**	
		NSE	**RSR**	**NSE**	**RSR**
Linear	**Band_ratios**	0.1	0.95	-1.56	1.6
	SDI	0.17	0.91	-2.29	1.81
ANN	**Band_ratios**	0.24	0.87	-0.13	1.06
	SDI	0.26	0.86	0.14	0.92
SVM	**Band_ratios**	0.35	0.8	0.33	0.82
	SDI	0.59	0.64	0.25	0.86
RF	**Band_ratios**	0.85	0.38	0.42	0.76
	SDI	0.89	0.37	***0.46***	***0.73***

2.6.3 Prediction of Fluvial Sediment Pulses:

Herein, the Reflectance-Turbidity modeling framework was implemented to predict turbidity for three different locations that experienced fluvial sediment pulses in Washington state under the two input availability scenarios. Based on the results for the reflectance turbidity model framework for the study area, a prediction model utilizing a Random Forest algorithm along with a predictor combination of reflectance band ratios and SDI was selected. In addition, the data rich scenario herein implemented a random data split, but the data scarce scenario was modified here that implemented a location-based split based on the experience of the location to a sediment pulse. Therefore, measured turbidity from the three selected locations comprised the test dataset, while the training data comprised of data from the rest 17 locations across the study area.

First, USGS Station no. 12166300 which recorded turbidity data shortly after the Oso landslide in March 2014 was evaluated for model accuracy. Under the data rich scenario, the model accurately predicted turbidity within the log transformed range of 2 to 3.5 log transformed FNU (Figure 2.6). However, it exhibited slight overprediction for turbidity values below 2 and underprediction for values above 3.5 log transformed FNU. This discrepancy can be attributed to pixel noise due to the 30-meter pixel size and the influence of channel-bed reflectance in shallow rivers. Additionally, higher turbidity levels were not accurately captured by Landsat Surface Reflectance dataset due to pixel color saturation, which is influenced by both pixel size and the nature of sensor used. Furthermore, the model's applicability was limited to non-cloudy days, and thus turbidity simulations during major precipitation events were not captured. Nonetheless, the approach successfully demonstrated declining turbidity trends from April to November, with monthly turbidity varying between 3 and 2.4 log transformed FNU, similar to the observed values. However, testing under data limited scenario was unsuccessful in capturing the sediment pulse generated after the landslide in late March 2014.

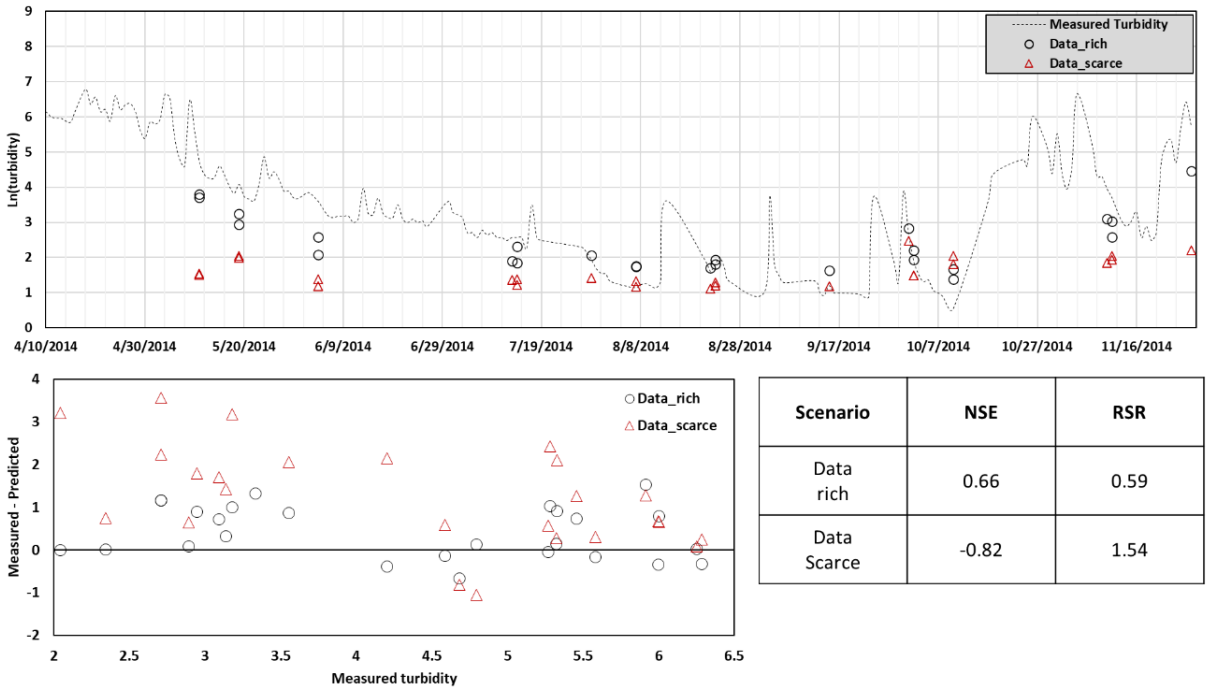

Scenario	NSE	RSR
Data rich	0.66	0.59
Data Scarce	-0.82	1.54

Figure 2.6 Model evaluation of the reflectance turbidity model for the Oso Landslide case under the data rich and data scarce scenario using a time series (a), a residual plot (b) and evaluation statistics (c).

Next, the framework was tested for the two input data scenarios for Toutle River at USGS Station no. 14242580, studied for being a suspended sediment-driven river because of the eruption of St. Mt. Helens (Major, 2004). Under both data availability scenarios, model predictions closely matched the observed data, which was supported by respective NSE (Data rich: 0.8, Data scarce: 0.44) and RSR (Data rich: 0.45, Data scarce: 0.75) values (Figure 2.7). Similar to results from the previous gauge station, it was observed that model consistently under predicted high turbidity values while performing better for mid to low observed turbidity values. The extent of the under prediction and over prediction for the peak high and peak low turbidity values under the data scarce scenario was higher as compared to the ones under the data rich scenario. Results showed that SDI was successful in identifying a donor location for the USGS station at Toutle River. More importantly, it indicates that the sediment transport across the river corridors was under the transport limited phase, minimizing the impact of pixel color saturation and so the model accuracy was similar to that observed during regional scale cross validation.

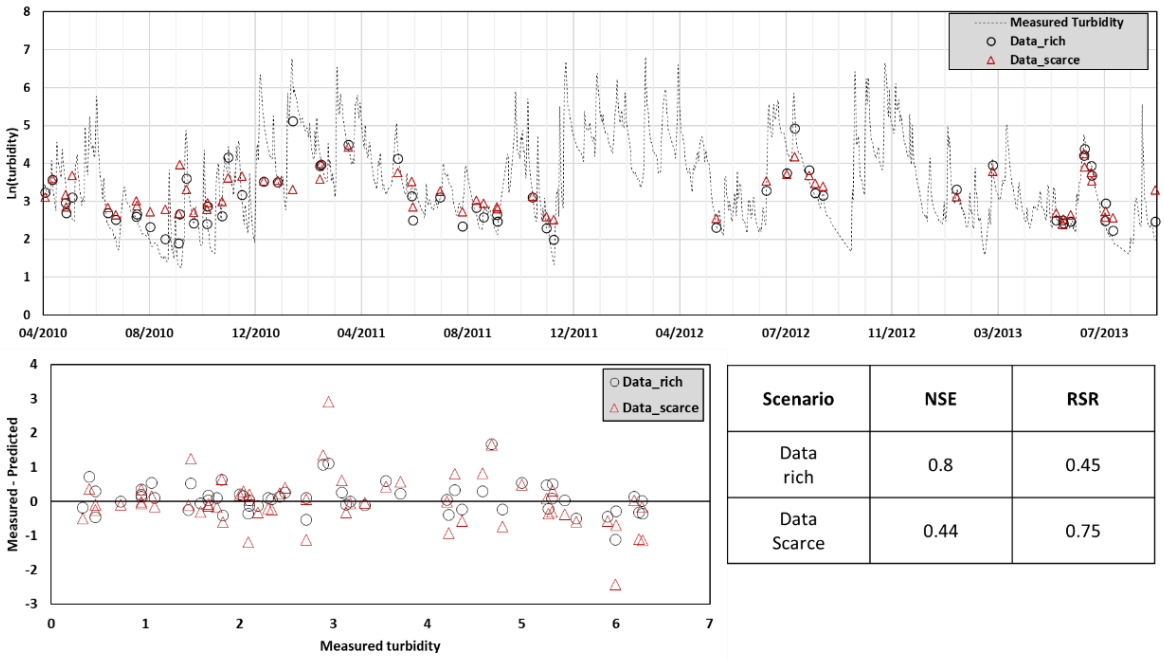

Scenario	NSE	RSR
Data rich	0.8	0.45
Data Scarce	0.44	0.75

Figure 2.7 Model evaluation of the reflectance turbidity model for the St. Mt. Helens Volcanic Eruption case under the data rich and data scarce scenario using a time series (a), a residual plot (b) and evaluation statistics (c).

Finally, the model was tested for Elwha River, which underwent two dam removals from 2011 to 2014. Under the data rich scenario, testing for Elwha River yielded mixed results. Turbidity simulations a few months after the dam removal in September 2011 consistently underpredicted daily turbidity due to pixel color saturation. However, once the initial phase of sediment pulse propagation concluded (post 2013), the model accurately predicted turbidity trends and values over the study period (Figure 2.8). The model exhibited higher efficiency in predicting mid turbidity values compared to high and low values. Aggregated results at monthly and yearly time steps demonstrated the model's success in predicting average flows and the declining trend in turbidity over the years. Under the data scarce scenario, prediction accuracy was substantially low (NSE: 0.1, RSR: 0.95). The model failed to consistently simulate peak low and high turbidity values and was best suited for predicting turbidity at aggregated time steps such as monthly or yearly.

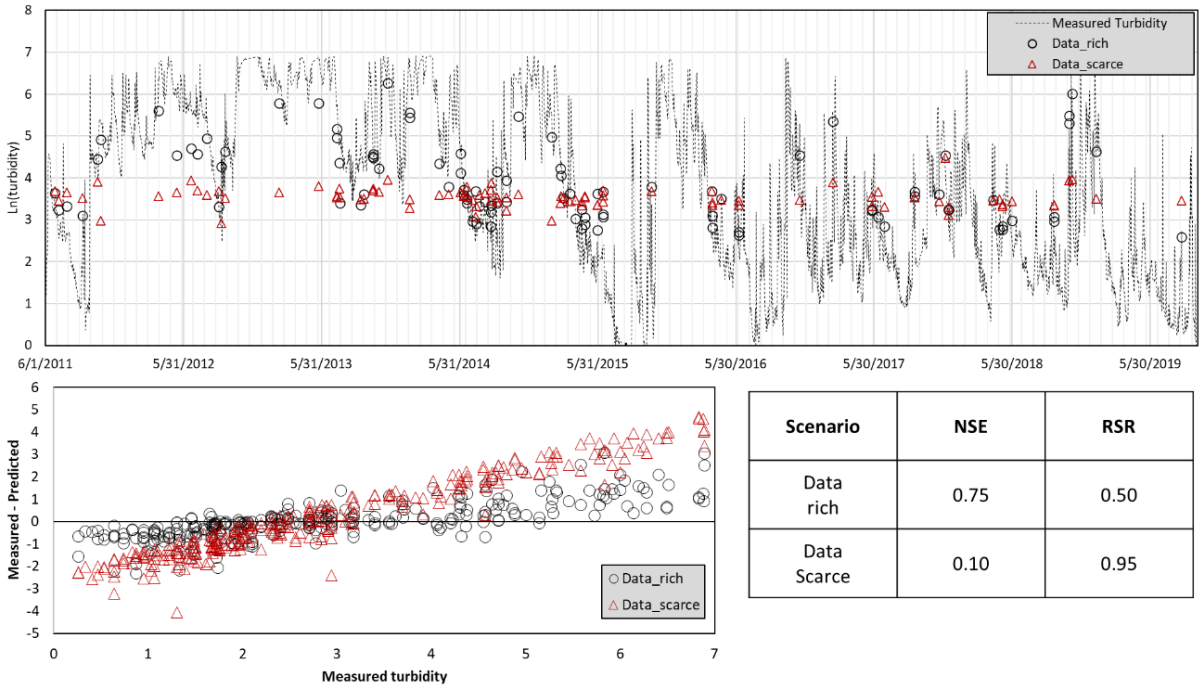

Scenario	NSE	RSR
Data rich	0.75	0.50
Data Scarce	0.10	0.95

Figure 2.8 Model evaluation of the reflectance turbidity model for the Elwha River under the data rich and data scarce scenario using a time series (a), a residual plot (b) and evaluation statistics (c).

2.7 Discussion:

The Reflectance-turbidity framework presented here allowed for prediction of turbidity for data scarce and data rich regions, while testing its potential in reconstruction of sediment pulses. Herein, the primary focus was on simulation of turbidity in the fluvial domain utilizing medium-scale satellite imagery (30m). In contrast, previous literature typically directed its attention towards coastal or estuarine settings (Brando & Dekker, 2003; Chen et al., 2007; Hellweger et al., 2004), or employed Moderate Resolution Imaging Spectroradiometer (MODIS) data to simulate Suspended Sediment Concentration (SSC), possible only in well-gauged systems (dos Santos et al., 2018; Espinoza-Villar et al., 2018; Liu et al., 2006; Mangiarotti et al., 2013; Robert et al., 2016; J.-J. Wang & Lu, 2010). From the context of sediment transport modeling, previous research primarily concentrated on predicting SSC using remote sensing under controlled conditions in terms of sediment transport, utilizing field-based settings (Simmons et al., 2010, 2017). By emphasizing turbidity dynamics in river environments, this study fills a gap in existing research and provides valuable insight into the factors influencing sediment transport modeling using reflectance-based prediction models.

In terms of regional scale analysis, this study investigated the impact of data quantity, predictor variables, and training algorithm altogether on model accuracy and transferability. Previous research often emphasized improving accuracy through the development of new band ratios or the exploration of physically informed predictors to relate turbidity and SSC, often using in situ data and not remote sensing based satellite imagery data (Bright et al., 2020; Holliday et al., 2003; Sehgal et al., 2022; Smith & Davis-Colley, 2001). While some studies focused solely on different algorithms, or were restricted to a reach or lab scale application of turbidity/SSC modeling (Francke et al., 2008; Kabir & Ahmari, 2020)., this study introduced SDI, which offered a quantitative measurement to indicate structural sediment similarity between river systems. The process of identification of similarity between multiple locations was similar to the suggestions by Dethier et al., (2020), who focused on data based clustering methods instead. In contrast, SDI was based on representation of erosional processes within the upslope drainage basin and its connectivity to the river network using elevation data. The rationale behind its development was based on suggestions from Long & Pavelsky, (2013), advising against predicting turbidity in unknown locations without knowledge of their optical signature.

Next, the development of SDI involved the utilization of the Index of Connectivity (I_C) to denote sediment connectivity (Borselli et al., 2008). I_C was chosen due to its simplicity and effectiveness, relying solely on elevation data to calculate surface roughness. In addition to Ic, several other indices also exist, simpler ones such as the one developed by Wohl et al., (2019), but they only focus towards hydrological connectivity, which could then be related to sediment connectivity. On the other hand, complex indices such as the one developed by Mahoney et al., (2018), representing functional connectivity of upslope sediment under a probabilistic framework require additional measured data, and computational power. By employing I_C, this study provided a straightforward and practical method for computing SDI, while enhancing the predictive capability of data-based turbidity modeling. Throughout the study, model performance was evaluated using NSE, and RSR which offer a more robust statistical evaluation, as compared to the widely used r^2, which serves more as a graphical performance measure, and is sensitive to peak high and low values, and does not offer a statistical quantitative comparison between measured and predicted data (Moriasi et al., 2007).

Despite the aforementioned advantages, there existed several limitations as well and should be acknowledged in this study. The use of Landsat satellite imagery, which has a 30m pixel size, is one such limitation. Although more advanced sensors with improved spatial resolution are available, Landsat was chosen for its extensive temporal coverage. Another limitation pertains to the regional scale framework employed in this study. While Dethier et al. (2020) conducted the analysis on a national scale, and others focused on specific watersheds or rivers (Robert et al., 2016; Wang et al., 2009), the spatial scale of the study lies somewhere in between. The reasoning behind that was to address the transferability of a predictive model on a regional scale, larger than a reach scale, but not as extensive as national or global scale. The results from this study suggest that, it can now be further expanded by future research to encompass larger spatial scales or explore specific case studies, allowing for a more comprehensive understanding of turbidity dynamics and its broader implications. Finally, this study opted to use turbidity data as a proxy for SSC due to its temporal continuity on a reach scale. Turbidity needs to be converted to SSC to make inferences on sediment transport dynamics for a river system under study, and previous researchers have used simple empirical relationships to convert turbidity to SSC. Overall, the relationship was observed to be linear with the slope of the regression varying from 0 to 2. Rymszewicz et al. (2017) tested the variation of SSC estimation based on different commercially available sensors, while Bright et al., (2020) and Bright & Mager, (2020) included the impact of sediment properties across different locations to develop the empirical relationship. The major advantage associated with the empirical conversion of turbidity to SSC is the non-requirement of in-situ data. However, this also adds uncertainty to the final estimation and needs to be represented in the final results to reduce subjectivity. The selection of a suitable empirical relationship can be further decided based on availability of measured turbidity and SSC data, and complexity of watershed properties resulting in the sediment delivery to the river network. This is out of the context of present study and needs further analysis to quantify the impact of different factors on uncertainty in turbidity to SSC conversion.

2.8 Conclusion:

The modeling framework developed in this study can be used to maximize the accuracy or inform the transferability of any model setup. The methodology can be successfully applied at various spatial scales, from regional to national scale. Overall, the performance of the reflectance

– turbidity model developed in this study was dependent on the input data, predictor quantity and quality, and learning algorithm used. Different algorithms tested in the initial phases of the study show that a random forest algorithm performed better at exploring the actual patterns in the training data. Second, model accuracy increased with the addition of predictors explaining the nature of sediment in the river due to structural properties of the watershed. Inclusion of the pixel-based SDI values along with reflectance ratios served as the most efficient combination of predictor variables as compared to all the others. However, SDI only represented the nature of sediment and not the quantity. Approximation of the functional connectivity of the upslope erosional sediment across a watershed required additional data on rainfall characteristics.

In addition, there existed several sources of uncertainty in turbidity prediction from space using Landsat imagery. First was pixel size, a 30 m spatial resolution made the application of this approach limited to only wider cross sections of the river corridors. A coarser pixel size also added noise to input data by misclassification of land pixels as water and vice versa. Second was channel bed reflectance. The effect was specifically observed during model application for low observed turbidity values. The third source of uncertainty was pixel color saturation. This was consistently observed for high turbidity flows across different locations across the study area. SR values did not respond to an increase in turbidity beyond a certain point and thus resulted in under prediction during the model testing phase. Out of all the three, it is the effect of color saturation that can be minimized. The addition of predictors to the model setup analyzing the functional properties of sediment transport across the watershed can prove to be vital and should be explored by future research. Fundamentally, optical satellite imagery is susceptible to cloud cover and some degree of loss in data quality and quantity must be accepted before the application of the approach. Despite that future work should focus on modern, much sophisticated satellite imagery programs such as Sentinel (ESA), Planet, and others with higher spatial, temporal, radiometric, and spectral resolution that can be used to enhance the accuracy of the modeling framework.

2.9 References:

Alber, A., & Piégay, H. (2011). Spatial disaggregation and aggregation procedures for characterizing fluvial features at the network-scale: Application to the Rhône basin (France). *Geomorphology*, *125*(3), 343–360.

Anderson, C. W., Wright, S. A., Schenk, L. N., Skalak, K., Curtis, J. A., East, A. E., & Benthem, A. (2019). Refining the Baseline Sediment Budget for the Klamath River, California. *SEDHYD 2019 Conference, 5*.

Anderson, S. W., Keith, M. K., Magirl, C. S., Wallick, J. R., Mastin, M. C., & Foreman, J. R. (2017). *Geomorphic response of the North Fork Stillaguamish River to the State Route 530 landslide near Oso, Washington*. US Geological Survey.

Ashida, K., & Michiue, M. (1972). Study on hydraulic resistance and bed-load transport rate in alluvial streams. *Proceedings of the Japan Society of Civil Engineers*, *1972*(206), 59–69.

Benda, L. E. E., Poff, N. L., Miller, D., Dunne, T., Reeves, G., Pess, G., & Pollock, M. (2004). The network dynamics hypothesis: how channel networks structure riverine habitats. *BioScience*, *54*(5), 413–427.

Blumm, M. C., & Illowsky, D. (2022). The World's Largest Dam Removal Project: The Klamath River Dams. *Available at SSRN 4061159*.

Borselli, L., Cassi, P., & Torri, D. (2008). Prolegomena to sediment and flow connectivity in the landscape: a GIS and field numerical assessment. *Catena*, *75*(3), 268–277.

Brando, V. E., & Dekker, A. G. (2003). Satellite hyperspectral remote sensing for estimating estuarine and coastal water quality. *IEEE Transactions on Geoscience and Remote Sensing*, *41*(6), 1378–1387.

Breiman, L. (2001). Random forests. *Machine Learning*, *45*, 5–32.

Brice, J. C. (1964). *Channel patterns and terraces of the Loup Rivers in Nebraska*. US Government Printing Office.

Bright, C. E., & Mager, S. M. (2020). A national-scale study of spatial variability in the relationship between turbidity and suspended sediment concentration and sediment

properties. *River Research and Applications*, *36*(8), 1449–1459.

Bright, C., Mager, S., & Horton, S. (2020). Response of nephelometric turbidity to hydrodynamic particle size of fine suspended sediment. *International Journal of Sediment Research*, *35*(5), 444–454.

Castro-Bolinaga, C. F., Diplas, P., & Bodnar, R. J. (2020). Modeling Hydro-Morphodynamic Processes During the Propagation of Fluvial Sediment Pulses: A Physics-Based Framework. *Journal of Geophysical Research: Earth Surface*, *125*(12), e2020JF005722.

Cavalli, M., Trevisani, S., Comiti, F., & Marchi, L. (2013). Geomorphometric assessment of spatial sediment connectivity in small Alpine catchments. *Geomorphology*, *188*, 31–41.

Chen, Z., Hu, C., & Muller-Karger, F. (2007). Monitoring turbidity in Tampa Bay using MODIS/Aqua 250-m imagery. *Remote Sensing of Environment*, *109*(2), 207–220.

Chib, S., & Greenberg, E. (1995). Understanding the metropolis-hastings algorithm. *The American Statistician*, *49*(4), 327–335.

Choubin, B., Solaimani, K., Rezanezhad, F., Roshan, M. H., Malekian, A., & Shamshirband, S. (2019). Streamflow regionalization using a similarity approach in ungauged basins: Application of the geo-environmental signatures in the Karkheh River Basin, Iran. *Catena*, *182*, 104128.

Cowan, W. L. (1956). Estimating hydraulic roughness coefficients. *Agricultural Engineering*, *37*(7), 473–475.

Crema, S., & Cavalli, M. (2018). SedInConnect: a stand-alone, free and open source tool for the assessment of sediment connectivity. *Computers & Geosciences*, *111*, 39–45.

Cui, Y., Dusterhoff, S. R., Wooster, J. K., & Downs, P. W. (2011). Practical considerations for modeling sediment transport dynamics in rivers. *Stream Restoration in Dynamic Fluvial Systems: Scientific Approaches, Analyses, and Tools"(Edited by Simon, A., Bennett, SJ, Castro, JM) American Geophysical Union, Washington DC*, 503–527.

Cui, Y., Parker, G., Braudrick, C., Dietrich, W. E., & Cluer, B. (2006). Dam removal express assessment models (DREAM). Part 1: model development and validation. *Journal of*

Hydraulic Research, *44*(3), 291–307.

Cui, Y., & Wilcox, A. (2008). Development and application of numerical models of sediment transport associated with dam removal. *Chapter*, *23*, 995–1020.

D. N. Moriasi, J. G. Arnold, M. W. Van Liew, R. L. Bingner, R. D. Harmel, & T. L. Veith. (2007). Model Evaluation Guidelines for Systematic Quantification of Accuracy in Watershed Simulations. *Transactions of the ASABE*, *50*(3), 885–900. https://doi.org/10.13031/2013.23153

Davies, R. B. (2002). Hypothesis testing when a nuisance parameter is present only under the alternative: linear model case. *Biometrika*, 484–489.

Dekker, A. G., & Peters, S. W. M. (1993). The use of the Thematic Mapper for the analysis of eutrophic lakes: a case study in the Netherlands. *International Journal of Remote Sensing*, *14*(5), 799–821.

Dethier, E. N., Renshaw, C. E., & Magilligan, F. J. (2020). Toward Improved Accuracy of Remote Sensing Approaches for Quantifying Suspended Sediment: Implications for Suspended-Sediment Monitoring. *Journal of Geophysical Research: Earth Surface*, *125*(7), e2019JF005033.

Ding, L., Chen, L., Ding, C., & Tao, J. (2019). Global trends in dam removal and related research: A systematic review based on associated datasets and bibliometric analysis. *Chinese Geographical Science*, *29*, 1–12.

dos Santos, A. L. M. R., Martinez, J. M., Filizola Jr, N. P., Armijos, E., & Alves, L. G. S. (2018). Purus River suspended sediment variability and contributions to the Amazon River from satellite data (2000–2015). *Comptes Rendus Geoscience*, *350*(1–2), 13–19.

Duda, J. J., & Bellmore, J. R. (2022). Dam Removal and River Restoration. *Encyclopedia of Inland Waters, Eds K. Tockner and T. Mehner (Oxford, UK: Elsevier Ltd). Doi*, *10*.

Duda, J. J., Freilich, J. E., & Schreiner, E. G. (2008). Baseline studies in the Elwha River ecosystem prior to dam removal: introduction to the special issue. *Northwest Science*, *82*(sp1), 1–12.

Duda, J. J., Warrick, J. A., & Magirl, C. S. (2011). Coastal and lower Elwha River, Washington, prior to dam removal—history, status, and defining characteristics. *Coastal Habitats of the Elwha River, Washington—Biological and Physical Patterns and Processes Prior to Dam Removal. US Geological Survey Scientific Investigations Report*, *5120*, 1–26.

East, A. E., Pess, G. R., Bountry, J. A., Magirl, C. S., Ritchie, A. C., Logan, J. B., Randle, T. J., Mastin, M. C., Minear, J. T., & Duda, J. J. (2015). Large-scale dam removal on the Elwha River, Washington, USA: River channel and floodplain geomorphic change. *Geomorphology*, *228*, 765–786.

Engelund, F., & Fredsøe, J. (1976). A sediment transport model for straight alluvial channels. *Hydrology Research*, *7*(5), 293–306.

Espinoza-Villar, R., Martinez, J.-M., Armijos, E., Espinoza, J.-C., Filizola, N., Dos Santos, A., Willems, B., Fraizy, P., Santini, W., & Vauchel, P. (2018). Spatio-temporal monitoring of suspended sediments in the Solimões River (2000–2014). *Comptes Rendus Geoscience*, *350*(1–2), 4–12.

Ferguson, R. I., Church, M., Rennie, C. D., & Venditti, J. G. (2015). Reconstructing a sediment pulse: Modeling the effect of placer mining on Fraser River, Canada. *Journal of Geophysical Research: Earth Surface*, *120*(7), 1436–1454.

Feyisa, G. L., Meilby, H., Fensholt, R., & Proud, S. R. (2014). Automated Water Extraction Index: A new technique for surface water mapping using Landsat imagery. *Remote Sensing of Environment*, *140*, 23–35.

Foley, M. M., Bellmore, J. R., O'Connor, J. E., Duda, J. J., East, A. E., Grant, G. E., Anderson, C. W., Bountry, J. A., Collins, M. J., & Connolly, P. J. (2017). Dam removal: Listening in. *Water Resources Research*, *53*(7), 5229–5246.

Foley, M. M., Duda, J. J., Beirne, M. M., Paradis, R., Ritchie, A., & Warrick, J. A. (2015). Rapid water quality change in the E lwha R iver estuary complex during dam removal. *Limnology and Oceanography*, *60*(5), 1719–1732.

Fox, C. A., Reo, N. J., Fessell, B., & Dituri, F. (2022). Native American tribes and dam removal: restoring the Ottaway, Penobscot and Elwha Rivers. *Water Alternatives*, *15*(1), 31–55.

Francke, T., López-Tarazón, J. A., & Schröder, B. (2008). Estimation of suspended sediment concentration and yield using linear models, random forests and quantile regression forests. *Hydrological Processes: An International Journal*, *22*(25), 4892–4904.

Gao, B.-C. (1996). NDWI—A normalized difference water index for remote sensing of vegetation liquid water from space. *Remote Sensing of Environment*, *58*(3), 257–266.

Gao, P. (2008). Understanding watershed suspended sediment transport. *Progress in Physical Geography*, *32*(3), 243–263.

Gelfenbaum, G., Stevens, A. W., Miller, I., Warrick, J. A., Ogston, A. S., & Eidam, E. (2015). Large-scale dam removal on the Elwha River, Washington, USA: Coastal geomorphic change. *Geomorphology*, *246*, 649–668.

Gesch, D., Oimoen, M., Greenlee, S., Nelson, C., Steuck, M., & Tyler, D. (2002). The national elevation dataset. *Photogrammetric Engineering and Remote Sensing*, *68*(1), 5–32.

Gitelson, A. A., Dall'Olmo, G., Moses, W., Rundquist, D. C., Barrow, T., Fisher, T. R., Gurlin, D., & Holz, J. (2008). A simple semi-analytical model for remote estimation of chlorophyll-a in turbid waters: Validation. *Remote Sensing of Environment*, *112*(9), 3582–3593.

Graf, W. L. (1999). Dam nation: A geographic census of American dams and their large-scale hydrologic impacts. *Water Resources Research*, *35*(4), 1305–1311.

Gran, K. B., & Czuba, J. A. (2017). Sediment pulse evolution and the role of network structure. *Geomorphology*, *277*, 17–30. https://doi.org/https://doi.org/10.1016/j.geomorph.2015.12.015

Guarino, J. (2013). Tribal advocacy and the art of dam removal: The Lower Elwha Klallam and the Elwha Dams. *American Indian Law Journal*, *2*(1), 114–145.

Guertault, L., Camenen, B., Paquier, A., & Peteuil, C. (2018). A one-dimensional process-based approach to study reservoir sediment dynamics during management operations. *Earth Surface Processes and Landforms*, *43*(2), 373–386.

Guertault, L., Camenen, B., Peteuil, C., Paquier, A., & Faure, J. B. (2016). One-dimensional modeling of suspended sediment dynamics in dam reservoirs. *Journal of Hydraulic*

Engineering, *142*(10), 4016033.

Guo, Y., Zhang, Y., Zhang, L., & Wang, Z. (2021). Regionalization of hydrological modeling for predicting streamflow in ungauged catchments: A comprehensive review. *Wiley Interdisciplinary Reviews: Water*, *8*(1), e1487.

Gupta, N., Atkinson, P. M., & Carling, P. A. (2013). Decadal length changes in the fluvial planform of the River Ganga: bringing a mega-river to life with Landsat archives. *Remote Sensing Letters*, *4*(1), 1–9.

Haefner, J. W. (2005). *Modeling biological systems:: principles and applications*. Springer Science & Business Media.

Hastings, W. K. (1970). *Monte Carlo sampling methods using Markov chains and their applications*.

Hearst, M. A., Dumais, S. T., Osuna, E., Platt, J., & Scholkopf, B. (1998). Support vector machines. *IEEE Intelligent Systems and Their Applications*, *13*(4), 18–28.

Hellweger, F. L., Schlosser, P., Lall, U., & Weissel, J. K. (2004). Use of satellite imagery for water quality studies in New York Harbor. *Estuarine, Coastal and Shelf Science*, *61*(3), 437–448.

Helsel, D. R., & Hirsch, R. M. (2002). Statistical methods in water resources. Hydrologic Analysis and Interpretation. *US Geological Survey Techniques of Water-Resources Investigations*, *510*.

Hilbert-Wolf, H. L., & Gerlak, A. K. (2022). The evolution of the modern dam conflict on the Snake River, USA. *Water International*, *47*(8), 1349–1369.

Hilldale, R. C., Carpenter, W. O., Goodwiller, B., Chambers, J. P., & Randle, T. J. (2015). Installation of impact plates to continuously measure bed load: Elwha River, Washington, USA. *Journal of Hydraulic Engineering*, *141*(3), 6014023.

Holliday, C. P., Rasmussen, T. C., & Miller, W. P. (2003). *Establishing the relationship between turbidity and total suspended sediment concentration*.

Hommes, L. (2022). The Ageing of Infrastructure and Ideologies: Contestations Around Dam

Removal in Spain. *Water Alternatives*, *15*(3), 592–613.

Hsu, N.-S., & Huang, C.-J. (2017). Estimation of flow duration curve at ungauged locations in Taiwan. *Journal of Hydrologic Engineering*, *22*(8), 5017009.

Ibraheem, N. A., Hasan, M. M., Khan, R. Z., & Mishra, P. K. (2012). Understanding color models: a review. *ARPN Journal of Science and Technology*, *2*(3), 265–275.

Isikdogan, F., Bovik, A., & Passalacqua, P. (2017). RivaMap: An automated river analysis and mapping engine. *Remote Sensing of Environment*, *202*, 88–97.

Iverson, R. M. (2015). Scaling and design of landslide and debris-flow experiments. *Geomorphology*, *244*, 9–20.

Iverson, R. M., & George, D. L. (2016). Modelling landslide liquefaction, mobility bifurcation and the dynamics of the 2014 Oso disaster. *Géotechnique*, *66*(3), 175–187.

Iverson, R. M., George, D. L., Allstadt, K., Reid, M. E., Collins, B. D., Vallance, J. W., Schilling, S. P., Godt, J. W., Cannon, C. M., & Magirl, C. S. (2015). Landslide mobility and hazards: implications of the 2014 Oso disaster. *Earth and Planetary Science Letters*, *412*, 197–208.

James, N. A., & Matteson, D. S. (2013). ecp: An R package for nonparametric multiple change point analysis of multivariate data. *ArXiv Preprint ArXiv:1309.3295*.

Jastram, J. D., Zipper, C. E., Zelazny, L. W., & Hyer, K. E. (2010). Increasing precision of turbidity-based suspended sediment concentration and load estimates. *Journal of Environmental Quality*, *39*(4), 1306–1316.

Jensen, J. R. (2009). *Remote sensing of the environment: An earth resource perspective 2/e*. Pearson Education India.

Jiang, L., Westphal Christensen, S., & Bauer-Gottwein, P. (2021). Calibrating 1D hydrodynamic river models in the absence of cross-section geometry using satellite observations of water surface elevation and river width. *Hydrology and Earth System Sciences*, *25*(12), 6359–6379.

Julien, P. Y. (2018). *River mechanics*. Cambridge University Press.

Kabir, S. M. I., & Ahmari, H. (2020). Evaluating the effect of sediment color on water radiance and suspended sediment concentration using digital imagery. *Journal of Hydrology*, *589*, 125189.

Karrasch, P., Henzen, D., Hunger, S., & Hörold, M. (2015). Determination of water body structures for small rivers using remote sensing data. *Remote Sensing for Agriculture, Ecosystems, and Hydrology XVII*, *9637*, 126–138.

Kellogg, K., Hoffman, P., Standley, S., Shaffer, S., Rosen, P., Edelstein, W., Dunn, C., Baker, C., Barela, P., & Shen, Y. (2020). NASA-ISRO synthetic aperture radar (NISAR) mission. *2020 IEEE Aerospace Conference*, 1–21.

Kendall, M. G. (1948). *Rank correlation methods.*

Khan, N. S., Roy, S. K., Mazumder, M. T. R., Talukdar, S., & Mallick, J. (2022). Assessing the long-term planform dynamics of Ganges–Jamuna confluence with the aid of remote sensing and GIS. *Natural Hazards*, *114*(1), 883–906.

Kirk, J. T. O. (1994). *Light and photosynthesis in aquatic ecosystems*. Cambridge university press.

Konrad, C. P. (2009). Simulating the recovery of suspended sediment transport and river-bed stability in response to dam removal on the Elwha River, Washington. *Ecological Engineering*, *35*(7), 1104–1115.

Lauer, D. T., Morain, S. A., & Salomonson, V. V. (1997). The Landsat program: Its origins, evolution, and impacts. *Photogrammetric Engineering and Remote Sensing*, *63*(7), 831–838.

Leisher, C., Hess, S., Dempsey, K., Payne Wynne, M. L., & Royte, J. (2022). Measuring the social changes from river restoration and dam removal. *Restoration Ecology*, *30*(1), e13500.

Leopold, L. B., Wolman, M. G., & Miller, J. P. (1964). Fluvial processes in geomorphology WH Freeman and Co. *San Francisco 522pp*.

Levins, R. (1966). The strategy of model building in population biology. *American Scientist*, *54*(4), 421–431.

Lindell, T., Pierson, D., & Premazzi, G. (1999). *Manual for monitoring European lakes using remote sensing techniques*.

Liu, C., He, B., Li, M., & Ren, X. (2006). Quantitative modeling of suspended sediment in middle Changjiang River from MODIS. *Chinese Geographical Science*, *16*, 79–82.

Long, C. M., & Pavelsky, T. M. (2013). Remote sensing of suspended sediment concentration and hydrologic connectivity in a complex wetland environment. *Remote Sensing of Environment*, *129*, 197–209.

Longbotham, N., Pacifici, F., Malitz, S., Baugh, W., & Camps-Valls, G. (2015). Measuring the spatial and spectral performance of WorldView-3. *Hyperspectral Imaging and Sounding of the Environment*, HW3B-2.

Ma, Y., & Huang, H. Q. (2016). Controls of channel morphology and sediment concentration on flow resistance in a large sand-bed river: A case study of the lower Yellow River. *Geomorphology*, *264*, 132–146.

Magirl, C. S., Hilldale, R. C., Curran, C. A., Duda, J. J., Straub, T. D., Domanski, M., & Foreman, J. R. (2015). Large-scale dam removal on the Elwha River, Washington, USA: Fluvial sediment load. *Geomorphology*, *246*, 669–686.

Mahoney, D. T., Fox, J. F., & Al Aamery, N. (2018). Watershed erosion modeling using the probability of sediment connectivity in a gently rolling system. *Journal of Hydrology*, *561*, 862–883.

Major, J. J. (2004). Posteruption suspended sediment transport at Mount St. Helens: Decadal-scale relationships with landscape adjustments and river discharges. *Journal of Geophysical Research: Earth Surface*, *109*(F1).

Major, J. J., Bertin, D., Pierson, T. C., Amigo, Á., Iroumé, A., Ulloa, H., & Castro, J. (2016). Extraordinary sediment delivery and rapid geomorphic response following the 2008–2009 eruption of Chaitén Volcano, Chile. *Water Resources Research*, *52*(7), 5075–5094.

Major, J. J., Pierson, T. C., Dinehart, R. L., & Costa, J. E. (2000). Sediment yield following severe volcanic disturbance—a two-decade perspective from Mount St. Helens. *Geology*, *28*(9), 819–822.

Mangiarotti, S., Martinez, J.-M., Bonnet, M.-P., Buarque, D. C., Filizola, N., & Mazzega, P. (2013). Discharge and suspended sediment flux estimated along the mainstream of the Amazon and the Madeira Rivers (from in situ and MODIS Satellite Data). *International Journal of Applied Earth Observation and Geoinformation*, *21*, 341–355.

Mann, H. B. (1945). Non-parametric test against trend. Econometrika 13, 245–259. *Search In*.

Matteson, D. S., & James, N. A. (2014). A nonparametric approach for multiple change point analysis of multivariate data. *Journal of the American Statistical Association*, *109*(505), 334–345.

Mauer, K. W. (2020). Monopoly's winners and losers: Elwha River Dam construction as social closure. *Journal of Environmental Studies and Sciences*, *10*(2), 137–147.

McCulloch, W. S., & Pitts, W. (1943). A logical calculus of the ideas immanent in nervous activity. *The Bulletin of Mathematical Biophysics*, *5*, 115–133.

McElreath, R. (2020). *Statistical rethinking: A Bayesian course with examples in R and Stan*. CRC press.

Metropolis, N., Rosenbluth, A., Rosenbluth, M., Teller, A., & Teller, E. (1953). Introduction of the metropolis algorithm for molecular-dynamics simulation. *J. Chem. Phys*, *21*, 1987.

Milliman, J. D., & Syvitski, J. P. M. (1992). Geomorphic/tectonic control of sediment discharge to the ocean: the importance of small mountainous rivers. *The Journal of Geology*, *100*(5), 525–544.

Mostafa, Y., & Abdelhafiz, A. (2017). Shadow identification in high resolution satellite images in the presence of water regions. *Photogrammetric Engineering & Remote Sensing*, *83*(2), 87–94.

Murphy, B. P., Czuba, J. A., & Belmont, P. (2019). Post-wildfire sediment cascades: A modeling framework linking debris flow generation and network-scale sediment routing. *Earth Surface Processes and Landforms*, *44*(11), 2126–2140.

Nash, J. E., & Sutcliffe, J. V. (1970). River flow forecasting through conceptual models part I—A discussion of principles. *Journal of Hydrology*, *10*(3), 282–290.

Nelson, A., & Dubé, K. (2016). Channel response to an extreme flood and sediment pulse in a mixed bedrock and gravel-bed river. *Earth Surface Processes and Landforms*, *41*(2), 178–195.

Nelson, P. A., Brew, A. K., & Morgan, J. A. (2015). Morphodynamic response of a variable-width channel to changes in sediment supply. *Water Resources Research*, *51*(7), 5717–5734.

O'CALLAGHAN, J., ROBERTSON, P., & Fraser, D. (1982). *Colour image display: it's not that simple.*

O'Hanley, J. R., Pompeu, P. S., Louzada, M., Zambaldi, L. P., & Kemp, P. S. (2020). Optimizing hydropower dam location and removal in the São Francisco river basin, Brazil to balance hydropower and river biodiversity tradeoffs. *Landscape and Urban Planning*, *195*, 103725.

Olden, J. D., Lawler, J. J., & Poff, N. L. (2008). Machine learning methods without tears: a primer for ecologists. *The Quarterly Review of Biology*, *83*(2), 171–193.

Palu, M. C., & Julien, P. Y. (2019). Modeling the sediment load of the Doce River after the Fundão tailings dam collapse, Brazil. *Journal of Hydraulic Engineering*, *145*(5), 5019002.

Pettitt, A. N. (1979). A non-parametric approach to the change-point problem. *Journal of the Royal Statistical Society: Series C (Applied Statistics)*, *28*(2), 126–135.

Piman, T., & Babel, M. S. (2013). Prediction of rainfall-runoff in an ungauged basin: case study in the mountainous region of Northern Thailand. *Journal of Hydrologic Engineering*, *18*(2), 285–296.

Popović, P., Devauchelle, O., Abramian, A., & Lajeunesse, E. (2021). Sediment load determines the shape of rivers. *Proceedings of the National Academy of Sciences*, *118*(49), e2111215118.

Pugliese, A., Farmer, W. H., Castellarin, A., Archfield, S. A., & Vogel, R. M. (2016). Regional flow duration curves: Geostatistical techniques versus multivariate regression. *Advances in Water Resources*, *96*, 11–22.

Rand, W. M. (1971). Objective criteria for the evaluation of clustering methods. *Journal of the American Statistical Association*, *66*(336), 846–850.

Randle, T. J., Bountry, J. A., Ritchie, A., & Wille, K. (2015). Large-scale dam removal on the Elwha River, Washington, USA: Erosion of reservoir sediment. *Geomorphology*, *246*, 709–728.

Rasmussen, P. P., Gray, J. R., Glysson, G. D., & Ziegler, A. C. (2009). Guidelines and procedures for computing time-series suspended-sediment concentrations and loads from in-stream turbidity-sensor and streamflow data. *US Geological Survey Techniques and Methods, Book*, *3*, 52.

Razavi, T., & Coulibaly, P. (2016). Improving streamflow estimation in ungauged basins using a multi-modelling approach. *Hydrological Sciences Journal*, *61*(15), 2668–2679.

Reneau, S. L., Katzman, D., Kuyumjian, G. A., Lavine, A., & Malmon, D. V. (2007). Sediment delivery after a wildfire. *Geology*, *35*(2), 151–154.

Ritchie, A. C., Warrick, J. A., East, A. E., Magirl, C. S., Stevens, A. W., Bountry, J. A., Randle, T. J., Curran, C. A., Hilldale, R. C., & Duda, J. J. (2018). Morphodynamic evolution following sediment release from the world's largest dam removal. *Scientific Reports*, *8*(1), 13279.

Robert, E., Grippa, M., Kergoat, L., Pinet, S., Gal, L., Cochonneau, G., & Martinez, J.-M. (2016). Monitoring water turbidity and surface suspended sediment concentration of the Bagre Reservoir (Burkina Faso) using MODIS and field reflectance data. *International Journal of Applied Earth Observation and Geoinformation*, *52*, 243–251.

Robertson, P. K., & O'Callaghan, J. F. (1988). The application of perceptual color spaces to the display of remotely sensed imagery. *IEEE Transactions on Geoscience and Remote Sensing*, *26*(1), 49–59.

Rojas, R. (2013). *Neural networks: a systematic introduction*. Springer Science & Business Media.

Roux, C., Alber, A., Bertrand, M., Vaudor, L., & Piégay, H. (2015). "FluvialCorridor": A new ArcGIS toolbox package for multiscale riverscape exploration. *Geomorphology*, *242*, 29–

37.

Ryan Bellmore, J., Duda, J. J., Craig, L. S., Greene, S. L., Torgersen, C. E., Collins, M. J., & Vittum, K. (2017). Status and trends of dam removal research in the United States. *WIREs Water* , *4*(2), e1164. https://doi.org/https://doi.org/10.1002/wat2.1164

Rymszewicz, A., O'sullivan, J. J., Bruen, M., Turner, J. N., Lawler, D. M., Conroy, E., & Kelly-Quinn, M. (2017). Measurement differences between turbidity instruments, and their implications for suspended sediment concentration and load calculations: A sensor inter-comparison study. *Journal of Environmental Management*, *199*, 99–108.

Schermerhorn, V. P. (1967). Relations between topography and annual precipitation in western Oregon and Washington. *Water Resources Research*, *3*(3), 707–711.

Schwarz, G. E., & Alexander, R. B. (1995). *State soil geographic (STATSGO) data base for the conterminous United States*.

Sehgal, D., Martinez-Carreras, N., Hissler, C., Bense, V., & Hoitink, T. A. J. F. (2022). *Influence of riverine suspended sediment carbon content and particle size on turbidity*. Copernicus Meetings.

Sharma, A., Castro-Bolinaga, C., & Nelson, N. (2022). An integrated modeling approach to evaluate the propagation of fluvial sediment pulses following dam removals: A case study from the Elwha River, Washington, USA. *Proceedings of the 39th IAHR World Congress*, 938–945. https://doi.org/10.3850/iahr-39wc252171192022365

Sharma, S., Waldman, J., Afshari, S., & Fekete, B. (2019). Status, trends and significance of American hydropower in the changing energy landscape. *Renewable and Sustainable Energy Reviews*, *101*, 112–122.

Simmons, S. M., Parsons, D. R., Best, J. L., Oberg, K. A., Czuba, J. A., & Keevil, G. M. (2017). An evaluation of the use of a multibeam echo-sounder for observations of suspended sediment. *Applied Acoustics*, *126*, 81–90.

Simmons, S. M., Parsons, D. R., Best, J. L., Orfeo, O., Lane, S. N., Kostaschuk, R., Hardy, R. J., West, G., Malzone, C., & Marcus, J. (2010). Monitoring suspended sediment dynamics using MBES. *Journal of Hydraulic Engineering*, *136*(1), 45–49.

Smith, D., & Davis-Colley, R. (2001). Turbidity suspended sediment and water clarity. *J Am Water Resour Assoc*, *37*, 1085–1101.

Smith, T., Marshall, L., & Sharma, A. (2014). Predicting hydrologic response through a hierarchical catchment knowledgebase: A Bayes empirical Bayes approach. *Water Resources Research*, *50*(2), 1189–1204.

Song, K., Wang, Z., Blackwell, J., Zhang, B., Li, F., Zhang, Y., & Jiang, G. (2011). Water quality monitoring using Landsat Themate Mapper data with empirical algorithms in Chagan Lake, China. *Journal of Applied Remote Sensing*, *5*(1), 53506.

Sousa, J., García-Sánchez, C., & Gorlé, C. (2018). Improving urban flow predictions through data assimilation. *Building and Environment*, *132*, 282–290.

Sousa, J., & Gorlé, C. (2019). Computational urban flow predictions with Bayesian inference: Validation with field data. *Building and Environment*, *154*, 13–22.

Steinschneider, S., Yang, Y.-C. E., & Brown, C. (2015). Combining regression and spatial proximity for catchment model regionalization: a comparative study. *Hydrological Sciences Journal*, *60*(6), 1026–1043.

Strick, R. J. P., Ashworth, P. J., Sambrook Smith, G. H., Nicholas, A. P., Best, J. L., Lane, S. N., Parsons, D. R., Simpson, C. J., Unsworth, C. A., & Dale, J. (2019). Quantification of bedform dynamics and bedload sediment flux in sandy braided rivers from airborne and satellite imagery. *Earth Surface Processes and Landforms*, *44*(4), 953–972.

Swain, J. B., & Patra, K. C. (2017). Streamflow estimation in ungauged catchments using regional flow duration curve: comparative study. *Journal of Hydrologic Engineering*, *22*(7), 4017010.

Syvitski, J., Ángel, J. R., Saito, Y., Overeem, I., Vörösmarty, C. J., Wang, H., & Olago, D. (2022). Earth's sediment cycle during the Anthropocene. *Nature Reviews Earth & Environment*, *3*(3), 179–196.

Syvitski, J. P. M., & Kettner, A. (2011). Sediment flux and the Anthropocene. *Philosophical Transactions of the Royal Society A: Mathematical, Physical and Engineering Sciences*, *369*(1938), 957–975.

Syvitski, J. P., Morehead, M. D., Bahr, D. B., & Mulder, T. (2000). Estimating fluvial sediment transport: the rating parameters. *Water Resources Research*, *36*(9), 2747–2760.

Tarolli, P., & Mudd, S. M. (2020). *Remote Sensing of Geomorphology* (Vol. 23). Elsevier.

Tegegne, G., & Kim, Y.-O. (2018). Modelling ungauged catchments using the catchment runoff response similarity. *Journal of Hydrology*, *564*, 452–466.

Umar, M., Rhoads, B. L., & Greenberg, J. A. (2018). Use of multispectral satellite remote sensing to assess mixing of suspended sediment downstream of large river confluences. *Journal of Hydrology*, *556*, 325–338.

Vahedifard, F., Madani, K., AghaKouchak, A., & Thota, S. K. (2021). Are we ready for more dam removals in the United States? *Environmental Research: Infrastructure and Sustainability*, *1*(1), 13001.

Van Liew, M. W., & Mittelstet, A. R. (2018). *Comparison of three regionalization techniques for predicting streamflow in ungaged watersheds in Nebraska, USA using SWAT model*.

Vercruysse, K., Grabowski, R. C., & Rickson, R. J. (2017). Suspended sediment transport dynamics in rivers: Multi-scale drivers of temporal variation. *Earth-Science Reviews*, *166*, 38–52.

Vermote, E., Justice, C., Claverie, M., & Franch, B. (2016). Preliminary analysis of the performance of the Landsat 8/OLI land surface reflectance product. *Remote Sensing of Environment*, *185*, 46–56.

Vogel, R. M., & Fennessey, N. M. (1995). Flow duration curves II: A review of applications in water resources planning 1. *JAWRA Journal of the American Water Resources Association*, *31*(6), 1029–1039.

Wang, J.-J., & Lu, X. X. (2010). Estimation of suspended sediment concentrations using Terra MODIS: An example from the Lower Yangtze River, China. *Science of the Total Environment*, *408*(5), 1131–1138.

Wang, J., Lu, X. X., Liew, S. C., & Zhou, Y. (2009). Retrieval of suspended sediment concentrations in large turbid rivers using Landsat ETM+: an example from the Yangtze

River, China. *Earth Surface Processes and Landforms*, *34*(8), 1082–1092.

Warrick, J. A., Bountry, J. A., East, A. E., Magirl, C. S., Randle, T. J., Gelfenbaum, G., Ritchie, A. C., Pess, G. R., Leung, V., & Duda, J. J. (2015). Large-scale dam removal on the Elwha River, Washington, USA: Source-to-sink sediment budget and synthesis. *Geomorphology*, *246*, 729–750.

Wen, C.-Y., & Chou, C.-M. (2004). Color image models and its applications to document examination. *Forensic Science Journal*, *3*(1), 23–32.

Wilcox, A. C., O'Connor, J. E., & Major, J. J. (2014). Rapid reservoir erosion, hyperconcentrated flow, and downstream deposition triggered by breaching of 38 m tall Condit Dam, White Salmon River, Washington. *Journal of Geophysical Research: Earth Surface*, *119*(6), 1376–1394.

Wohl, E., Bledsoe, B. P., Jacobson, R. B., Poff, N. L., Rathburn, S. L., Walters, D. M., & Wilcox, A. C. (2015). The natural sediment regime in rivers: Broadening the foundation for ecosystem management. *BioScience*, *65*(4), 358–371.

Wohl, E., Brierley, G., Cadol, D., Coulthard, T. J., Covino, T., Fryirs, K. A., Grant, G., Hilton, R. G., Lane, S. N., & Magilligan, F. J. (2019). Connectivity as an emergent property of geomorphic systems. *Earth Surface Processes and Landforms*, *44*(1), 4–26.

Xu, H. (2005). A study on information extraction of water body with the modified normalized difference water index (MNDWI). *JOURNAL OF REMOTE SENSING-BEIJING-*, *9*(5), 595.

Zhang, M., Dong, Q., Cui, T., Xue, C., & Zhang, S. (2014). Suspended sediment monitoring and assessment for Yellow River estuary from Landsat TM and ETM+ imagery. *Remote Sensing of Environment*, *146*, 136–147.

Zhang, Y., Chiew, F. H. S., Li, M., & Post, D. (2018). Predicting runoff signatures using regression and hydrological modeling approaches. *Water Resources Research*, *54*(10), 7859–7878.

3 CONSTRUCTION, CALIBRATION, AND VALIDATION OF HYDRO-MORPHODYNAMIC MODELS FOR DATA-SCARCE REGIONS USING REMOTE SENSING

3.1 Abstract:

Maintaining spatiotemporal continuity in monitoring sediment transport across river corridors is a major challenge globally. Complex process based numerical models have been widely used to understand the channel and landscape evolution processes, but the model setup process requires intensive data input, and additional data to further calibrate model parameters. In this study, a remote sensing based methodology was developed to construct, and calibrate a 1D hydrodynamic numerical model for potential applications in data scarce regions, and the performance of the method was evaluated for Elwha River in Washington. The method used a supervised classification method for river channels with considerable shadow pixels to extract a river mask. Next, channel attributes such as width, sinuosity, and slope were extracted, and similar cross sections were identified using a multivariate change point approach. Testing the approach on Elwha resulted in four segments, for which the hydraulic calibration of the model was successful in simulating the water surface elevation (NSE: 0.93, PBIAS: -7%, RSR: 0.27). The sediment transport sub model provided accurate SSC simulations across the mid discharge values 70 – 100 m^3/s associated with exceedance probabilities ranging from 0.4 to 0.04. Finally, aerial imagery-based channel aggradation-degradation through 2015 to 2017 were accurately reproduced by the numerical model (56 m vs 48 m). Results suggest that remote sensing datasets were successful in supplementing data requirements for a numerical model setup, and calibration, and that the methodology has the potential to accurately simulate the hydromorphodynamic processes for a data rich and data scarce region alike.

3.2 Introduction:

River systems across the world are acted upon by the natural process of sediment transport, whereby sediment is carried from upslope areas towards major oceans, serving as essential sinks (Syvitski et al., 2022; Syvitski & Kettner, 2011). This global phenomenon has been the subject of interest for previous researchers who have explored the various factors influencing sediment transport across river systems. These factors include climate change,

discharge patterns, basin geology, human activities, and the size of the upslope basin (Milliman & Syvitski, 1992; Syvitski et al., 2022).

To better understand the complex dynamics of sediment transport, it becomes crucial to quantify the impact of the aforementioned factors on upstream sediment supply. This quantification provides valuable insights into the rate of sediment outflow from river systems, as well as sheds light on the fate of sediment during its downstream journey. To achieve this, pervious researchers have extensively relied on process-based numerical models, which offer detailed spatial and temporal information, complementing the measured data and enhancing our overall understanding of the system (Cui et al., 2006, 2011; Gao, 2008).

The application of numerical models in studying sediment transport dynamics has encompassed various scenarios involving sediment supply disturbances. Numerous projects have employed these models to simulate the impact of dam removals (Castro-Bolinaga et al., 2020; Konrad, 2009; Palu & Julien, 2019), mining-related activities (Ferguson et al., 2015), landslides (Iverson, 2015), and reservoir sediment management (Guertault et al., 2016, 2018). Specifically for dam removals, previous researchers have associated the sediment pulses generated post removals with high suspended sediment concentrations (SSC), hyperconcentrated flows, significant channel-bed aggradation and degradation, and severe bank failure (Castro-Bolinaga et al., 2020; East et al., 2015; Foley et al., 2017; Konrad, 2009; Palu & Julien, 2019; Wilcox et al., 2014). By investigating scenarios pertaining to similar conditions, valuable insights can be gained targeting the intricate mechanisms driving sediment transport within river systems. However, the applicability and accuracy of numerical models heavily depend on the availability of reliable input and/or validation data. Input data pertaining to channel geometry, such as shape, depth, width, and the nature of channel bed sediment, plays a pivotal role in model construction, as these data directly influence sediment transport modes and rates. Additional data such as erosion and deposition levels are also important for model validation and accuracy. In regions where measured data is scarce or no longer accessible, remote sensing techniques have emerged as viable alternatives for obtaining the required input data to construct and apply process-based numerical models.

Remote sensing has proven to be a valuable tool, with methods such as Lidar and aerial imagery scanning, offering spatially continuous scans that capture crucial information about river systems (Leopold et al., 1964; Sehgal et al., 2022; Syvitski et al., 2000). Numerous researchers

have extensively utilized aerial imagery and Lidar scans to analyze the long-term morphological evolution of river channels across different regions worldwide (Gupta et al., 2013; Khan et al., 2022; Strick et al., 2019; Tarolli & Mudd, 2020). In particular, these techniques have facilitated the extraction of longitudinal channel characteristics, such as channel width (Alber & Piégay, 2011; Isikdogan et al., 2017), sinuosity (Brice, 1964), and water surface slope derived from elevation data (Roux et al., 2015).

One crucial step preceding the extraction of these channel attributes is the evaluation of a river mask, which defines the extent of the river system within the remotely sensed area. Traditionally, an index-based approach has been employed, involving the computation of indices such as Normalized Difference Water Index (NDWI) (Gao, 1996), Modified Normalized Difference Water Index (MNDWI) (Xu, 2005), or Automated Water Extraction Index (AWEI) (Feyisa et al., 2014). However, this approach has limitations when it comes to quantifying pixels affected by vegetation or topographical shadows, and in determining site-specific thresholds for accurate water pixel classification, thereby reducing its transferability (Mostafa & Abdelhafiz, 2017). Machine learning-based supervised classification methods provide an opportunity to overcome these limitations.

To simplify the construction of numerical models and minimize computational costs while maintaining reasonable accuracy, several simplifications have been proposed including reducing the dimensionality of the numerical model and simplifying channel geometry. Specifically, in the context of channel geometry, previous researchers have employed spatial aggregation techniques, which involve identifying and grouping homogeneous cross sections within a river system (Alber & Piégay, 2011). This aggregation is achieved through changepoint analysis, utilizing methods such as the Mann Kendall test (Kendall, 1948; Mann, 1945), Hubert's test (Roux et al., 2015), and Pettit test (Pettitt, 1979). Alber & Piégay (2011) suggested that the choice of an appropriate aggregation method should take into account factors such as the nature of input data, the sensitivity of changepoint detection on significance level, and the number of variables selected for the changepoint analysis.

The present study aims to develop a methodology that combines remote sensing techniques and process-based numerical modeling to simulate sediment transport in rivers situated in data-scarce environments. The objectives of this study are twofold: (1) to utilize publicly available remote sensing-based aerial imagery and elevation data for extracting channel

characteristics and aggregating similar features across space; and (2) to establish, calibrate, and validate a one-dimensional (1D) numerical model capable of simulating hydrodynamics and sediment transport at the reach scale. By achieving these objectives, valuable insights can be gained regarding sediment dynamics in challenging data-scarce scenarios, contributing to the broader understanding of river systems and their intricate processes.

3.3 Study Area:

The Elwha River, which runs 72 km through the Olympic Peninsula in Northern Washington into the Strait of Juan de Fuca, was chosen to assess the potential of remote sensing-based numerical model construction and validation. This river was selected because it underwent two dam removals over the last decade: Elwha Dam (32-m high) in 2011 and Glines Canyon Dam (64-m high) in 2014. Therefore, extensive monitored data on sediment transport and morphological changes across the river are publicly available (East et al., 2015; Foley et al., 2015, 2017; Magirl et al., 2015; Ritchie et al., 2018; Warrick et al., 2015), allowing to critically assess the performance of the developed methodology The dams had impounded around 21 million m^3 of sediment in the reservoirs, and the removal project presented an opportunity to study the impact of sediment release at a scale not explored before. Glines Canyon Dam trapped the majority of the sediment (16 million m^3), with the sediment primarily composed of 44% silt- and clay sized material and 56% coarse sediment. The smaller Elwha Dam trapped 4.9 million m^3 of sediment primarily composed of 47% silt and clay fraction, and 53% coarse material (Randle et al., 2015). Previous research classified the river as a single, wandering gravel bed channel, while braded morphology was only observed along the lower sections of the river where multiple mainstem channels were separated by large bars or vegetated islands (East et al., 2015). Specifically, the numerical model was constructed and validated for a short sub-section of the river, which measures 2.6 km in length, located downstream of both former dam sites and including the USGS 12046260 gage station (Figure 3.1).

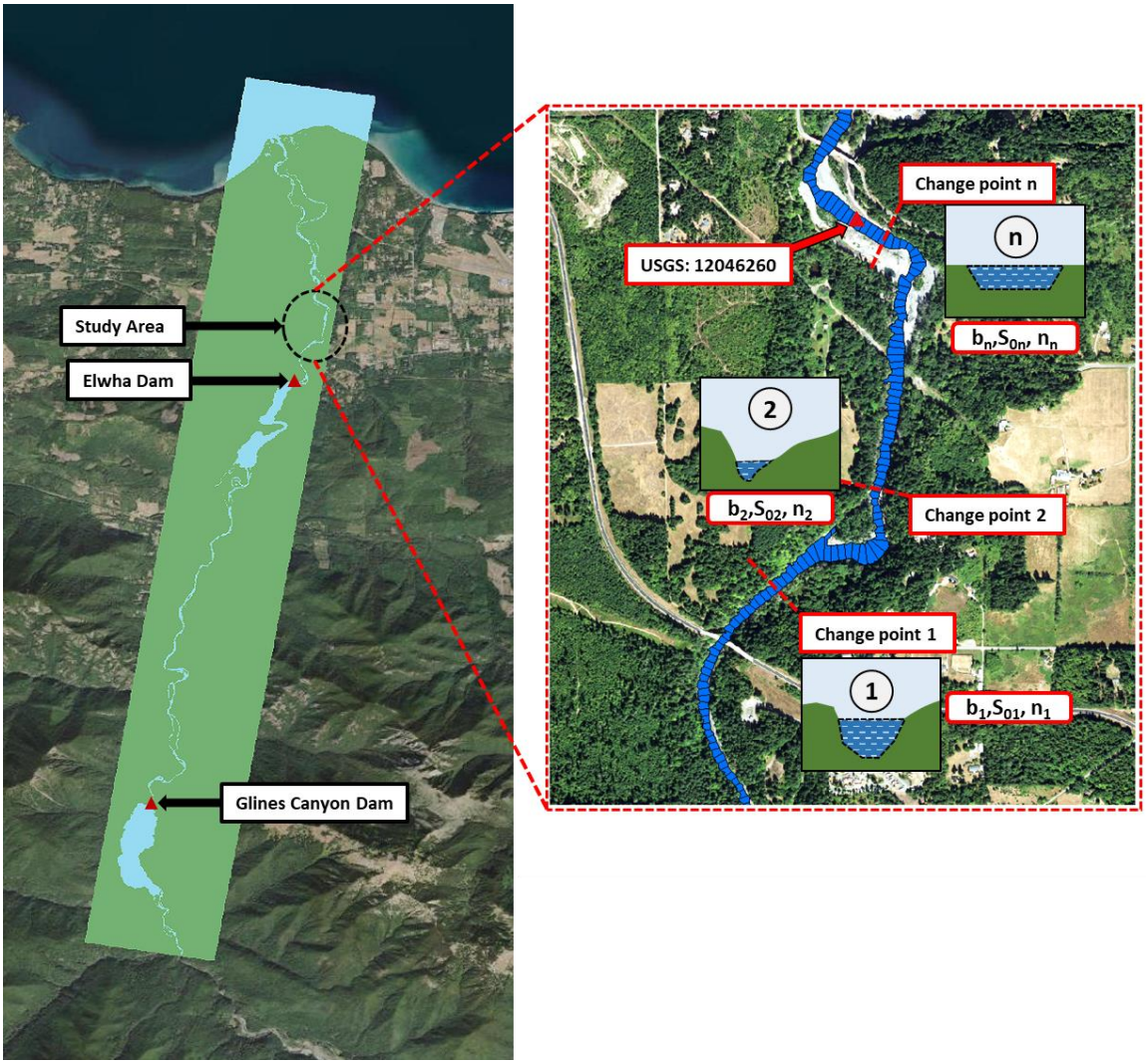

Figure 3.1 The sub-section of the Elwha River that was selected for the study (left). Cross sections across the study area were different in terms of width, and slope. To simplify the numerical model setup for the study reach, a changepoint analysis was used identifying similar cross sections in terms of channel geometry (right).

Input data comprised of a combination of publicly available aerial imagery, streamflow, turbidity, suspended sediment concentration (SSC), and river cross-sectional data (Table 3.1). It was intended to be used in construction of channel geometry for the numerical model. Based on suggestions from Castro-Bolinaga et al., (2020), the period between 2015 to 2017 as the evaluation period for this study as the initial pulse propagation phase associated with a downstream transport of 40% of the reservoir sediment ended by 2014.The evaluation period

was important to guide the model validation process using aerial imagery based channel aggradation/degradation rates.

Table 3.1 Complete list of input data used for the study in addition to its source and units.

Data	Units	Source
Aerial Imagery	1m x 1m pixels; Four bands	https://datagateway.nrcs.usda.gov/
Streamflow	m3/sec (Daily)	USGS: 12045500
Turbidity	FNU (Daily)	USGS: 12046260
SSC	Mg/L (Daily)	Sharma (2023a)
Elevation	30m x 30m pixels	https://apps.nationalmap.gov/downloader/

3.4 Methodology:

3.4.1 Overview

The model construction and validation workflow was divided into three steps: (1) extraction of channel attributes; (2) spatial aggregation of these attributes; and (3) construction, calibration, and validation of the 1D hydro-morphodynamic numerical model. Different channel attributes and validation metrics including channel width, sinuosity, slope, longitudinal aggradation, and longitudinal degradation were extracted using publicly available aerial imagery data from the National Agricultural Imagery Program (NAIP) for the years 2015 and 2017, as well as the National Elevation Dataset (Gesch et al., 2002). Subsequently, spatial aggregation of different sections of the reach was conducted using a Univariate Hubert's test and a multivariate e-divisive test (Matteson & James, 2014). This facilitated the aggregation of the extracted channel attributes, allowing for a much uniform and simplified channel geometry for the hydro-morphodynamic numerical model. The final step involved constructing a 1D numerical model, calibrating the hydraulics and sediment transport, and validating the morphodynamic subcomponent of the model for the study area throughout the evaluation period.

3.4.2 Channel attribute extraction

3.4.2.1 Water mask:

A river mask, encompassing both water and non-water pixels for the study reach, was generated as a binary raster utilizing NAIP imagery. During the initial visual inspection, it was observed that the NAIP imagery data contained significant noise attributed to shadows. Consequently, a supervised classification method was employed instead of an index and threshold-based approach in order to extract water pixels more effectively. To achieve this, two algorithms, namely, the Support Vector Machine algorithm and the random forest algorithm, were utilized to train a model capable of classifying the input imagery into five distinct categories: Water; Vegetation; Bare and Urban; Shadow on water; and Shadow on land. ESRI's ArcMap 10.7.1 was used to build up training data for each category, and then perform image classification using the "Spatial analyst" extension. Subsequently, the "Shadow on water" and "Water" pixels were merged into a single category labeled as "Water," while the remaining three categories were reclassified as "Non-Water". To ensure accuracy and precision, a final inspection was conducted, and manual corrections were applied to the cross-sections associated with bridge crossings, overhanging vegetation, or any instances of erroneous classification. This verification guaranteed reliability of the generated river mask, minimizing the potential for inaccuracies and ensuring the accurate representation of the water and non-water regions within the study reach.

3.4.2.2 Longitudinal Riverscape attributes:

By utilizing the developed river mask, boundaries of the study river reach within the designated region were precisely delineated, providing a foundation for extraction of various essential channel attributes, including the channel centerline (Karrasch et al., 2015), active channel width, and channel sinuosity (Alber & Piégay, 2011; Roux et al., 2015). To evaluate the elevation profile of the river network, publicly available USGS elevation data were incorporated (Gesch et al., 2002). This dataset was utilized to quantify the water surface elevation throughout the entire river network, that served as a proxy for estimating the channel bed slope.

To ensure accurate computation and minimize potential errors, the entire study area was divided into 20-m spatial units referred to as disaggregated geographical objects (DGOs). This division into units with uniform length was not only helpful in simplifying channel attribute extraction such as channel width and sinuosity between two consecutive DGOs, but it also

helped in finalizing the finite volume length for the hydro-morphodynamic numerical model to 20m.

3.4.2.3 Spatial aggregation:

Changepoint analysis was employed to identify spatially homogeneous reach sections throughout the study area. Data for width, slope, and sinuosity were utilized in this analysis, enabling the detection of multiple changepoints through both univariate and multivariate analyses.

Previous research in the field of geomorphology has highlighted the effectiveness of Hubert's test for spatial aggregation of data (Roux et al., 2015). This mean-based univariate test has proven successful in detecting multiple change points and exhibits lesser sensitivity to the alpha level compared to the univariate Pettit test (Pettitt, 1979) and the Mann Kendall test (Kendall, 1948; Mann, 1945). The assumption underlying the use of Hubert's test is that the mean and variance serve as representative measures of the spatial data being analyzed. To verify the accuracy of this assumption, a multivariate non-parametric test was employed. This test utilized differences in data distribution to identify homogeneous segments across the study river reach. Results obtained from both the univariate and multivariate tests were then compared using the Rand index (Rand, 1971). The Rand index serves as a measure of similarity between two clusters of data, assessing the agreement between pairs of data points in terms of their assignment to the same or different clusters.

By evaluating the Rand index, the level of agreement between the clusters or segments identified through the univariate and multivariate tests was determined. This comparison facilitated the final segmentation of the data, leading to the identification of distinct and homogeneous reaches within the study reach. The Rand index, ranging from 0 to 1, provided a quantitative measure of the agreement achieved, where a value of 1 indicated a perfect agreement between the clusters or segments, while a value of 0 indicated no agreement between them.

3.4.3 Model Construction and Calibration

3.4.3.1 Overview of the Numerical Model:

Castro-Bolinaga et al. (2020) developed a one-dimensional (1-D) adaptive morphodynamic model for water flow, sediment transport, and riverbed evolution in alluvial rivers. The model was formulated based on the St. Venant shallow water equations and the Exner

equation for sediment mass conservation. It considered the movement of uniform granular material as both bedload and suspended load. In this study, the model also considered non-uniform sediment transport conditions, including fractional rates of bedload and suspended load transport, entrainment, deposition, and temporal variation of the riverbed material gradation. Additional details and revised equations can be found in the original publication, which also provides comprehensive information on empirical closure relations and numerical methods. A simplified version of the model, constructed using remote sensing, had a spatial resolution of 20m, with each individual spatial object depicted as a Designated Geomorphic Object (DGO), similar to Alber & Piégay, (2011). Further, sections having uniform channel width, bed slope, and sinuosity from the NAIP imagery analysis were identified using suitable changepoint methods described previously in detail and channel geometry setup accordingly for the numerical model.

3.4.3.2 Hydraulic Calibration:

Channel geometry was defined by assuming a rectangular cross-sectional shape and utilizing the changepoint analysis-based channel attributes such as channel width, and channel slope. Next, discharge data from the nearest USGS gage station (12045500) were used alongside changepoint analysis based aggregated spatial data on channel geometry to evaluate Manning's roughness. The hydraulic calibration focused on adjusting the Manning's roughness coefficient for the evaluation period while minimizing error in simulating water surface elevation. The measured water surface elevation was derived from measured stage discharge relationship developed using channel data from USGS 12045500. It was assumed that the stage discharge relationship developed was constant throughout the study reach. Next, the performance of the numerical model during hydraulic calibration was evaluated using several metrics, including the Nash-Sutcliffe Efficiency (NSE) (Nash & Sutcliffe, 1970), Percent Bias (PBIAS), and the Root Mean Square Error to Standard Deviation Ratio (RSR) (Moriasi et al., 2007). These metrics provided a comprehensive assessment of the model's ability to accurately represent the observed water surface elevation.

Mathematically, these metrics can be calculated as follows:

$$NSE = 1 - \left[\frac{\sum_{i=1}^{n}\left(Y_i^{obs} - Y_i^{sim}\right)^2}{\sum_{i=1}^{n}\left(Y_i^{obs} - Y^{mean}\right)^2}\right] \qquad \text{(Equation 3.2)}$$

$$PBIAS = \left[\frac{\sum_{i=1}^{n}\left(Y_i^{obs} - Y_i^{sim}\right)*(100)}{\sum_{i=1}^{n}\left(Y_i^{obs}\right)}\right] \quad \text{(Equation 3.3)}$$

$$RSR = \frac{RMSE}{STDEV_{obs}} = \left[\frac{\sqrt{\sum_{i=1}^{n}\left(Y_i^{obs} - Y_i^{sim}\right)^2}}{\sqrt{\sum_{i=1}^{n}\left(Y_i^{obs} - Y^{mean}\right)^2}}\right] \quad \text{(Equation 3.4)}$$

where, Y_i^{obs} = value of the ith observation, Y_i^{sim}= value of the ith simulated value and Y^{mean}= mean of the observed values.

3.4.3.3 Sediment Transport Calibration:

The sediment transport calibration process was divided into two steps to ensure accuracy and reliability. In the first step, the focus was on selecting an appropriate sediment transport formula that could effectively represent the Suspended Sediment Concentration (SSC) along the study reach. Two empirical bedload sediment transport equations, namely Ashida & Michiue, (1972) and Engelund & Fredsøe, (1976) were tested in conjunction with the particle size distribution specific to the Elwha River as determined by Hilldale et al., (2015). These equations were implemented within the sediment transport sub-model. Next, reach averaged numerical model simulated SSC values were compared to turbidity-based SSC data from USGS 12046260. Turbidity data from the gage station were converted to SSC using a regression. Previous researchers observed that the that the connection between turbidity and SSC was influenced by the physical characteristics of the suspended sediment and the flow, along with a saturation point evident in turbidity measuring instruments beyond a certain sensor-specific range (Bright et al., 2020; Rymszewicz et al., 2017; Sehgal et al., 2022). Physically, the lower turbidity levels represent finer sediment in suspension and thus drives a different turbidity-SSC response (lower regression coefficient), as compared to the higher turbidity levels that represents a mixture of fine and coarse sediment, and thus leads to a different regression coefficient (Anderson et al., (2017)). For this study, an approach that sequentially identified breakpoints along the turbidity spectrum using the method developed by Davies, (2002) was used to convert turbidity to SSC. Such an approach was focused on identifying structural changes in the turbidity vs. SSC relationship for the measured dataset.

Finally, a comparison evaluating the agreement (R^2) between the numerical model simulated SSC and the measured SSC data (turbidity to SSC) from the USGS gage station

location (12046260) on the Elwha River between 2015 and 2017, ultimately led to the selection of the more accurate sediment transport empirical equation used in the numerical model.

Next step of the analysis focused on validating the morphological changes along the study reach using Aggradation-Degradation areal estimates derived from NAIP data. The analysis aimed to identify pixels that transitioned from non-water to water for the evaluation period, indicating degradation, while the opposite scenario indicated aggradation. This pixel-by-pixel analysis was performed using raster map algebra, enabling the quantification of aggradation and degradation areas for each DGO. To account for changes in the surrounding floodplain, an additional 20 m buffer was considered. Lastly, the aggradation and degradation areas were normalized by the DGO and buffer widths, resulting in values per unit length.

Subsequently, a regression relationship was established between changes in predicted channel-bed elevation and discharge for each segment derived from the changepoint analysis along the study reach. This regression equation was then employed to simulate channel-bed aggradation and degradation for all discharge values throughout the evaluation period. The process generated a cumulative estimate of channel-bed changes over time and was performed for two scenarios: one utilizing the Flow Duration Curve (FDC) and using the probability of exceedance as a weight for different discharges throughout the evaluation period (FDC), and the other without it (W/O FDC). Flow duration curve was introduced in the analysis to test the efficacy of using discharge frequencies to understand NAIP generated morphological data. Previous researchers have used similar methods to determine rating coefficients to determine sediment concentrations or sediment loads using discharge (Syvitski et al., 2000; Vogel & Fennessey, 1995). Finally, a quantitative comparison was conducted for both scenarios from the numerical model's estimates of bed changes (m) with the estimates derived from the NAIP data, specifically focusing on aggradation and degradation patterns (m).

3.5 Results and Discussion:

3.5.1 Channel Attribute Extraction and Segmentation:

Support Vector Machine (SVM) image classification outperformed the classification based on Random Forest for the study reach. Using a minimum of 5,000 pixels to train each category (Figure 3.2 (a)), two images from 2015 and 2017 were successfully classified into five categories (Figure 3.2 (c)). However, some misclassifications occurred in the pixels located around the intersection of the river and landmass, where some “shadow on water" pixels were

erroneously classified as "shadow on land". To address these errors, a manual correction method was employed to remove the misclassified pixels. Furthermore, in areas near bridge crossings and their associated shadows, manual reclassification of pixels was conducted to ensure accurate classification of water pixels (Figure 3.2 (d)).

The significance of utilizing a supervised classification approach is highlighted by the fact that, in certain cross sections across the study reach, shadow areas accounted for approximately 35% of the total water area. This underscores the importance of accurately classifying shadow pixels to obtain reliable results. The resulting classification allowed for the identification of a reach length of 2.6 kilometers selected for further analysis (Figure 3.2 (b)).

One major limitation of this approach is the absence of validation data to assess the accuracy of the classification. The only available validation dataset, the NLCD 2011 classification using Landsat by the USGS, could not be utilized due to its coarser spatial resolution (30 meters) and the lack of classification data on shadows. Therefore, it was not possible to quantitatively validate the classification results using an independent dataset. This limitation emphasizes the need for additional validation data sources and methods to ensure the accuracy and reliability of the classification results.

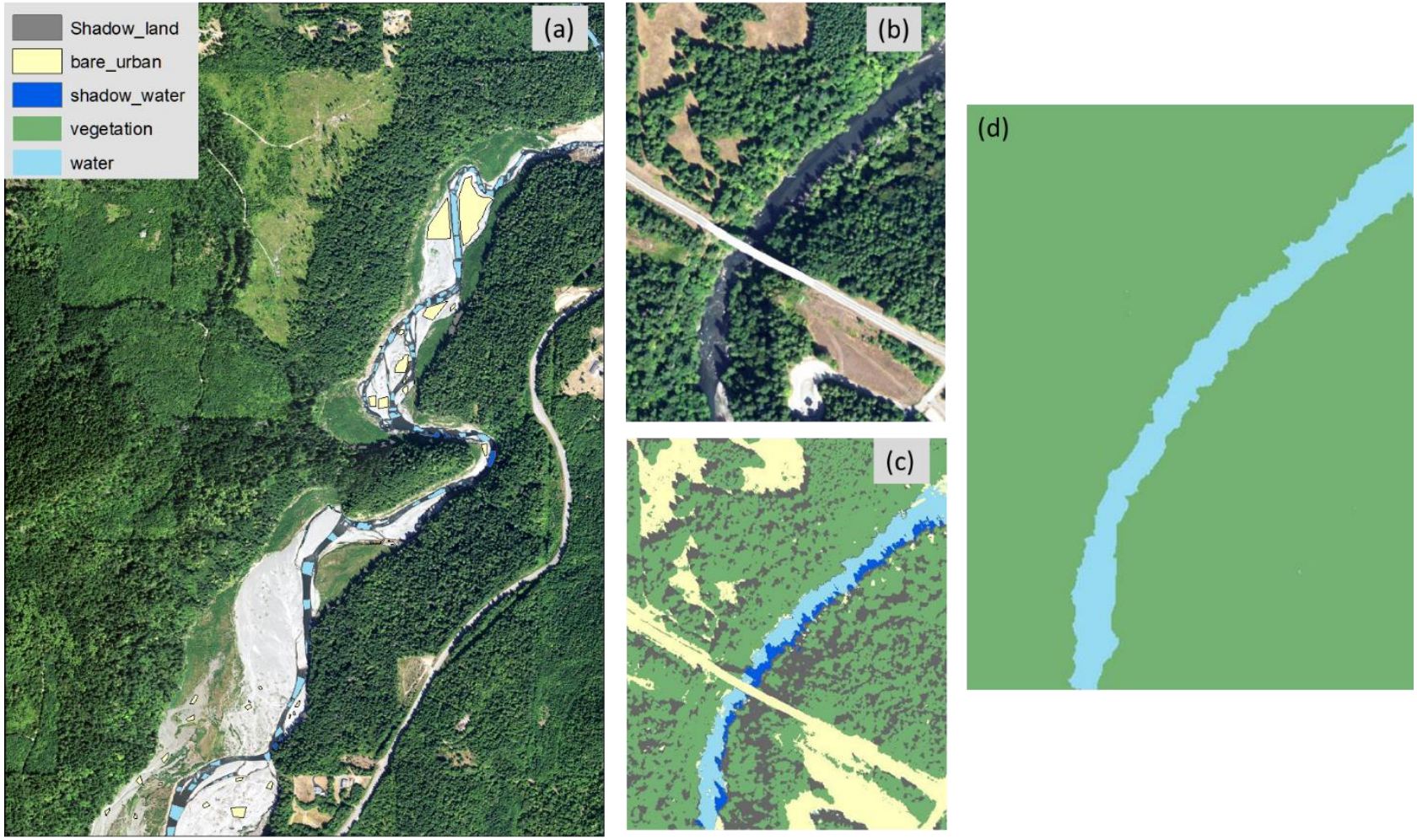

Figure 3.2 Training samples used for the SVM classifier (a). Zoomed in view of sub reach (b) and its initial classification (c), which was further improved manually to obtain the final river mask (d).

Attribute extraction for the study reach showed that the channel width across the 2.6-kilometer reach ranged from 17 to 75 meters, with an average width of approximately 30 meters. Notably, higher width values were observed around DGO: 37 and then around DGO: 67, while lower values were observed along other cross sections located throughout the study reach (Figure 3.3). Similarly, sinuosity values greater than 1 were observed around DGO: 37, DGO: 67: DGO: 104 gradually decreasing beyond those sections. Sinuosity values for the channel bends ranged from 1.05 to 1.24, while the average sinuosity for the remaining cross sections averaged around 0.99. Since sinuosity has a theoretical influence on channel roughness (Cowan, 1956), it was considered as input for the changepoint analysis but not used to construct the numerical model.

The average slope of the water surface across the reach was determined to be 0.001%. The slope values varied between 0% and 0.1%, with the maximum values observed around DGO 1-10, 50, and 60. The water surface slope, derived using the elevation dataset, was utilized as a proxy for the channel-bed slope along the study reach.

For changepoint analysis, a Univariate Hubert's test with an alpha level of 0.05 was conducted separately for width, sinuosity, and slope. The results yielded different change point locations as shown in Figure 3.3. Specifically, the univariate tests identified three changepoints for the channel width data, four changepoints for the sinuosity data, and two changepoints for the slope data. However, the results from the three univariate changepoint analysis indicated disparate locations for the changepoints, resulting in a lack of alignment and an asymmetrical division of the study reach. On the other hand, the multivariate test resulted in three change points, allowing for a more consistent segmentation of the study reach.

When comparing the Rand index values between each of the univariate tests and the multivariate test, the values were approximately 0.51 for width, 0.5 for sinuosity, and 0.5 for slope. These Rand index values suggest moderate agreement between the univariate and multivariate segmentation approaches. It indicates that some data points were assigned to the same clusters in both segmentation procedures, while others were assigned to different clusters. The overall level of agreement between the two methods was moderate, and therefore, change points identified from the multivariate approach were selected to establish the geometry for the numerical model.

Future research is needed to explore the potential of assigning weights to the different channel attributes used in the multivariate approach. Overall, the analysis and segmentation of

channel attributes provided valuable insights into the dynamics of the study reach, enabling the identification of significant change points and informing the setup of the numerical model. Segment 1 extended from DGO 1 to DGO 36, with a width of 25m, and slope of 0.0039. Segment 2 extended from DGO 37 to 66, with a width of 35m, and a slope of 0.004. Segment 3 extended from DGO 67 to DGO 104, with a width of 34m and slope of 0.00031. Segment 4 extended from DGO 104 to DGO 129, with a width of 39m, and slope of 0.0044. Overall, Segment 3 was the largest (length = 740m), followed by Segment 1 (length = 720m), Segment 2 (length = 600m), and Segment 4 (length = 520m).

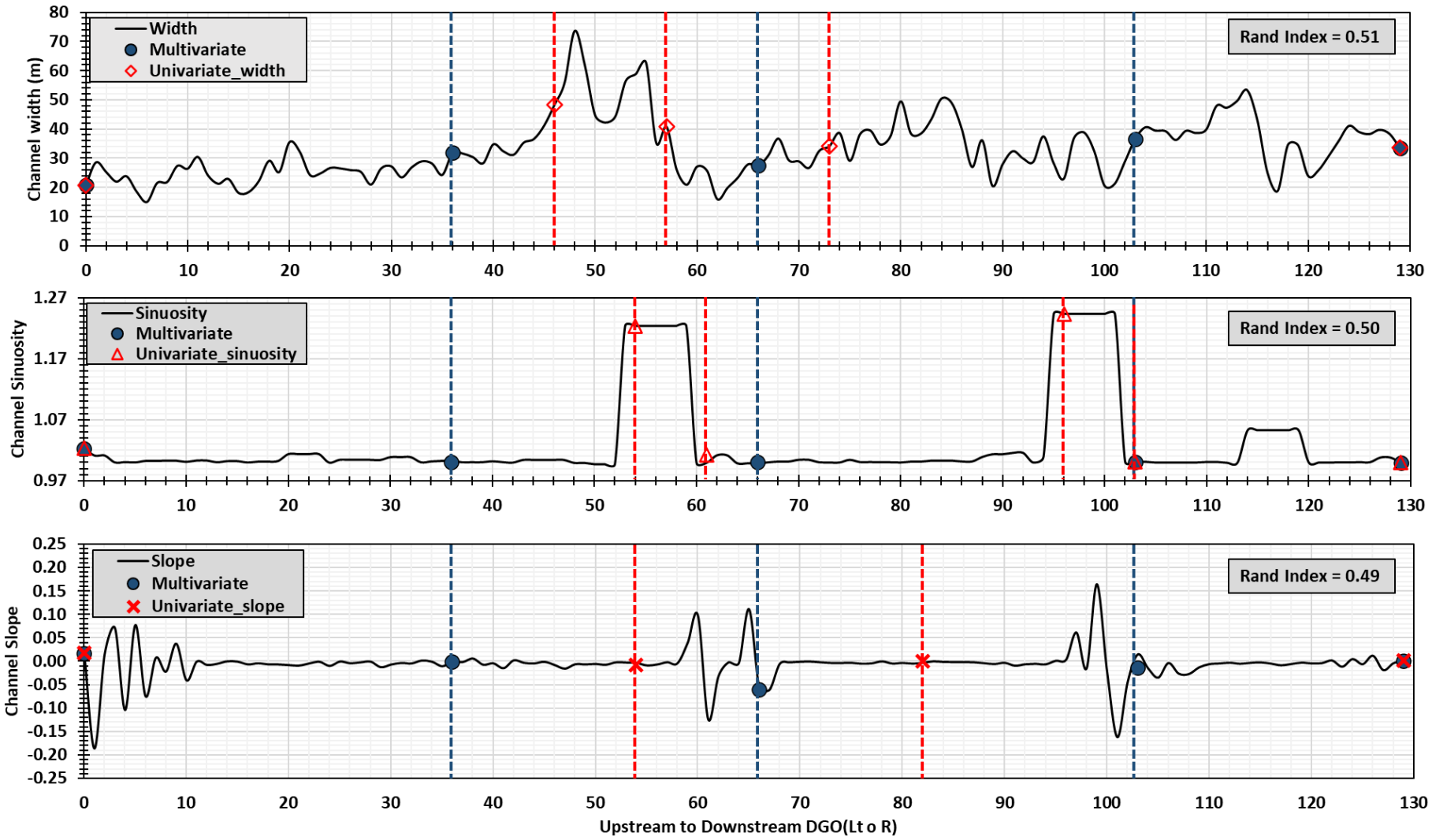

Figure 3.3 Channel width, sinuosity, and slope across the riverlength for Elwha alongwith location of different changepoints for the multivariate test (blue), and the univariate test (red).

3.5.2 Hydraulic Calibration

The hydraulic calibration process involved selecting a range of discharge values from 8 to 101 m^3/s. These values were chosen as a subset of the daily discharge values recorded between 2015 and 2017, which ranged from 8 m^3/s to 151 m^3/s. The calibration dataset was similar to the total dataset in terms of data distribution as well, with similar median, 25^{th} and 75^{th} quartile values (Figure 3.4 (a)). To calibrate the model, Manning's roughness coefficients were computed for each segment using NAIP based channel geometry data, and stage discharge relationship from USGS 12045500. Next, median values were selected as the initial parameters for calibration. Manning roughness varied from 0.016 to 0.099 across the four segments, with segment 1 attributed with the minimal range (0.016 to 0.039), followed by Segment 3 (0.031 to 0.075), Segment 2 (0.04 to 0.095), and Segment 4 (0.041 to 0.099). The selected values for the segments were 0.024 (Segment 1), 0.059 (Segment 2), 0.046 (Segment 3), and 0.061 (Segment 4) (Figure 3.4 (b)). These chosen roughness values were found to be in line with observations from natural rivers reported in the literature by previous researchers (e.g., Julien, 2018).

Visual inspection revealed a close match between the simulated stage-discharge curve and the measured data (Figure 3.4 (c)). Furthermore, quantitative evaluation of the model using statistical measures supported the results. The Nash-Sutcliffe Efficiency (NSE) was found to be 0.93, indicating a strong agreement between the simulated and measured values. The Percent Bias (PBIAS) was -6.8%, suggesting a slight underprediction of the simulated values compared to the measured data. The Root Mean Square Residual (RSR) value of 0.27 indicated a good fit of the model. Similar metrics were observed by Jiang et al., (2021), where water surface elevation was successfully calibrated for Songhua River in China using satellite based observations of channel width. In this study, it was observed that the simulation error was relatively higher for higher discharge values. This may be attributed to the limitations of the 1D model in accurately simulating water surface elevation as the model approached bankfull conditions, specifically around 200 m^3/s. Despite this, the overall simulation error remained low. Based on these results, no adjustments were made to the Manning's roughness coefficients for each segment. Consequently, the calibration process was deemed successful, and the analysis

proceeded to the next stage.

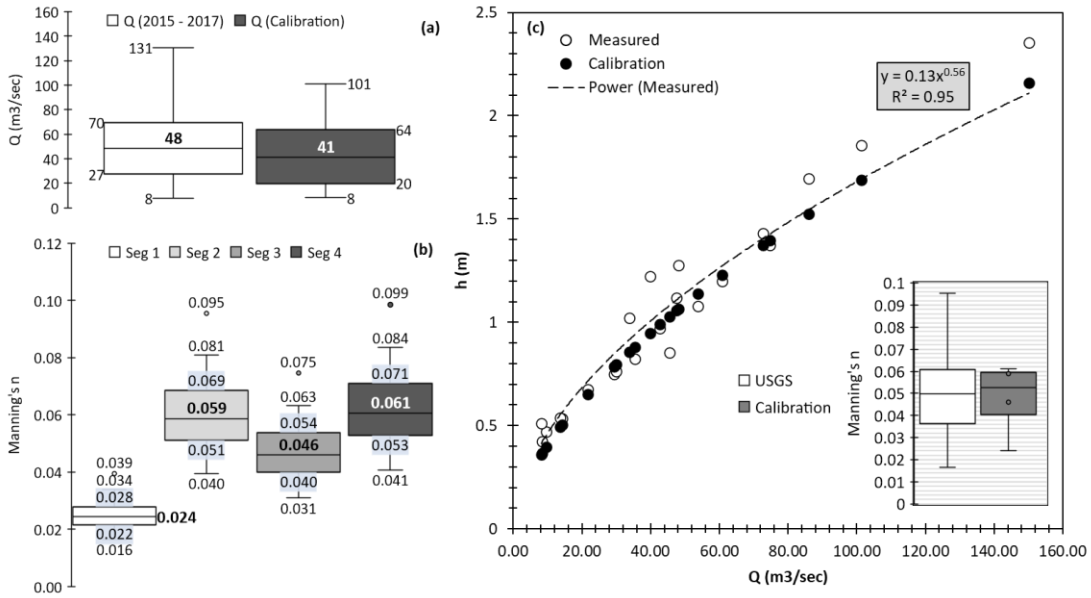

Figure 3.4 Discharge data used for the calibration (a), and its associated manning's roughness for each of the four segments (b). Water surface elevation (Y axis) plotted against the measured discharge (c) (USGS: 12045500) (X axis) for the river using measured data (hollow circle) and numerical model simulation after calibration (solid circle).

3.5.3 Sediment Transport Calibration

A visual examination comparing measured SSC and measured turbidity revealed a linear relationship, indicating as expected that SSC increases as turbidity increases (Figure 3.5). However, conducting a sequential breakpoint analysis of the SSC-turbidity regression identified two breakpoints at turbidity values of 1,125 FNU (Formazin Nephelometric Units) and 118 FNU, thereby yielding three segments. The slope of the regression line varied across these three segments were 1.9, 3.13, and 13.76 (Figure 3.5).

A suitable regression slope was determined by referring back to the daily measured turbidity from USGS 12046260 used for estimating SSC during the study period, and calibrating the sediment transport sub model. Next, SSC values derived from continuously measured turbidity were compared with predictions from the numerical model using two different sediment transport formulas. A visual comparison revealed that two empirical equations consistently overpredicted SSC across various discharge ranges (Figure 3.5). The simulation error was highest during low flow rates compared to mid-range and higher flow rates. This discrepancy can

be attributed to the fact that turbidity during low flow events is not solely influenced by suspended sediment. As flow rates increase, turbidity becomes more dominated by suspended sediment transport, making it a more reliable proxy for SSC estimation. Among the two equations considered, the Ashida and Michue (1972) equation had similar R^2 to Engelund and Hansen (1976), 0.56 vs 0.56 respectively. So, the simpler equation by Ashida and Michue (1972) was chosen. Comparing results from the two equations against turbidity generated SSC highlighted the significance of turbidity as an inherent optical property of water, with the potential to estimate SSC, particularly in regions where data availability is limited. In addition to using measured turbidity, previous research by Long & Pavelsky, (2013) and Sharma et al. (2022) successfully utilized satellite imagery to predict turbidity for both data rich and data scarce regions.

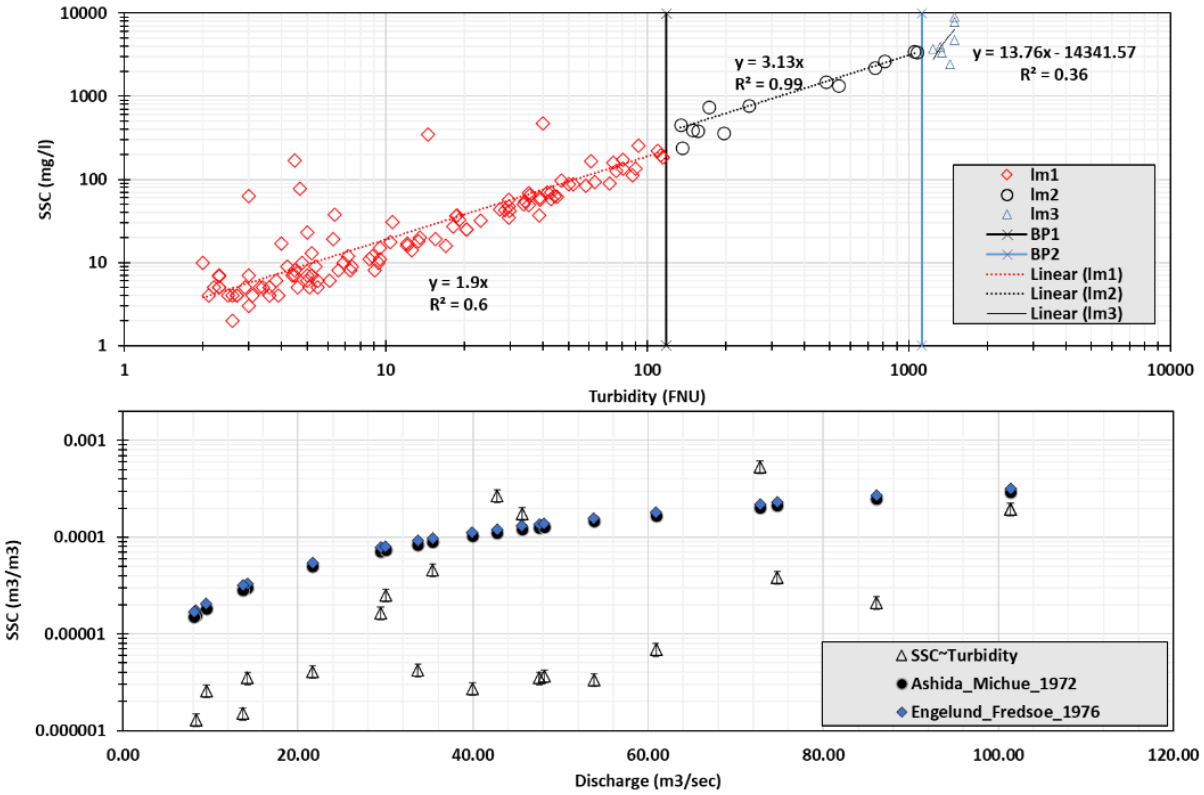

Figure 3.5 Piecewise linear regression between SSC (response) and turbidity (predictor) yielding two breakpoints at 118 FNU, and 1125 FNU respectively (Above). Next, a comparison between turbidity derived SSC with error (Y axis) (hollow triangle), and the numerical model derived SSC, across different discharges (X axis) for the model employing Ashida and Michue (1972) (Solid circle), and the one employing Engelund and Fredsoe (1976) (solid diamond).

By utilizing the Ashida & Michiue (1972) equation for sediment transport simulation and examining the regression analysis between the change in bed elevation per section and flow rates, it was observed that segment two and four exhibited positive regression coefficients indicating degradation, while segment one and three showed negative regression coefficients representing aggradation (Figure 3.6 (a)). This analysis provided evidence for the morphological changes occurring within each segment of the Elwha River.

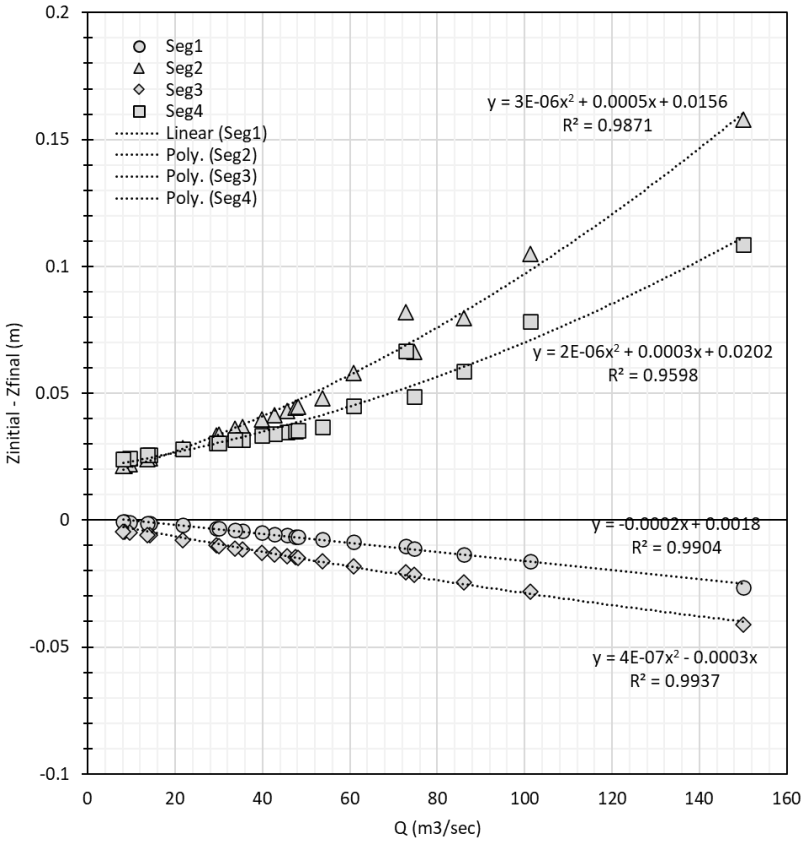

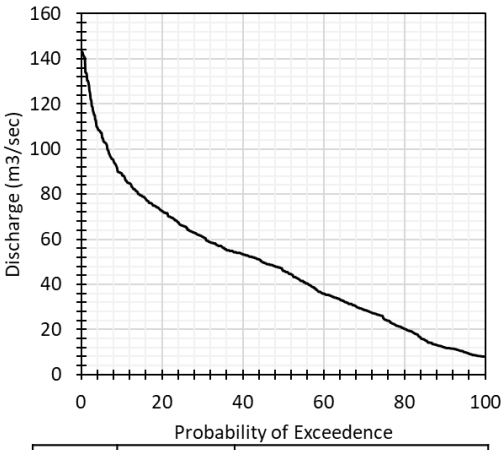

Segment	NAIP		Numerical Model			
			w/o FDC		FDC	
	Δz (m)	Δz/Δzt	Δz (m)	Δz/Δzt	Δz (m)	Δz/Δzt
Δz_1	-13.6	-0.26	-5.5	-0.11	-1.6	-0.08
Δz_2	31.0	0.60	34.7	0.71	12.6	0.65
Δz_3	11.1	0.21	-9.3	-0.19	-3.2	-0.17
Δz_4	23.5	0.45	28.8	0.59	11.4	0.59
Δz_t	52.0	1.00	48.7	1.00	19.2	1.00

Figure 3.6 Change in bed elevation for each segment expressed as a regression along with the associated flow duration curve for the upstream boundary. A final comparison of the spatial trends of the change in bed elevation across the different segments showed similar results between the numerical simulations and NAIP imagery analysis.

Next, the net cumulative change in bed elevation from 2015 to 2017 simulated from the numerical model (+48 m) was slightly higher than the one observed from NAIP imagery (+56 m). This difference could be attributed to the distinct physical interpretations of the two methods. While the process-based numerical model simulates vertical change in the channel bed across the

river length for input conditions, NAIP imagery measures the area in and around the channel that was aggraded or degraded, but in transverse direction. Despite this disparity, the overall morphological changes, and the changes per segment yielded promising results. The numerical simulation successfully captured the pronounced degradation observed in segment four and two, but under predicted changes in bed elevation for segment one and three experiencing aggradation (Figure 3.6 (c). In addition to the cumulative channel-bed changes, results showed that inclusion of probability of exceedance as a weighing factor to estimate the ratio of the cumulative bed change per segment to the cumulative change for the entire reach ($\Delta z/\Delta zt$) yielded promising results. Inclusion of FDC helped to accurately identify spatial patterns in morphology through time for the Elwha river. Numerical simulations with FDC weights were a close match to NAIP results for segment two, three, and four as compared to estimates not using the probability of exceedance as a weighing factor. Overall, Segment three had the lowest percent degradation, while 59% of the total degradation was simulated for Segment four. Herein, aerial imagery-based analysis successfully helped us to denote morphological changes across space, and through time can potentially be used to track lateral bank movement, and channel bar migration. Using a simplified numerical model can also aid in such analysis. However, developing a time series using regression analysis does not consider the dynamic nature of channel geometry through time, and is a subject that needs to be further investigated by future researchers.

3.6 Conclusion:

Results of this study demonstrate the effectiveness of remote sensing-based datasets, such as aerial imagery and elevation data, in extracting various channel attributes, including width, sinuosity, and slope. By employing a supervised classification methods, it becomes possible to extract shadow-affected pixels, generate a reliable river mask, and subsequently obtain various channel attributes required for numerical model setup.

Furthermore, the implementation of a multivariate change point method allowed for additional simplification of the longitudinal channel data, facilitating the numerical model setup.

The calibration of the numerical model for the Elwha River proved successful in accurately simulating the hydraulics and sediment concentrations across the river channel. This highlights the potential of the method employed in the study to contribute to the understanding of river dynamics and aid in the prediction of sediment transport in similar environments. Notably, it is important to note that the method utilized in this research, which combined NAIP imagery

and the numerical model, not only provided spatial trends regarding the morphological evolution of the channel, but numerical model predictions were also able to provide a quantitative measure of the aggradation-degradation process occurring within the Elwha River. This suggests the potential of the integrated numerical modeling and remote sensing-based approach to obtain a more comprehensive assessment of the morphological patterns through river corridors.

One notable advantage of this study is its applicability beyond the Elwha River system and its specific geographical area. The methodology presented here can be adapted and applied to other river systems, regardless of whether they possess abundant or limited data. Therefore, the findings of this research hold promise for studying and managing rivers in diverse settings, making important contributions to the field of river geomorphology and sediment dynamics.

3.7 References:

Alber, A., & Piégay, H. (2011). Spatial disaggregation and aggregation procedures for characterizing fluvial features at the network-scale: Application to the Rhône basin (France). *Geomorphology*, *125*(3), 343–360.

Anderson, C. W., Wright, S. A., Schenk, L. N., Skalak, K., Curtis, J. A., East, A. E., & Benthem, A. (2019). Refining the Baseline Sediment Budget for the Klamath River, California. *SEDHYD 2019 Conference*, *5*.

Anderson, S. W., Keith, M. K., Magirl, C. S., Wallick, J. R., Mastin, M. C., & Foreman, J. R. (2017). *Geomorphic response of the North Fork Stillaguamish River to the State Route 530 landslide near Oso, Washington*. US Geological Survey.

Ashida, K., & Michiue, M. (1972). Study on hydraulic resistance and bed-load transport rate in alluvial streams. *Proceedings of the Japan Society of Civil Engineers*, *1972*(206), 59–69.

Benda, L. E. E., Poff, N. L., Miller, D., Dunne, T., Reeves, G., Pess, G., & Pollock, M. (2004). The network dynamics hypothesis: how channel networks structure riverine habitats. *BioScience*, *54*(5), 413–427.

Blumm, M. C., & Illowsky, D. (2022). The World's Largest Dam Removal Project: The Klamath River Dams. *Available at SSRN 4061159*.

Borselli, L., Cassi, P., & Torri, D. (2008). Prolegomena to sediment and flow connectivity in the landscape: a GIS and field numerical assessment. *Catena*, *75*(3), 268–277.

Brando, V. E., & Dekker, A. G. (2003). Satellite hyperspectral remote sensing for estimating estuarine and coastal water quality. *IEEE Transactions on Geoscience and Remote Sensing*, *41*(6), 1378–1387.

Breiman, L. (2001). Random forests. *Machine Learning*, *45*, 5–32.

Brice, J. C. (1964). *Channel patterns and terraces of the Loup Rivers in Nebraska*. US Government Printing Office.

Bright, C. E., & Mager, S. M. (2020). A national-scale study of spatial variability in the relationship between turbidity and suspended sediment concentration and sediment properties. *River Research and Applications*, *36*(8), 1449–1459.

Bright, C., Mager, S., & Horton, S. (2020). Response of nephelometric turbidity to hydrodynamic particle size of fine suspended sediment. *International Journal of Sediment Research*, *35*(5), 444–454.

Castro-Bolinaga, C. F., Diplas, P., & Bodnar, R. J. (2020). Modeling Hydro-Morphodynamic Processes During the Propagation of Fluvial Sediment Pulses: A Physics-Based Framework. *Journal of Geophysical Research: Earth Surface*, *125*(12), e2020JF005722.

Cavalli, M., Trevisani, S., Comiti, F., & Marchi, L. (2013). Geomorphometric assessment of spatial sediment connectivity in small Alpine catchments. *Geomorphology*, *188*, 31–41.

Chen, Z., Hu, C., & Muller-Karger, F. (2007). Monitoring turbidity in Tampa Bay using MODIS/Aqua 250-m imagery. *Remote Sensing of Environment*, *109*(2), 207–220.

Chib, S., & Greenberg, E. (1995). Understanding the metropolis-hastings algorithm. *The American Statistician*, *49*(4), 327–335.

Choubin, B., Solaimani, K., Rezanezhad, F., Roshan, M. H., Malekian, A., & Shamshirband, S. (2019). Streamflow regionalization using a similarity approach in ungauged basins: Application of the geo-environmental signatures in the Karkheh River Basin, Iran. *Catena*, *182*, 104128.

Cowan, W. L. (1956). Estimating hydraulic roughness coefficients. *Agricultural Engineering*, *37*(7), 473–475.

Crema, S., & Cavalli, M. (2018). SedInConnect: a stand-alone, free and open source tool for the assessment of sediment connectivity. *Computers & Geosciences*, *111*, 39–45.

Cui, Y., Dusterhoff, S. R., Wooster, J. K., & Downs, P. W. (2011). Practical considerations for modeling sediment transport dynamics in rivers. *Stream Restoration in Dynamic Fluvial Systems: Scientific Approaches, Analyses, and Tools"(Edited by Simon, A., Bennett, SJ, Castro, JM) American Geophysical Union, Washington DC*, 503–527.

Cui, Y., Parker, G., Braudrick, C., Dietrich, W. E., & Cluer, B. (2006). Dam removal express assessment models (DREAM). Part 1: model development and validation. *Journal of Hydraulic Research*, *44*(3), 291–307.

Cui, Y., & Wilcox, A. (2008). Development and application of numerical models of sediment transport associated with dam removal. *Chapter*, *23*, 995–1020.

D. N. Moriasi, J. G. Arnold, M. W. Van Liew, R. L. Bingner, R. D. Harmel, & T. L. Veith. (2007). Model Evaluation Guidelines for Systematic Quantification of Accuracy in Watershed Simulations. *Transactions of the ASABE*, *50*(3), 885–900. https://doi.org/10.13031/2013.23153

Davies, R. B. (2002). Hypothesis testing when a nuisance parameter is present only under the

alternative: linear model case. *Biometrika*, 484–489.

Dekker, A. G., & Peters, S. W. M. (1993). The use of the Thematic Mapper for the analysis of eutrophic lakes: a case study in the Netherlands. *International Journal of Remote Sensing*, *14*(5), 799–821.

Dethier, E. N., Renshaw, C. E., & Magilligan, F. J. (2020). Toward Improved Accuracy of Remote Sensing Approaches for Quantifying Suspended Sediment: Implications for Suspended-Sediment Monitoring. *Journal of Geophysical Research: Earth Surface*, *125*(7), e2019JF005033.

Ding, L., Chen, L., Ding, C., & Tao, J. (2019). Global trends in dam removal and related research: A systematic review based on associated datasets and bibliometric analysis. *Chinese Geographical Science*, *29*, 1–12.

dos Santos, A. L. M. R., Martinez, J. M., Filizola Jr, N. P., Armijos, E., & Alves, L. G. S. (2018). Purus River suspended sediment variability and contributions to the Amazon River from satellite data (2000–2015). *Comptes Rendus Geoscience*, *350*(1–2), 13–19.

Duda, J. J., & Bellmore, J. R. (2022). Dam Removal and River Restoration. *Encyclopedia of Inland Waters, Eds K. Tockner and T. Mehner (Oxford, UK: Elsevier Ltd). Doi*, *10*.

Duda, J. J., Freilich, J. E., & Schreiner, E. G. (2008). Baseline studies in the Elwha River ecosystem prior to dam removal: introduction to the special issue. *Northwest Science*, *82*(sp1), 1–12.

Duda, J. J., Warrick, J. A., & Magirl, C. S. (2011). Coastal and lower Elwha River, Washington, prior to dam removal—history, status, and defining characteristics. *Coastal Habitats of the Elwha River, Washington—Biological and Physical Patterns and Processes Prior to Dam Removal. US Geological Survey Scientific Investigations Report*, *5120*, 1–26.

East, A. E., Pess, G. R., Bountry, J. A., Magirl, C. S., Ritchie, A. C., Logan, J. B., Randle, T. J., Mastin, M. C., Minear, J. T., & Duda, J. J. (2015). Large-scale dam removal on the Elwha River, Washington, USA: River channel and floodplain geomorphic change. *Geomorphology*, *228*, 765–786.

Engelund, F., & Fredsøe, J. (1976). A sediment transport model for straight alluvial channels. *Hydrology Research*, *7*(5), 293–306.

Espinoza-Villar, R., Martinez, J.-M., Armijos, E., Espinoza, J.-C., Filizola, N., Dos Santos, A., Willems, B., Fraizy, P., Santini, W., & Vauchel, P. (2018). Spatio-temporal monitoring of

suspended sediments in the Solimões River (2000–2014). *Comptes Rendus Geoscience*, *350*(1–2), 4–12.

Ferguson, R. I., Church, M., Rennie, C. D., & Venditti, J. G. (2015). Reconstructing a sediment pulse: Modeling the effect of placer mining on Fraser River, Canada. *Journal of Geophysical Research: Earth Surface*, *120*(7), 1436–1454.

Feyisa, G. L., Meilby, H., Fensholt, R., & Proud, S. R. (2014). Automated Water Extraction Index: A new technique for surface water mapping using Landsat imagery. *Remote Sensing of Environment*, *140*, 23–35.

Foley, M. M., Bellmore, J. R., O'Connor, J. E., Duda, J. J., East, A. E., Grant, G. E., Anderson, C. W., Bountry, J. A., Collins, M. J., & Connolly, P. J. (2017). Dam removal: Listening in. *Water Resources Research*, *53*(7), 5229–5246.

Foley, M. M., Duda, J. J., Beirne, M. M., Paradis, R., Ritchie, A., & Warrick, J. A. (2015). Rapid water quality change in the E lwha R iver estuary complex during dam removal. *Limnology and Oceanography*, *60*(5), 1719–1732.

Fox, C. A., Reo, N. J., Fessell, B., & Dituri, F. (2022). Native American tribes and dam removal: restoring the Ottaway, Penobscot and Elwha Rivers. *Water Alternatives*, *15*(1), 31–55.

Francke, T., López-Tarazón, J. A., & Schröder, B. (2008). Estimation of suspended sediment concentration and yield using linear models, random forests and quantile regression forests. *Hydrological Processes: An International Journal*, *22*(25), 4892–4904.

Gao, B.-C. (1996). NDWI—A normalized difference water index for remote sensing of vegetation liquid water from space. *Remote Sensing of Environment*, *58*(3), 257–266.

Gao, P. (2008). Understanding watershed suspended sediment transport. *Progress in Physical Geography*, *32*(3), 243–263.

Gelfenbaum, G., Stevens, A. W., Miller, I., Warrick, J. A., Ogston, A. S., & Eidam, E. (2015). Large-scale dam removal on the Elwha River, Washington, USA: Coastal geomorphic change. *Geomorphology*, *246*, 649–668.

Gesch, D., Oimoen, M., Greenlee, S., Nelson, C., Steuck, M., & Tyler, D. (2002). The national elevation dataset. *Photogrammetric Engineering and Remote Sensing*, *68*(1), 5–32.

Gitelson, A. A., Dall'Olmo, G., Moses, W., Rundquist, D. C., Barrow, T., Fisher, T. R., Gurlin, D., & Holz, J. (2008). A simple semi-analytical model for remote estimation of chlorophyll-a in turbid waters: Validation. *Remote Sensing of Environment*, *112*(9), 3582–3593.

Graf, W. L. (1999). Dam nation: A geographic census of American dams and their large-scale hydrologic impacts. *Water Resources Research*, *35*(4), 1305–1311.

Gran, K. B., & Czuba, J. A. (2017). Sediment pulse evolution and the role of network structure. *Geomorphology*, *277*, 17–30. https://doi.org/https://doi.org/10.1016/j.geomorph.2015.12.015

Guarino, J. (2013). Tribal advocacy and the art of dam removal: The Lower Elwha Klallam and the Elwha Dams. *American Indian Law Journal*, *2*(1), 114–145.

Guertault, L., Camenen, B., Paquier, A., & Peteuil, C. (2018). A one-dimensional process-based approach to study reservoir sediment dynamics during management operations. *Earth Surface Processes and Landforms*, *43*(2), 373–386.

Guertault, L., Camenen, B., Peteuil, C., Paquier, A., & Faure, J. B. (2016). One-dimensional modeling of suspended sediment dynamics in dam reservoirs. *Journal of Hydraulic Engineering*, *142*(10), 4016033.

Guo, Y., Zhang, Y., Zhang, L., & Wang, Z. (2021). Regionalization of hydrological modeling for predicting streamflow in ungauged catchments: A comprehensive review. *Wiley Interdisciplinary Reviews: Water*, *8*(1), e1487.

Gupta, N., Atkinson, P. M., & Carling, P. A. (2013). Decadal length changes in the fluvial planform of the River Ganga: bringing a mega-river to life with Landsat archives. *Remote Sensing Letters*, *4*(1), 1–9.

Haefner, J. W. (2005). *Modeling biological systems:: principles and applications*. Springer Science & Business Media.

Hastings, W. K. (1970). *Monte Carlo sampling methods using Markov chains and their applications*.

Hearst, M. A., Dumais, S. T., Osuna, E., Platt, J., & Scholkopf, B. (1998). Support vector machines. *IEEE Intelligent Systems and Their Applications*, *13*(4), 18–28.

Hellweger, F. L., Schlosser, P., Lall, U., & Weissel, J. K. (2004). Use of satellite imagery for water quality studies in New York Harbor. *Estuarine, Coastal and Shelf Science*, *61*(3), 437–448.

Helsel, D. R., & Hirsch, R. M. (2002). Statistical methods in water resources. Hydrologic Analysis and Interpretation. *US Geological Survey Techniques of Water-Resources Investigations*, *510*.

Hilbert-Wolf, H. L., & Gerlak, A. K. (2022). The evolution of the modern dam conflict on the Snake River, USA. *Water International*, *47*(8), 1349–1369.

Hilldale, R. C., Carpenter, W. O., Goodwiller, B., Chambers, J. P., & Randle, T. J. (2015). Installation of impact plates to continuously measure bed load: Elwha River, Washington, USA. *Journal of Hydraulic Engineering*, *141*(3), 6014023.

Holliday, C. P., Rasmussen, T. C., & Miller, W. P. (2003). *Establishing the relationship between turbidity and total suspended sediment concentration*.

Hommes, L. (2022). The Ageing of Infrastructure and Ideologies: Contestations Around Dam Removal in Spain. *Water Alternatives*, *15*(3), 592–613.

Hsu, N.-S., & Huang, C.-J. (2017). Estimation of flow duration curve at ungauged locations in Taiwan. *Journal of Hydrologic Engineering*, *22*(8), 5017009.

Ibraheem, N. A., Hasan, M. M., Khan, R. Z., & Mishra, P. K. (2012). Understanding color models: a review. *ARPN Journal of Science and Technology*, *2*(3), 265–275.

Isikdogan, F., Bovik, A., & Passalacqua, P. (2017). RivaMap: An automated river analysis and mapping engine. *Remote Sensing of Environment*, *202*, 88–97.

Iverson, R. M. (2015). Scaling and design of landslide and debris-flow experiments. *Geomorphology*, *244*, 9–20.

Iverson, R. M., & George, D. L. (2016). Modelling landslide liquefaction, mobility bifurcation and the dynamics of the 2014 Oso disaster. *Géotechnique*, *66*(3), 175–187.

Iverson, R. M., George, D. L., Allstadt, K., Reid, M. E., Collins, B. D., Vallance, J. W., Schilling, S. P., Godt, J. W., Cannon, C. M., & Magirl, C. S. (2015). Landslide mobility and hazards: implications of the 2014 Oso disaster. *Earth and Planetary Science Letters*, *412*, 197–208.

James, N. A., & Matteson, D. S. (2013). ecp: An R package for nonparametric multiple change point analysis of multivariate data. *ArXiv Preprint ArXiv:1309.3295*.

Jastram, J. D., Zipper, C. E., Zelazny, L. W., & Hyer, K. E. (2010). Increasing precision of turbidity-based suspended sediment concentration and load estimates. *Journal of Environmental Quality*, *39*(4), 1306–1316.

Jensen, J. R. (2009). *Remote sensing of the environment: An earth resource perspective 2/e*. Pearson Education India.

Jiang, L., Westphal Christensen, S., & Bauer-Gottwein, P. (2021). Calibrating 1D hydrodynamic

river models in the absence of cross-section geometry using satellite observations of water surface elevation and river width. *Hydrology and Earth System Sciences*, *25*(12), 6359–6379.

Julien, P. Y. (2018). *River mechanics*. Cambridge University Press.

Kabir, S. M. I., & Ahmari, H. (2020). Evaluating the effect of sediment color on water radiance and suspended sediment concentration using digital imagery. *Journal of Hydrology*, *589*, 125189.

Karrasch, P., Henzen, D., Hunger, S., & Hörold, M. (2015). Determination of water body structures for small rivers using remote sensing data. *Remote Sensing for Agriculture, Ecosystems, and Hydrology XVII*, *9637*, 126–138.

Kellogg, K., Hoffman, P., Standley, S., Shaffer, S., Rosen, P., Edelstein, W., Dunn, C., Baker, C., Barela, P., & Shen, Y. (2020). NASA-ISRO synthetic aperture radar (NISAR) mission. *2020 IEEE Aerospace Conference*, 1–21.

Kendall, M. G. (1948). *Rank correlation methods.*

Khan, N. S., Roy, S. K., Mazumder, M. T. R., Talukdar, S., & Mallick, J. (2022). Assessing the long-term planform dynamics of Ganges–Jamuna confluence with the aid of remote sensing and GIS. *Natural Hazards*, *114*(1), 883–906.

Kirk, J. T. O. (1994). *Light and photosynthesis in aquatic ecosystems*. Cambridge university press.

Konrad, C. P. (2009). Simulating the recovery of suspended sediment transport and river-bed stability in response to dam removal on the Elwha River, Washington. *Ecological Engineering*, *35*(7), 1104–1115.

Lauer, D. T., Morain, S. A., & Salomonson, V. V. (1997). The Landsat program: Its origins, evolution, and impacts. *Photogrammetric Engineering and Remote Sensing*, *63*(7), 831–838.

Leisher, C., Hess, S., Dempsey, K., Payne Wynne, M. L., & Royte, J. (2022). Measuring the social changes from river restoration and dam removal. *Restoration Ecology*, *30*(1), e13500.

Leopold, L. B., Wolman, M. G., & Miller, J. P. (1964). Fluvial processes in geomorphology WH Freeman and Co. *San Francisco 522pp*.

Levins, R. (1966). The strategy of model building in population biology. *American Scientist*, *54*(4), 421–431.

Lindell, T., Pierson, D., & Premazzi, G. (1999). *Manual for monitoring European lakes using remote sensing techniques*.

Liu, C., He, B., Li, M., & Ren, X. (2006). Quantitative modeling of suspended sediment in middle Changjiang River from MODIS. *Chinese Geographical Science*, *16*, 79–82.

Long, C. M., & Pavelsky, T. M. (2013). Remote sensing of suspended sediment concentration and hydrologic connectivity in a complex wetland environment. *Remote Sensing of Environment*, *129*, 197–209.

Longbotham, N., Pacifici, F., Malitz, S., Baugh, W., & Camps-Valls, G. (2015). Measuring the spatial and spectral performance of WorldView-3. *Hyperspectral Imaging and Sounding of the Environment*, HW3B-2.

Ma, Y., & Huang, H. Q. (2016). Controls of channel morphology and sediment concentration on flow resistance in a large sand-bed river: A case study of the lower Yellow River. *Geomorphology*, *264*, 132–146.

Magirl, C. S., Hilldale, R. C., Curran, C. A., Duda, J. J., Straub, T. D., Domanski, M., & Foreman, J. R. (2015). Large-scale dam removal on the Elwha River, Washington, USA: Fluvial sediment load. *Geomorphology*, *246*, 669–686.

Mahoney, D. T., Fox, J. F., & Al Aamery, N. (2018). Watershed erosion modeling using the probability of sediment connectivity in a gently rolling system. *Journal of Hydrology*, *561*, 862–883.

Major, J. J. (2004). Posteruption suspended sediment transport at Mount St. Helens: Decadal-scale relationships with landscape adjustments and river discharges. *Journal of Geophysical Research: Earth Surface*, *109*(F1).

Major, J. J., Bertin, D., Pierson, T. C., Amigo, Á., Iroumé, A., Ulloa, H., & Castro, J. (2016). Extraordinary sediment delivery and rapid geomorphic response following the 2008–2009 eruption of Chaitén Volcano, Chile. *Water Resources Research*, *52*(7), 5075–5094.

Major, J. J., Pierson, T. C., Dinehart, R. L., & Costa, J. E. (2000). Sediment yield following severe volcanic disturbance—a two-decade perspective from Mount St. Helens. *Geology*, *28*(9), 819–822.

Mangiarotti, S., Martinez, J.-M., Bonnet, M.-P., Buarque, D. C., Filizola, N., & Mazzega, P. (2013). Discharge and suspended sediment flux estimated along the mainstream of the Amazon and the Madeira Rivers (from in situ and MODIS Satellite Data). *International*

Journal of Applied Earth Observation and Geoinformation, *21*, 341–355.

Mann, H. B. (1945). Non-parametric test against trend. Econometrika 13, 245–259. *Search In*.

Matteson, D. S., & James, N. A. (2014). A nonparametric approach for multiple change point analysis of multivariate data. *Journal of the American Statistical Association*, *109*(505), 334–345.

Mauer, K. W. (2020). Monopoly's winners and losers: Elwha River Dam construction as social closure. *Journal of Environmental Studies and Sciences*, *10*(2), 137–147.

McCulloch, W. S., & Pitts, W. (1943). A logical calculus of the ideas immanent in nervous activity. *The Bulletin of Mathematical Biophysics*, *5*, 115–133.

McElreath, R. (2020). *Statistical rethinking: A Bayesian course with examples in R and Stan*. CRC press.

Metropolis, N., Rosenbluth, A., Rosenbluth, M., Teller, A., & Teller, E. (1953). Introduction of the metropolis algorithm for molecular-dynamics simulation. *J. Chem. Phys*, *21*, 1987.

Milliman, J. D., & Syvitski, J. P. M. (1992). Geomorphic/tectonic control of sediment discharge to the ocean: the importance of small mountainous rivers. *The Journal of Geology*, *100*(5), 525–544.

Mostafa, Y., & Abdelhafiz, A. (2017). Shadow identification in high resolution satellite images in the presence of water regions. *Photogrammetric Engineering & Remote Sensing*, *83*(2), 87–94.

Murphy, B. P., Czuba, J. A., & Belmont, P. (2019). Post-wildfire sediment cascades: A modeling framework linking debris flow generation and network-scale sediment routing. *Earth Surface Processes and Landforms*, *44*(11), 2126–2140.

Nash, J. E., & Sutcliffe, J. V. (1970). River flow forecasting through conceptual models part I—A discussion of principles. *Journal of Hydrology*, *10*(3), 282–290.

Nelson, A., & Dubé, K. (2016). Channel response to an extreme flood and sediment pulse in a mixed bedrock and gravel-bed river. *Earth Surface Processes and Landforms*, *41*(2), 178–195.

Nelson, P. A., Brew, A. K., & Morgan, J. A. (2015). Morphodynamic response of a variable-width channel to changes in sediment supply. *Water Resources Research*, *51*(7), 5717–5734.

O'CALLAGHAN, J., ROBERTSON, P., & Fraser, D. (1982). *Colour image display: it's not that*

simple.

O'Hanley, J. R., Pompeu, P. S., Louzada, M., Zambaldi, L. P., & Kemp, P. S. (2020). Optimizing hydropower dam location and removal in the São Francisco river basin, Brazil to balance hydropower and river biodiversity tradeoffs. *Landscape and Urban Planning*, *195*, 103725.

Olden, J. D., Lawler, J. J., & Poff, N. L. (2008). Machine learning methods without tears: a primer for ecologists. *The Quarterly Review of Biology*, *83*(2), 171–193.

Palu, M. C., & Julien, P. Y. (2019). Modeling the sediment load of the Doce River after the Fundão tailings dam collapse, Brazil. *Journal of Hydraulic Engineering*, *145*(5), 5019002.

Pettitt, A. N. (1979). A non-parametric approach to the change-point problem. *Journal of the Royal Statistical Society: Series C (Applied Statistics)*, *28*(2), 126–135.

Piman, T., & Babel, M. S. (2013). Prediction of rainfall-runoff in an ungauged basin: case study in the mountainous region of Northern Thailand. *Journal of Hydrologic Engineering*, *18*(2), 285–296.

Popović, P., Devauchelle, O., Abramian, A., & Lajeunesse, E. (2021). Sediment load determines the shape of rivers. *Proceedings of the National Academy of Sciences*, *118*(49), e2111215118.

Pugliese, A., Farmer, W. H., Castellarin, A., Archfield, S. A., & Vogel, R. M. (2016). Regional flow duration curves: Geostatistical techniques versus multivariate regression. *Advances in Water Resources*, *96*, 11–22.

Rand, W. M. (1971). Objective criteria for the evaluation of clustering methods. *Journal of the American Statistical Association*, *66*(336), 846–850.

Randle, T. J., Bountry, J. A., Ritchie, A., & Wille, K. (2015). Large-scale dam removal on the Elwha River, Washington, USA: Erosion of reservoir sediment. *Geomorphology*, *246*, 709–728.

Rasmussen, P. P., Gray, J. R., Glysson, G. D., & Ziegler, A. C. (2009). Guidelines and procedures for computing time-series suspended-sediment concentrations and loads from in-stream turbidity-sensor and streamflow data. *US Geological Survey Techniques and Methods, Book*, *3*, 52.

Razavi, T., & Coulibaly, P. (2016). Improving streamflow estimation in ungauged basins using a multi-modelling approach. *Hydrological Sciences Journal*, *61*(15), 2668–2679.

Reneau, S. L., Katzman, D., Kuyumjian, G. A., Lavine, A., & Malmon, D. V. (2007). Sediment delivery after a wildfire. *Geology*, *35*(2), 151–154.

Ritchie, A. C., Warrick, J. A., East, A. E., Magirl, C. S., Stevens, A. W., Bountry, J. A., Randle, T. J., Curran, C. A., Hilldale, R. C., & Duda, J. J. (2018). Morphodynamic evolution following sediment release from the world's largest dam removal. *Scientific Reports*, *8*(1), 13279.

Robert, E., Grippa, M., Kergoat, L., Pinet, S., Gal, L., Cochonneau, G., & Martinez, J.-M. (2016). Monitoring water turbidity and surface suspended sediment concentration of the Bagre Reservoir (Burkina Faso) using MODIS and field reflectance data. *International Journal of Applied Earth Observation and Geoinformation*, *52*, 243–251.

Robertson, P. K., & O'Callaghan, J. F. (1988). The application of perceptual color spaces to the display of remotely sensed imagery. *IEEE Transactions on Geoscience and Remote Sensing*, *26*(1), 49–59.

Rojas, R. (2013). *Neural networks: a systematic introduction*. Springer Science & Business Media.

Roux, C., Alber, A., Bertrand, M., Vaudor, L., & Piégay, H. (2015). "FluvialCorridor": A new ArcGIS toolbox package for multiscale riverscape exploration. *Geomorphology*, *242*, 29–37.

Ryan Bellmore, J., Duda, J. J., Craig, L. S., Greene, S. L., Torgersen, C. E., Collins, M. J., & Vittum, K. (2017). Status and trends of dam removal research in the United States. *WIREs Water* , *4*(2), e1164. https://doi.org/https://doi.org/10.1002/wat2.1164

Rymszewicz, A., O'sullivan, J. J., Bruen, M., Turner, J. N., Lawler, D. M., Conroy, E., & Kelly-Quinn, M. (2017). Measurement differences between turbidity instruments, and their implications for suspended sediment concentration and load calculations: A sensor inter-comparison study. *Journal of Environmental Management*, *199*, 99–108.

Schermerhorn, V. P. (1967). Relations between topography and annual precipitation in western Oregon and Washington. *Water Resources Research*, *3*(3), 707–711.

Schwarz, G. E., & Alexander, R. B. (1995). *State soil geographic (STATSGO) data base for the conterminous United States*.

Sehgal, D., Martinez-Carreras, N., Hissler, C., Bense, V., & Hoitink, T. A. J. F. (2022). *Influence of riverine suspended sediment carbon content and particle size on turbidity*. Copernicus

Meetings.

Sharma, A., Castro-Bolinaga, C., & Nelson, N. (2022). An integrated modeling approach to evaluate the propagation of fluvial sediment pulses following dam removals: A case study from the Elwha River, Washington, USA. *Proceedings of the 39th IAHR World Congress*, 938–945. https://doi.org/10.3850/iahr-39wc252171192022365

Sharma, S., Waldman, J., Afshari, S., & Fekete, B. (2019). Status, trends and significance of American hydropower in the changing energy landscape. *Renewable and Sustainable Energy Reviews*, *101*, 112–122.

Simmons, S. M., Parsons, D. R., Best, J. L., Oberg, K. A., Czuba, J. A., & Keevil, G. M. (2017). An evaluation of the use of a multibeam echo-sounder for observations of suspended sediment. *Applied Acoustics*, *126*, 81–90.

Simmons, S. M., Parsons, D. R., Best, J. L., Orfeo, O., Lane, S. N., Kostaschuk, R., Hardy, R. J., West, G., Malzone, C., & Marcus, J. (2010). Monitoring suspended sediment dynamics using MBES. *Journal of Hydraulic Engineering*, *136*(1), 45–49.

Smith, D., & Davis-Colley, R. (2001). Turbidity suspended sediment and water clarity. *J Am Water Resour Assoc*, *37*, 1085–1101.

Smith, T., Marshall, L., & Sharma, A. (2014). Predicting hydrologic response through a hierarchical catchment knowledgebase: A Bayes empirical Bayes approach. *Water Resources Research*, *50*(2), 1189–1204.

Song, K., Wang, Z., Blackwell, J., Zhang, B., Li, F., Zhang, Y., & Jiang, G. (2011). Water quality monitoring using Landsat Themate Mapper data with empirical algorithms in Chagan Lake, China. *Journal of Applied Remote Sensing*, *5*(1), 53506.

Sousa, J., García-Sánchez, C., & Gorlé, C. (2018). Improving urban flow predictions through data assimilation. *Building and Environment*, *132*, 282–290.

Sousa, J., & Gorlé, C. (2019). Computational urban flow predictions with Bayesian inference: Validation with field data. *Building and Environment*, *154*, 13–22.

Steinschneider, S., Yang, Y.-C. E., & Brown, C. (2015). Combining regression and spatial proximity for catchment model regionalization: a comparative study. *Hydrological Sciences Journal*, *60*(6), 1026–1043.

Strick, R. J. P., Ashworth, P. J., Sambrook Smith, G. H., Nicholas, A. P., Best, J. L., Lane, S. N., Parsons, D. R., Simpson, C. J., Unsworth, C. A., & Dale, J. (2019). Quantification of

bedform dynamics and bedload sediment flux in sandy braided rivers from airborne and satellite imagery. *Earth Surface Processes and Landforms*, *44*(4), 953–972.

Swain, J. B., & Patra, K. C. (2017). Streamflow estimation in ungauged catchments using regional flow duration curve: comparative study. *Journal of Hydrologic Engineering*, *22*(7), 4017010.

Syvitski, J., Ángel, J. R., Saito, Y., Overeem, I., Vörösmarty, C. J., Wang, H., & Olago, D. (2022). Earth's sediment cycle during the Anthropocene. *Nature Reviews Earth & Environment*, *3*(3), 179–196.

Syvitski, J. P. M., & Kettner, A. (2011). Sediment flux and the Anthropocene. *Philosophical Transactions of the Royal Society A: Mathematical, Physical and Engineering Sciences*, *369*(1938), 957–975.

Syvitski, J. P., Morehead, M. D., Bahr, D. B., & Mulder, T. (2000). Estimating fluvial sediment transport: the rating parameters. *Water Resources Research*, *36*(9), 2747–2760.

Tarolli, P., & Mudd, S. M. (2020). *Remote Sensing of Geomorphology* (Vol. 23). Elsevier.

Tegegne, G., & Kim, Y.-O. (2018). Modelling ungauged catchments using the catchment runoff response similarity. *Journal of Hydrology*, *564*, 452–466.

Umar, M., Rhoads, B. L., & Greenberg, J. A. (2018). Use of multispectral satellite remote sensing to assess mixing of suspended sediment downstream of large river confluences. *Journal of Hydrology*, *556*, 325–338.

Vahedifard, F., Madani, K., AghaKouchak, A., & Thota, S. K. (2021). Are we ready for more dam removals in the United States? *Environmental Research: Infrastructure and Sustainability*, *1*(1), 13001.

Van Liew, M. W., & Mittelstet, A. R. (2018). *Comparison of three regionalization techniques for predicting streamflow in ungaged watersheds in Nebraska, USA using SWAT model*.

Vercruysse, K., Grabowski, R. C., & Rickson, R. J. (2017). Suspended sediment transport dynamics in rivers: Multi-scale drivers of temporal variation. *Earth-Science Reviews*, *166*, 38–52.

Vermote, E., Justice, C., Claverie, M., & Franch, B. (2016). Preliminary analysis of the performance of the Landsat 8/OLI land surface reflectance product. *Remote Sensing of Environment*, *185*, 46–56.

Vogel, R. M., & Fennessey, N. M. (1995). Flow duration curves II: A review of applications in

water resources planning 1. *JAWRA Journal of the American Water Resources Association*, *31*(6), 1029–1039.

Wang, J.-J., & Lu, X. X. (2010). Estimation of suspended sediment concentrations using Terra MODIS: An example from the Lower Yangtze River, China. *Science of the Total Environment*, *408*(5), 1131–1138.

Wang, J., Lu, X. X., Liew, S. C., & Zhou, Y. (2009). Retrieval of suspended sediment concentrations in large turbid rivers using Landsat ETM+: an example from the Yangtze River, China. *Earth Surface Processes and Landforms*, *34*(8), 1082–1092.

Warrick, J. A., Bountry, J. A., East, A. E., Magirl, C. S., Randle, T. J., Gelfenbaum, G., Ritchie, A. C., Pess, G. R., Leung, V., & Duda, J. J. (2015). Large-scale dam removal on the Elwha River, Washington, USA: Source-to-sink sediment budget and synthesis. *Geomorphology*, *246*, 729–750.

Wen, C.-Y., & Chou, C.-M. (2004). Color image models and its applications to document examination. *Forensic Science Journal*, *3*(1), 23–32.

Wilcox, A. C., O'Connor, J. E., & Major, J. J. (2014). Rapid reservoir erosion, hyperconcentrated flow, and downstream deposition triggered by breaching of 38 m tall Condit Dam, White Salmon River, Washington. *Journal of Geophysical Research: Earth Surface*, *119*(6), 1376–1394.

Wohl, E., Bledsoe, B. P., Jacobson, R. B., Poff, N. L., Rathburn, S. L., Walters, D. M., & Wilcox, A. C. (2015). The natural sediment regime in rivers: Broadening the foundation for ecosystem management. *BioScience*, *65*(4), 358–371.

Wohl, E., Brierley, G., Cadol, D., Coulthard, T. J., Covino, T., Fryirs, K. A., Grant, G., Hilton, R. G., Lane, S. N., & Magilligan, F. J. (2019). Connectivity as an emergent property of geomorphic systems. *Earth Surface Processes and Landforms*, *44*(1), 4–26.

Xu, H. (2005). A study on information extraction of water body with the modified normalized difference water index (MNDWI). *JOURNAL OF REMOTE SENSING-BEIJING-*, *9*(5), 595.

Zhang, M., Dong, Q., Cui, T., Xue, C., & Zhang, S. (2014). Suspended sediment monitoring and assessment for Yellow River estuary from Landsat TM and ETM+ imagery. *Remote Sensing of Environment*, *146*, 136–147.

Zhang, Y., Chiew, F. H. S., Li, M., & Post, D. (2018). Predicting runoff signatures using

regression and hydrological modeling approaches. *Water Resources Research*, *54*(10), 7859–7878.

4 INVERSE MODELING THE UPSTREAM SUPPLY TIME SERIES FOR SEDIMENT PULSES GENERATED AFTER DAM REMOVALS UTILIZING NUMERICAL MODELING AND REMOTE SENSING

4.1 Abstract:

In recent decades, dam removal has gained importance as a river restoration practice owing to the associated ecological and benefits, and a rapidly aging infrastructure. However, lack of monitoring data on a river's response to the sediment pulse created as a result of dam removal leads to subjectivity regarding its pros and cons amongst the stakeholders involved in the dam removal movement, and the general public. This study aimed at developing a modeling approach to reconstruct fluvial sediment pulses spatiotemporally after dam removals, using numerical modeling, and remote sensing. A critical assessment of the developed approach for the Elwha River showed that post two dam removals, the annual upstream sediment supply inversely modeled using the Landsat based Suspended Sediment Concentration data varied from 194 mg/l (7.32e-05 m^3/m^3), to 97 mg/l (3.67e-05 m^3/m^3) through 2012 to 2017. The efficiency of the method was contingent upon the availability of cloud free Landsat data, upstream flow rate, and on the proposed parameter range based on the Landsat SSC data. Overall, the numerical simulated SSC through time were a close match to the measured SSC during the initial pulse propagation phase (2012 – 2014). Thereafter, a consistent overprediction was observed during the falling limb of the Measured SSC hydrograph. Despite limitations to data continuity due to overcast conditions, and using a simplified 1D numerical model, the integration of Landsat based SSC, and process based numerical model through an MCMC based inverse modeling framework was successful in estimating the upstream external sediment supply rates through time. The applicability of the methodology is not only limited to dam removals, but can be used for any sediment disturbance scenario for any geographical location.

4.2 Introduction:

Sediment supply plays a vital role in shaping the downstream river response to environmental changes, particularly when fluvial sediment pulses are introduced into the system (Benda et al., 2004; Popović et al., 2021; Vercruysse et al., 2017; Wohl et al., 2015). A sediment pulse refers to a sudden and substantial increase in loose sediment entering a river, resulting from natural events like floods, wildfires, volcanic eruption, and landslides, or human-induced

practices involving dam removals and mining activities. Understanding how the upstream sediment supply affects the downstream river response to such sediment pulses is vital for assessing the geomorphic and ecological consequences of these events.

Fundamentally, a river's response to changes in upstream sediment supply is a complex and dynamic process, influenced by various factors such as the grain size distribution of channel bed, size of supplied sediment, channel geometry, channel hydraulics, and channel morphology (Ritchie et al., 2018). When a sediment pulse occurs, the downstream river response depends on the sediment supply rate, its grain size distribution, and the capacity of the channel to accommodate the increased sediment load. If the upstream sediment supply is greater than the river's transport capacity, the excess sediment accumulates, resulting in channel-bed and floodplain aggradation. This can lead to changes in channel morphology, increased flood risk, and alterations to the river's ecosystem. In contrast, if the sediment supply is lower than the transport capacity, the river may experience degradation, leading to channel incision and loss of sediment storage capacity. Furthermore, the downstream river response to a sediment pulse also depends on the temporal and spatial distribution of sediment inputs (Gran & Czuba, 2017). If the sediment pulse is brief and localized, the downstream river response may be relatively minor, with the system able to absorb and transport the excess sediment without significant long-term effects. However, prolonged or sustained sediment pulses, especially when combined with other factors like vegetation loss or changes in water flow, can have far-reaching consequences on river morphology, sediment transport dynamics, and ecosystem health.

In case of dam removals, understanding the relationship between upstream sediment supply and the downstream river response is crucial. With less than 10% of removals associated with monitored data, it is difficult to make suggestions to the stakeholders, decision makers, and the general public about the pros and cons of the practice for river restoration (Duda & Bellmore, 2022; Bellmore et al., 2017). Modeling can help to reconstruct past sediment pulses and understand their effects on river systems. Process-based numerical models can simulate sediment transport processes, allowing investigation into how sediment pulses affect river morphology, hydrodynamics, and downstream sediment dynamics (Castro-Bolinaga et al., 2020; Cui et al., 2006, 2011; Cui & Wilcox, 2008; Murphy et al., 2019). However, applying a model requires intensive measured input data for construction and calibration. Inclusion of channel attribute based on remote sensing extraction presents a solution to develop simplified models (Jiang et al.,

(2021); Sharma (2023b)). In addition, combining remote sensing data with ground-based measurements and predictive modeling approaches can enhance the reconstruction of sediment pulses in river systems, specifically in data scarce regions.

Remote sensing offers a wide range of data with different levels of spatial and temporal coverage. This has allowed previous researchers to analyze sediment dynamics at scale, and its long-term impacts on river systems (Dethier et al., 2020; Long & Pavelsky, 2013; M. Zhang et al., 2014). Multispectral and hyperspectral sensors utilized by different satellite missions capture data in multiple bands across the electromagnetic spectrum. By analyzing the spectral characteristics of the reflected or emitted light from river water surface, sediment concentrations can be estimated following the occurrence of sediment pulses. When coupling remote sensing estimates with physics-based numerical models, further insights into a river's response and the factors driving it can be obtained. Inverse modeling can be particularly useful to integrate remote sensing estimates and process-based models. Inverse modeling is an approach that can be used to infer or estimate unknown parameters or conditions based on observed data. Previous researchers have suggested using Grid approximation methods, or Monte Carlo Markov Chain (MCMC) methods to sample from the parameter space and achieve the desired objective function and return the optimal parameter value (McElreath, 2020). However, inverse modeling efforts targeting quantification of the upstream sediment supply post sediment pulses has been limited in fluid dynamics, but missing altogether in river mechanics (Sousa et al., 2018; Sousa & Gorlé, 2019). Specifically for dam removals, the restoration efforts in the Elwha River serve as a benchmark example for the dam removal movement as a whole, emphasizing the importance of prioritizing the restoration of rivers and their ecosystems. Additionally, the project's extensive monitored data on sediment transport and morphological changes across the river, well-documented in scientific literature, can be utilized to develop and test a method quantifying the upstream sediment supply (Castro-Bolinaga et al., 2020; East et al., 2015; Foley et al., 2017; Konrad, 2009; Magirl et al., 2015; Warrick et al., 2015). The objectives of the study were to (1) develop a method to optimize a process-based 1D numerical model using Landsat-based Suspended Sediment Concentration (SSC) data and MCMC sampling for a model parameter representing the upstream volumetric sediment supply concentration (Cs) and test it for the Elwha River dam removals, and to (2) reconstruct the sediment pulse using the optimized

numerical model from 2012 to 2017, while analyzing spatial trends in downstream numerical model SSC (C_N) and Landsat based SSC (Landsat SSC).

4.3 Study Area:

The Elwha River dams, comprising the Elwha Dam and the Glines Canyon Dam, were constructed in the early 20th century on the Elwha River in Washington state, USA, to generate hydroelectricity (Guarino, 2013; Mauer, 2020). The construction and subsequent operation for decades significantly disrupted the river's natural ecosystem, causing the decline of various fish species, including the iconic salmon population (Duda et al., 2008, 2011; Guarino, 2013). In recognition of the ecological damage and the importance of restoring the river's natural processes, and the economic limitations pertaining to dam rehabilitation, an act (Elwha River Ecosystem and Fisheries Act) was passed by the congress in 1992 approving removal of both the dams. The removal process, carried out from 2011 to 2014, constituted the largest dam removal project in U.S. history. The removal of the dams had a profound impact on the river's ecosystem, allowing it to flow freely and restore natural sediment transport. Consequently, downstream transport of 10.5 million tons of sediment led to the formation of 32ha delta in the estuary region, providing conducive environment for expansion of the native flora and fauna, particularly salmon populations pos removal, began to recover (East et al., 2015; Gelfenbaum et al., 2015; Magirl et al., 2015; Randle et al., 2015).

A reach on the Elwha, running 2.6 kms was selected for the study (Figure 4.1). It was located downstream of the two dams, and close to USGS 12046260 which was used as a source of measured SSC data. Channel attribute assignment, and its subsequent numerical model calibrated setup by Sharma (2023b) was used for the study to construct the pulse for the evaluation period, from 2012 to 2017. The study area comprised of four distinct segments, each with variable width, slope, length, and manning's roughness provided in Figure 4.1. The construction and calibration process of the numerical model for the study reach can be referred to in the original study.

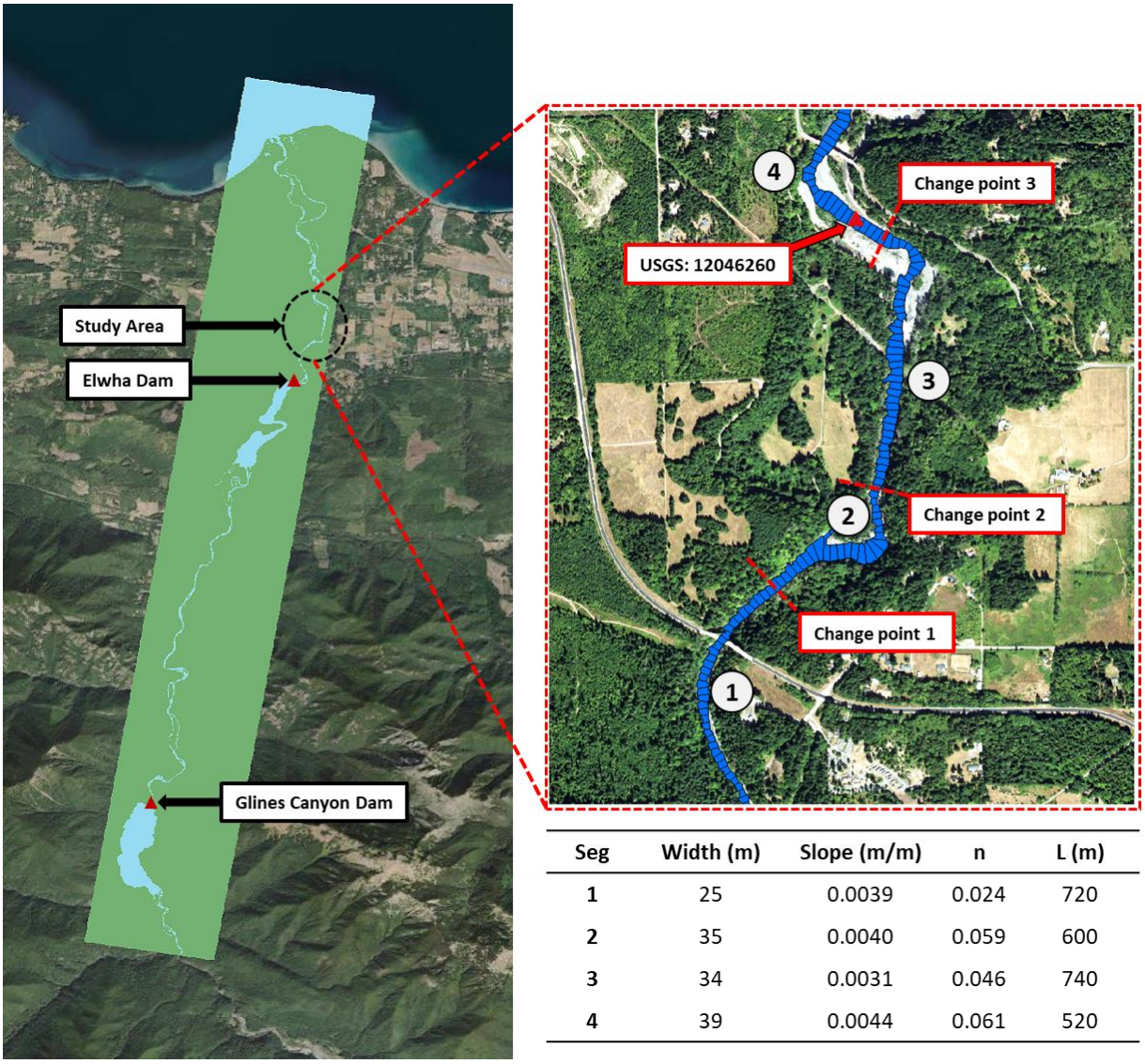

Seg	Width (m)	Slope (m/m)	n	L (m)
1	25	0.0039	0.024	720
2	35	0.0040	0.059	600
3	34	0.0031	0.046	740
4	39	0.0044	0.061	520

Figure 4.1 A sub section of the Elwha located downstream of the two dams was selected for the study (left). A 1D numerical model constructed and calibrated by Sharma (2023b) was used to test the inverse modeling framework. The model used changepoint analysis to simplify channel geometry (Width (m), Slope (m/m), and Length (m)), and calibrate channel bed roughness (n)). The details for each segment have been provided in the table on the bottom right.

4.4 Methodology:

4.4.1 Overview

The methodology used for the study can be divided into four different steps. First, a 1D numerical model successfully constructed, calibrated, and validated using remotely sensed data for the study reach was selected (Sharma, 2023b) (Figure 4.2 left). Second, Landsat 7 and 8

imagery was used to estimate SSC for different water pixels along the study area using a prediction model developed by Sharma (2023a). Third, an inverse method was used to optimize a model parameter Cs, representing the upstream sediment supply suspended sediment concentration throughout the evaluation period. Finally, a time series was created for the upstream sediment supply (Figure 4.2 right) and inferences made on the overall downstream river response. The reconstructed sediment pulse through space and time offered valuable insights into the patterns and dynamics of sediment movement, enhancing our knowledge of sediment-related processes along the study reach. This methodology can be applied in various settings to gain a better understanding of sediment transport and its implications for ecosystem health and management.

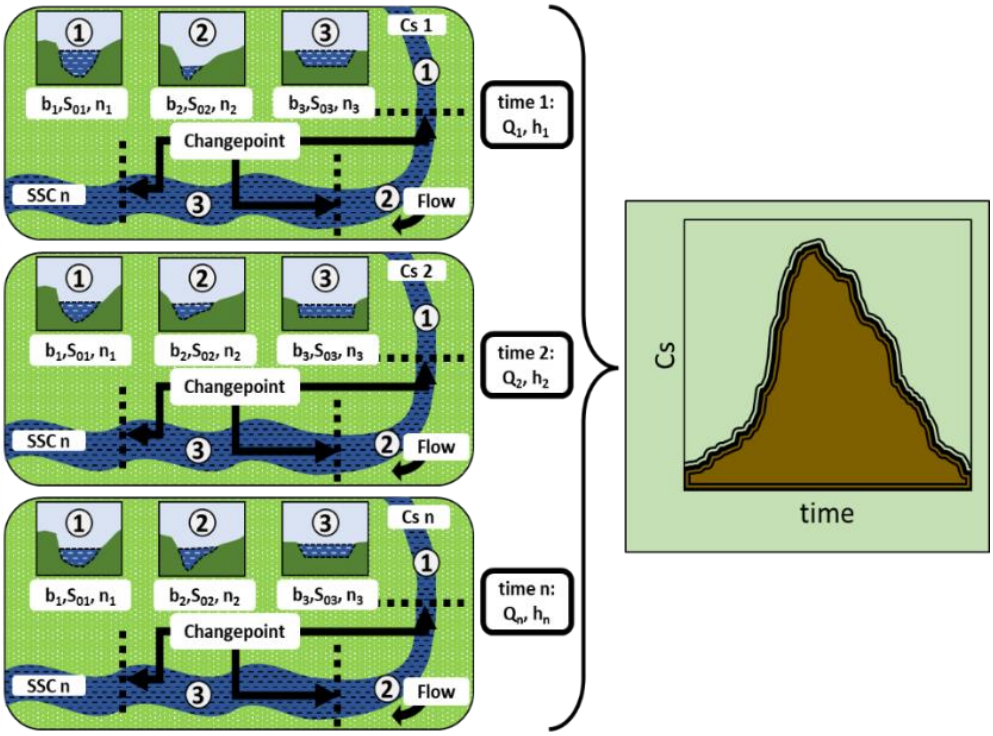

Figure 4.2 Framework developed to optimize the upstream sediment supply concentration (m^3/m^3) for the 1D numerical model for the study area through 2012 to 2017, post dam removals. The resultant Cs time series provided information about the rivers downstream response (Landsat SSC) to availability of upstream sediment.

4.4.2 Measured data:

A combination of discharge data, turbidity data, and SSC data were used throughout the study. Detailed information about the source, units, data quantity, and temporal coverage have been provided in table 4.1. Discharge data for USGS: 12045500 were obtained for the study area coinciding with the Landsat availability during the evaluation period. The data were used to estimate the corresponding flow depth using the stage-discharge curve developed for the Elwha River by Sharma (2023 b). Additional channel attribute information by Sharma (2023b) such as bed roughness, width, bed slope, and reach length were used to develop numerical modeling scenarios through the evaluation period. Next, Landsat 7 and 8 sensors were used to extract cloud free water pixels for the study reach. The resulting surface reflectance along with pixel location was extracted using Google's Earth Engine. Landsat-based turbidity predictions derived from a random forest modeling framework specific to Washington (Sharma, (2023a)) were used as input data for the study. To convert these turbidity values into suspended sediment concentration (SSC), regression coefficients from Sharma, (2023b) were used. In addition, SSC data from Curran et al., (2018) was used as measured data to compare with the downstream numerical model SSC simulations (C_N).

Table 4.1 Different data used for the study included Landsat surface reflectance data based SSC, SSC predictions from Curran et al., (2018), and Measured SSC at USGS: 12046260 from 2012 to 2017.

Source	Units	Data points	Data coverage
Landsat 7	Turbidity	55	2/9/2012 to 12/12/2017
Landsat 8	Turbidity	57	7/1/2013 to 12/11/2017
Curran et al., (2018)	SSC (mg/l)	92	9/5/2011 to 9/30/2016
Sharma (2023 b)	SSC (mg/l)	100	1/1/2013 to 12/31/2017
Discharge (USGS 12045500)	m^3/sec	112	2/9/2012 to 12/12/2017

4.4.3 1D Numerical Model setup:

Castro-Bolinaga et al. (2020) developed a one-dimensional (1-D) adaptive morphodynamic model for water flow, sediment transport, and riverbed evolution in alluvial rivers. The model was formulated based on the St. Venant shallow water equations and the Exner equation for sediment mass conservation. It considered the movement of uniform granular material as both bedload and suspended load. In this study, the model of also considered non-uniform sediment transport conditions, including fractional rates of bedload and suspended load transport, entrainment, deposition, and temporal variation of the riverbed material gradation. Additional details and revised equations can be found in the original publication, which also provides comprehensive information on empirical closure relations and numerical methods. A simplified version of the model, constructed using remote sensing, had a spatial resolution of 20m, with each individual spatial object depicted as a Designated Geomorphic Object (DGO), similar to Alber & Piégay, (2011). The model was further simplified by identifying similar sections having identical channel width, bed slope, and sinuosity using a multivariate changepoint approach (James & Matteson, 2013; Matteson & James, 2014). In total, four segments were identified and were used as the spatial step for calibrating the sediment transport component of the numerical model (Sharma, 2023b).

4.4.4 Inverse Modeling Framework:

The methodology developed in this study involved parameter optimization using the Metropolis-Hastings algorithm for the Markov Chain Monte Carlo (MCMC) sampling method (Chib & Greenberg, 1995; Hastings, 1970; Metropolis et al., 1953) in combination with adaptive scaling. The goal was to identify the optimal value of Cs that minimized the difference between CN and Landsat SSC on a daily time step (Figure 4.3). Root Mean Square Error (RMSE) was selected as the objective function for the optimization process, with the Landsat SSC data used to define the proposed parameter range (Cs). The optimization proceeded through a series of 50 iterations, finalized through trial and error considering solution convergence by MCMC while effective exploration of the input parameter space. The MCMC approach used in the study was a simplification of the probability based MCMC (Appendix 6.1). Herein, discrete RMSE values representing model fit were used as a proposal acceptance criterion, while conventional MCMC compares the ratio of posterior probabilities, which was based on both the likelihood and the prior distribution.

In each iteration, a value for Cs was proposed constrained within the Landsat SSC range for the day. The Numerical Model was run to evaluate RMSE between spatially detailed Landsat SSC and model simulated CN. The exponential difference between the previously accepted RMSE and current proposal RMSE was computed and stored as acceptance likelihood. Next, the acceptance or rejection surrounding each proposal was performed randomly. This process of random acceptance and rejection was critical to effectively explore parameter space. Throughout the optimization process, the best parameter value and its corresponding RMSE were continuously tracked. The proposal standard deviation was adaptively adjusted based on the proposal rate, allowing for efficient exploration of the parameter space. The scaling factor controlled the rate of adjustment, enabling fine-tuning of the proposals and improving the convergence of the optimization process. The significance of this methodology lies in its ability to iteratively search for the parameter value that best aligned with the observed data. The optimization approach provided a practical and effective framework for inverse modeling the upstream sediment supply leading to a measured SSC response downstream. Finally, RMSE associated with the optimized Cs values through the evaluation period were compared with different factors such as discharge, number of DGO's, Landsat SSC data, and Cs values itself for correlation. This was done to identify factors that contributed to optimization error.

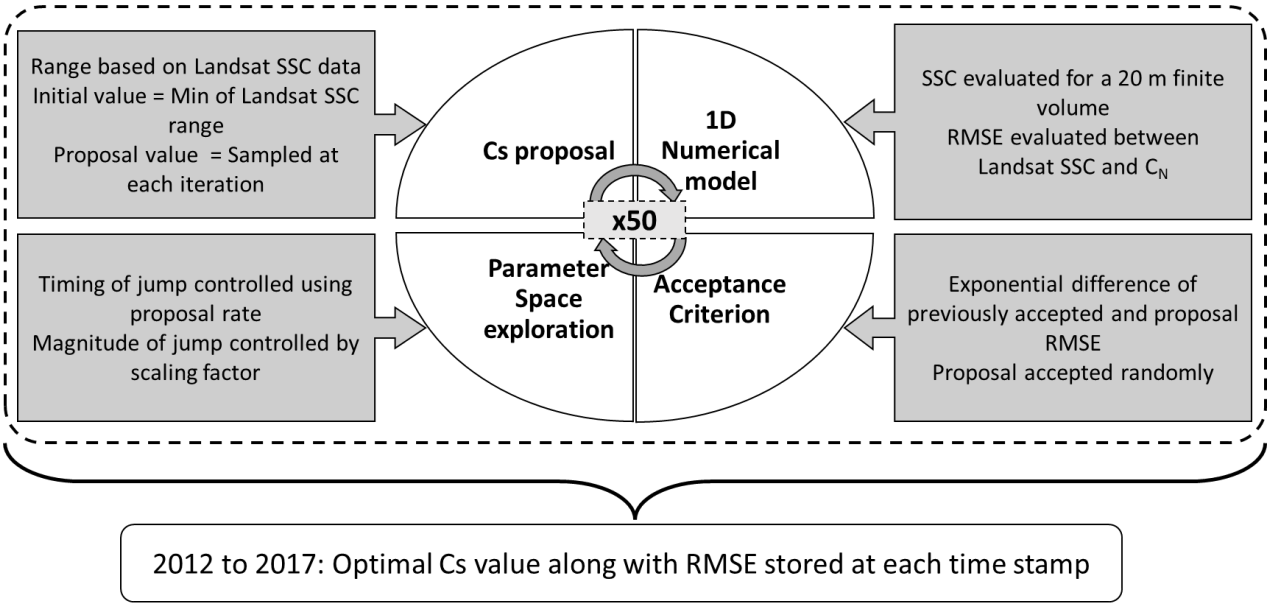

Figure 4.3 Conceptual framework depicting the inverse modeling framework developed in the study to optimize the upstream sediment supply concentration (Cs) per time step.

4.5 Results and Discussion:

4.5.1 Establishing Initial Model Parameters using Landsat-based SSC Range:

The analysis of USGS 12046260 daily discharge data (m^3/sec) coinciding with Landsat 7 and 8 scenes for the Elwha River from 2012 to 2017 revealed a mix of upstream flow conditions, varying from 103 m^3/sec to 6 m^3/sec, with an average of 32 m^3/sec associated with a probability of exceedance of around 75% by (Sharma, (2023b)). For the evaluation period, the majority of Landsat scenes were captured during the months from March to October. The limited availability during other months could be attributed to various factors such as cloud cover and data acquisition schedules (16-day temporal resolution for Landsat). Further, the total number of DGOs per scene also varied considerably across the study period. The number of DGOs per scene ranged from 1 to 64, with an average of around 12 DGO's available with Landsat SSC estimates (Figure 4.4). It was observed that the spatial extraction of water pixels during low flow days and high flow days was inefficient and yielded lesser number of DGO's as compared to flow around mean flow, where maximum spatial coverage in terms of Landsat based SSC estimates was observed. Another factor that impacted data coverage was the choice of satellite sensor. It was observed that number of DGOs available for the Landsat 7 sensor, owing primarily to the scan line error prevalent for the sensor as compared to the more spatially continuous data from Landsat 8. This was specifically observed in 2012, where Landsat 8 data was not available. Overall, Landsat SSC varied from 1.55 E-05 to 0.00018 m^3/m^3. Higher values of SSC were consistently estimated during 2012, 2013, and 2014, and decreased through time. This can be attributed to the large availability of reservoir sediment and subsequent riverine flow conditions during the initial part of the sediment pulse leading to higher transport rates downstream.

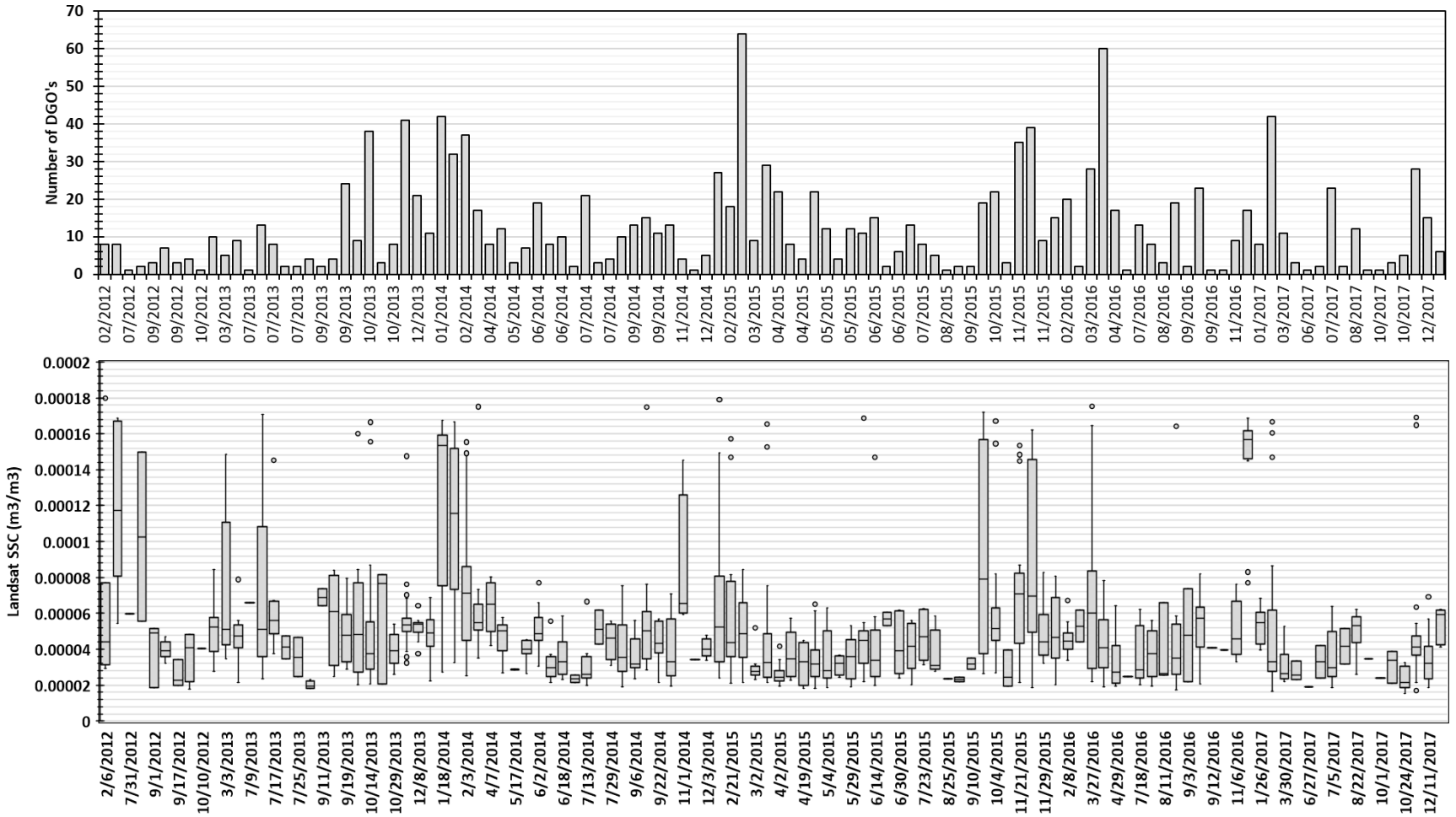

Figure 4.4 Variability in the number of water pixels available per Landsat scene through time shown above using a bar plot along with the spatial variation in the SSC range estimated using machine learning based turbidity predictions from a regional scale reflectance model developed and tested for the state of Washington.

4.5.2 Analyzing post optimization Upstream Sediment Supply Concentration results:

The MCMC optimization process was followed by the examination of trends in the concentration of upstream sediment supply (Cs) (Figure 4.5 a). The optimized value for Cs ranged from 1.67e-05 to 6.27e-04 m^3/m^3 over time, with a median value of approximately 4.34e-05 m^3/m^3. Cs consistently remained higher than the median for 2012, 2013, and 2014 considering total Landsat coverage each year. In contrast, it was below the median for 69% scenes captured during 2017. In addition, years 2014 and 2015 were associated with the highest variability in Cs (Figure 4.5 b). Similar observations were made by East et al., (2015), who attributed the pronounced geomorphic adjustments along the Elwha river during the initial phase of the sediment pulse in 2013 to an increased sediment supply upstream. Konrad (2009) concluded that the propogation of sediment pulses after dam removals was a two stage process, the first stage was the transport limited accompanied by high sediment concentrations even at low flow conditions, while the second stage was the supply limited phase, where only high flow conditions were accompanied by high sediment concentration. A comparison between the optimized value of Cs and the proposal range based on each Landsat scene revealed that, in most cases during 2012 to 2014, optimized Cs approached the upper end of the proposal range, while it was around the mean or lower end of the proposed range during 2015 to 2017.

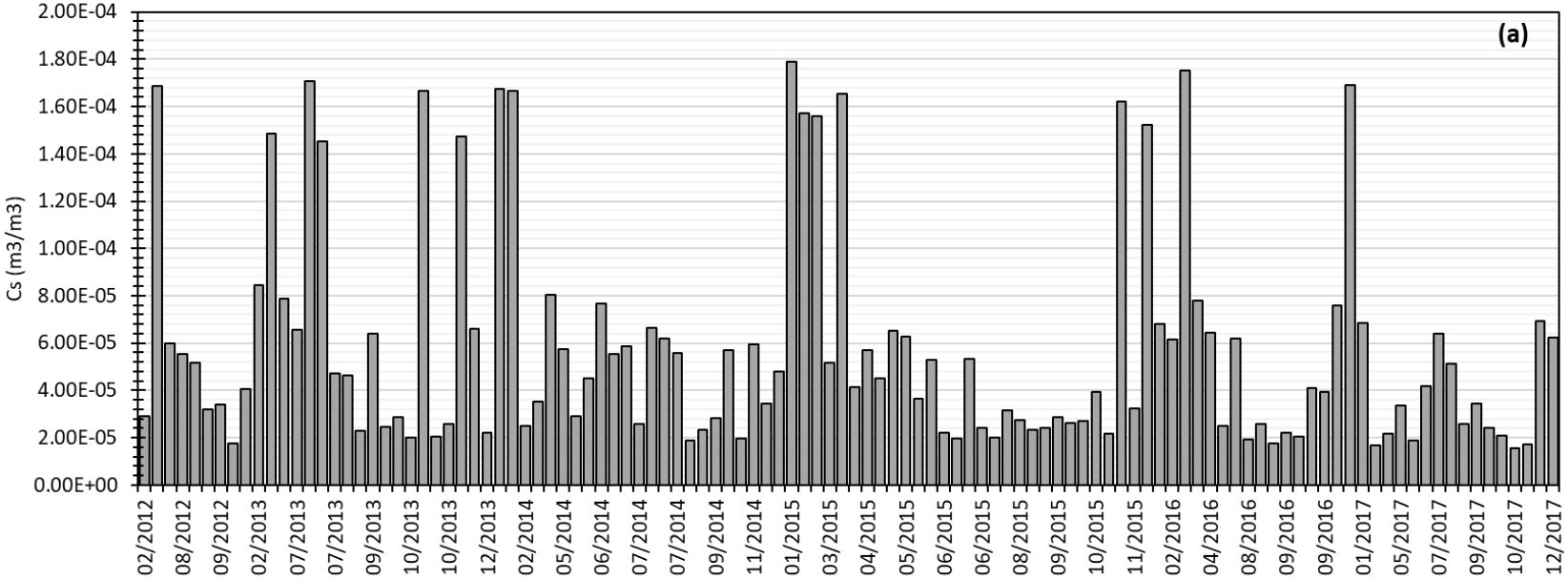

(b) Year	Total Scenes	Cs > Median Cs	High Cs percentage
2012	9	4	44
2013	19	12	63
2014	23	14	61
2015	29	13	45
2016	16	8	50
2017	16	5	31

Figure 4.5 A bar plot (a) showed the variability of the upstream sediment supply concentration (m^3/m^3) through 2012 to 2017 for the Elwha River. Comparing Cs values per year with the overall median value of Cs (4.44e-5 m3/m3) showed higher values for 2013 and 2014, and lower values for 2017 (b).

Next, a correlation matrix showed different factors affecting Cs, and optimization accuracy for the study (Figure 4.6 a). Results showed strong correlation between Cs and Landsat SSC throughout the evaluation period (R^2 = 0.74), which supported the importance of quantifying Cs to understand the downstream river response (Figure 4.6 b). A lower R^2 value (0.21) observed between number of DGO's per scene and Cs showed that data quantity did not explicitly explain trends in C_S through time (Figure 4.6 c). However, it did not overrule the impact of spatial distribution of measured data on Cs, and overall optimization accuracy. Throughout the optimization process, the Root Mean Square Error (RMSE) between the spatially explicit C_N and Landsat SSC ranged from 9.98e-06 to 1.56e-04 m^3/m^3 (Figure 4.6 d). The optimized value for Cs was determined to achieve the lowest RMSE, indicating the best fit between the C_N and Landsat SSC. However, it was crucial to note that MCMC based optimization might lead to errors, as well as the Landsat SSC predictions used as measured data for the study exhibited errors too, particularly when it came to predicting peak low and high measured SSC values (Sharma 2023 (a)). Next, the post-optimization RMSE values were thoroughly examined, with a focus on their relationship with Landsat SSC, flow rate, and the number of DGOs per scene. The findings revealed that the variability in RMSE could be primarily attributed to flow rate, demonstrating a strong correlation with an R-squared value of 0.6 (Figure 4.6 d). As flow rate played a significant role in sediment transport dynamics, it had a direct impact on the accuracy of the model predictions, with higher flow rates resulting in increased RMSE values. In addition, results showed that other factors, such as the grain size distribution of the channel bed, might have a crucial role in shaping the RMSE values observed through time. However, the model construction for this study relied on the grain size data obtained from a sampling conducted by Hilldale et al., (2015). The assumption of a constant grain size distribution throughout the study period might have introduced some discrepancies between the model predictions and the observed data. Given the complexities and limitations associated with the influence of grain size distribution and its temporal variations, it was suggested that future researchers delve into a comprehensive analysis to explore these factors in greater detail. Such investigations would contribute to a deeper understanding of the dynamics of sediment transport and provide valuable insights for improving the accuracy of sediment transport models.

Nonetheless, these findings showcased the potential of combining numerical modeling with satellite imagery to enhance our understanding of sediment transport dynamics in channels.

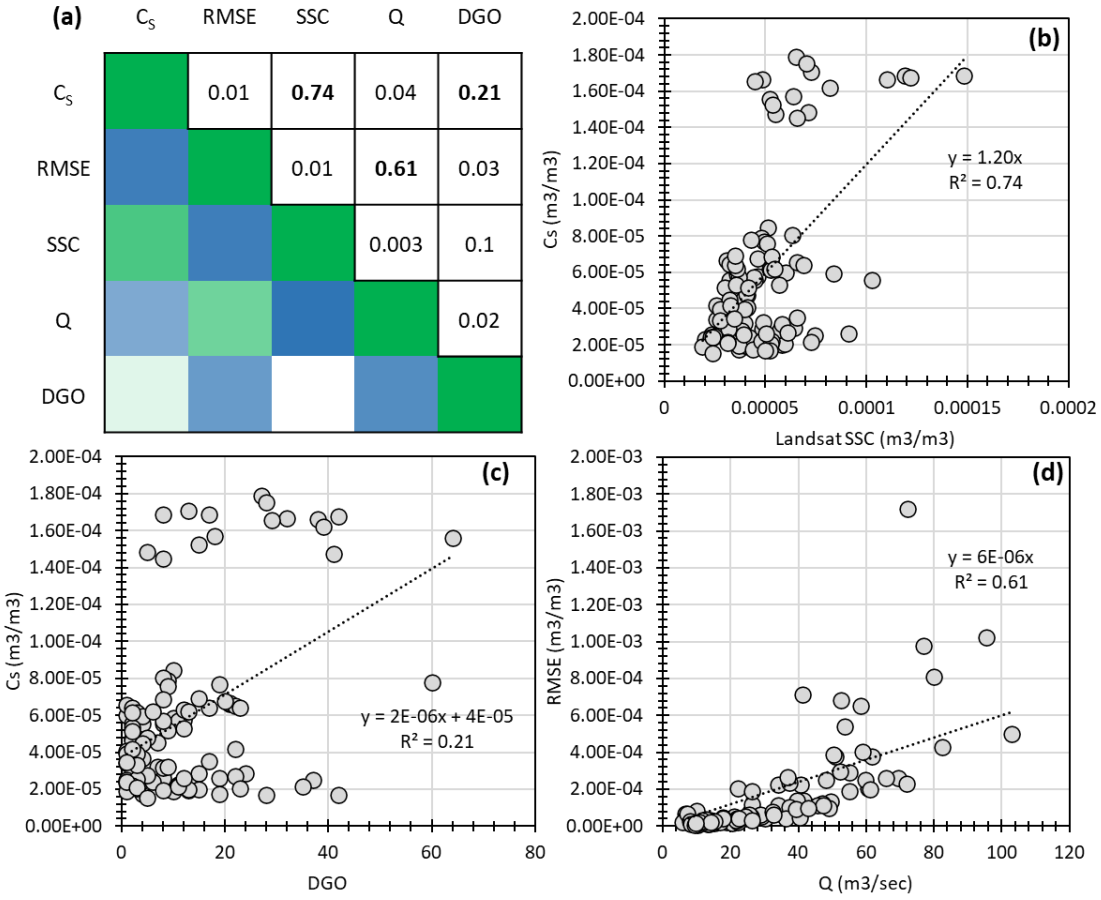

Figure 4.6 A correlation matrix (a) showed Landsat SSC and DGO's per scene to be correlated with Cs. A strong correlation was observed between Cs and Landsat SSC (b), and a weak correlation was observed with the number of DGO's available per scene (c). Finally, optimization accuracy for the MCMC based approach was explored using a regression between flow rate Q (m3/sec) and RMSE (m3/m3) (d).

4.5.3 Spatial Variability in Downstream Suspended Sediment Concentration:

Figure 4.7 illustrated the trends in C_N throughout the evaluation period. On average, Cs was highest in 2013, with a value of 194 mg/l (7.32e-05 m^3/m^3), while it reached a minimum in 2017, with a concentration of 97 mg/l (3.67e-05 m^3/m^3). Subsequently, after 2014, there was a consistent decline in the mean annual Cs over time. Interestingly, the downstream concentration was not significantly influenced by the upstream sediment supply, indicating a decoupling of these two variables. When examining the spatial distribution of Landsat coverage, it was observed that the first segment had minimal coverage. This can be attributed to its relatively narrow average width of approximately 25 meters, compared to wider segments found in other parts of the river, measuring around 34 meters, 35 meters, and 39 meters (Sharma, 2023b). Consequently, the limited Landsat coverage in the first segment resulted in less available data for analysis. Throughout the different years, results showed that Landsat SSC was minimal in segment 1 and gradually increased downstream, particularly during the years 2012, 2013, and 2014. However, after 2014, there was a noticeable declining trend in annual Landsat SSC across all four segments of the river. The upstream end exhibited the highest concentrations, which subsequently decreased with each downstream segment.

In the comparison between the annual mean C_N and the discrete SSC predictions obtained using Landsat, it was observed that the Landsat SSC closely approximated C_N values for the years 2015 and 2013. These two years exhibited minimal RMSE values of 8.51E-05 m^3/m^3 and 8.55E-05 m^3/m^3, respectively. On the other hand, the C_N for 2016 and 2017 were associated with the highest RMSE values of 0.00018 m^3/m^3 and 0.00032 m^3/m^3, respectively. From these results, two inferences were drawn. Firstly, it was inferred that the numerical model simulated a base level SSC, which originated from the channel bed and remained consistent even under low flow conditions. This finding suggests that the channel bed played a significant role in determining the sediment concentration. Secondly, the entire framework of the numerical model assumed a constant value for SSC at each time step, implying that dynamic system properties such as channel geometry and bed grain size were treated as constants throughout the simulation period. Overall, the comparison highlighted the accuracy of the Landsat SSC predictions in capturing the C_N values for specific years. However, it also revealed higher RMSE values for C_N in certain years, indicating discrepancies between the modeled and observed data. Previous research also showed that both riverine and coastal sediment distributions across the Elwha River got finer

after the dams were removed (East et al., 2015; Gelfenbaum et al., 2015; Warrick et al., 2015). Randle et al., (2015) suggested that 40% of the total sediment trapped in the dam reservoirs were supplied to the lower reaches of the Elwha during the first two years post removal.

After 2013, the simulated SSC range exhibited a larger range (max – min) for subsequent years, which may be attributed to the flushing of the otherwise coarser reservoir sediment that was trapped in the middle Elwha region (located upstream of the study area and not included in the model setup) during 2012 to 2013. This flushing phenomenon occurred after 2013, with the sediment subsequently being transported downstream to the study reach by predominantly higher flow events. When comparing the spatial trends of Landsat SSC and the C_N through time, it was found that they generally exhibited similar patterns. This suggested that both the Landsat imagery and the numerical modeling approach were able to capture and represent the overall trends in sediment concentration within the study reach. However, it was important to note that there may still be some differences and discrepancies between the two approaches, as reflected by the wider extent of the C_N as compared to Landsat SSC range. These differences could be influenced by various factors, including the resolution (spatial, temporal, and spectral) and limitations of the Landsat imagery, as well as the assumptions and simplifications made in the numerical model.

Further, the spatial variation in C_N were observed across different segments of the study area (Figure 4.7). C_N was highest in Segment 2, followed by Segment 4, then Segment 3, and finally Segment 1 consistently for the different years. This spatial variation in SSC might be attributed to the interplay of sediment depositional and erosional processes within each segment. Lower C_N values in certain segments can be explained by pronounced sediment deposition. The deposition of sediment reduced the concentration of suspended sediment in the water column. On the other hand, higher C_N values indicated substantial erosion and suspension of sediment, which might be attributed to higher shear stress. Increased erosional forces led to the entrainment and suspension of sediment particles, contributing to higher C_N values. The differences in channel geometry and Manning's roughness among the different segments provided insights into the higher erosional forces observed in certain segments. The width of the channel was found to be greatest in Segment 4, followed by Segment 2, then Segment 3, and finally Segment 1. Similarly, the channel slope was highest in Segment 4, followed by Segment 2, Segment 1, and Segment 3. Additionally, Manning's roughness was found to be highest in Segment 2, followed by Segment

4, Segment 3, and finally Segment 1. The correlation observed between SSC concentration and Manning's roughness suggested that channel shape played a crucial role in the erosion and suspension of channel sediment, influencing the C_N values observed in different segments varying in width, slope, and sinuosity, discussed in detail by previous researchers as well (Konrad, 2009; Ma & Huang, 2016; Nelson et al., 2015).

Figure 4.7 Numerical model simulated SSC range (grey area) with accompanied mean (black) SSC through river length shown for each year (2012 to 2017) (a through f), as compared to spatially discrete yearly Landsat based SSC range (solid point). The mean (blue), max (green), and min (red) upstream sediment concentration per year are also shown.

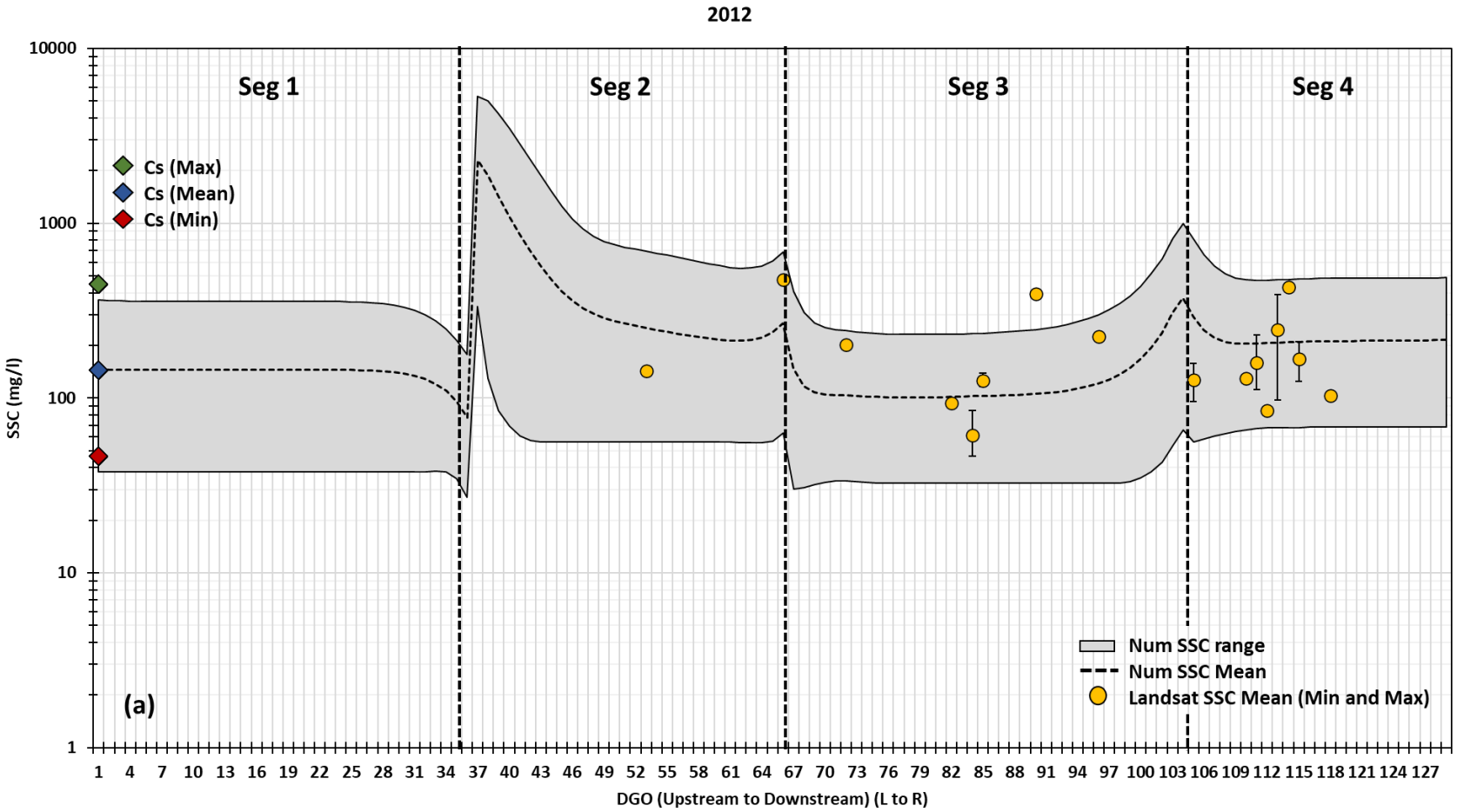
2012
Seg 1
Seg 2
Seg 3
Seg 4
Cs (Max)
Cs (Mean)
Cs (Min)
Num SSC range
Num SSC Mean
Landsat SSC Mean (Min and Max)
(a)
SSC (mg/l)
DGO (Upstream to Downstream) (L to R)

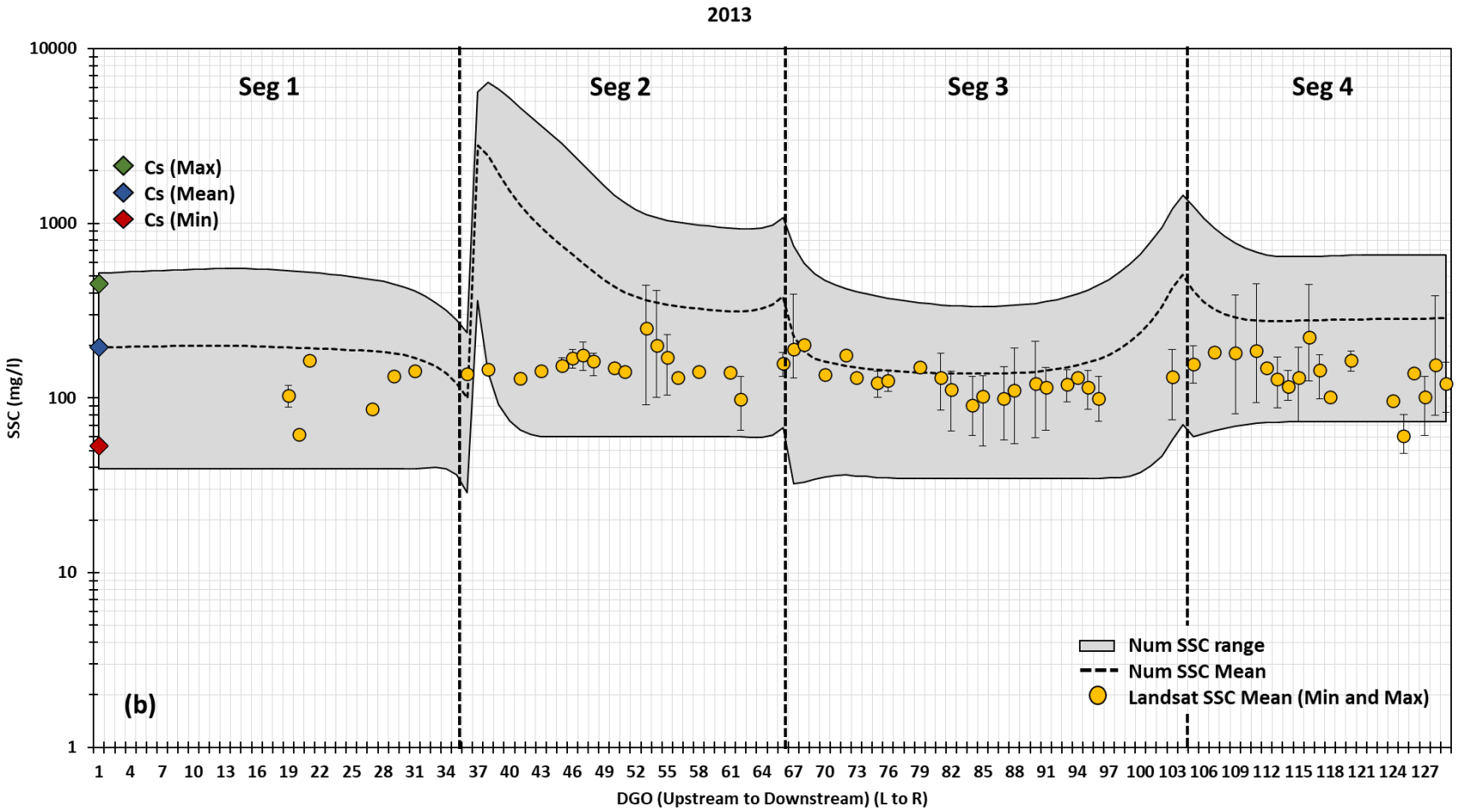
2013
Seg 1
Seg 2
Seg 3
Seg 4
Cs (Max)
Cs (Mean)
Cs (Min)
(b)
Num SSC range
Num SSC Mean
Landsat SSC Mean (Min and Max)
SSC (mg/l)
10000
1000
100
10
1
1 4 7 10 13 16 19 22 25 28 31 34 37 40 43 46 49 52 55 58 61 64 67 70 73 76 79 82 85 88 91 94 97 100 103 106 109 112 115 118 121 124 127
DGO (Upstream to Downstream) (L to R)

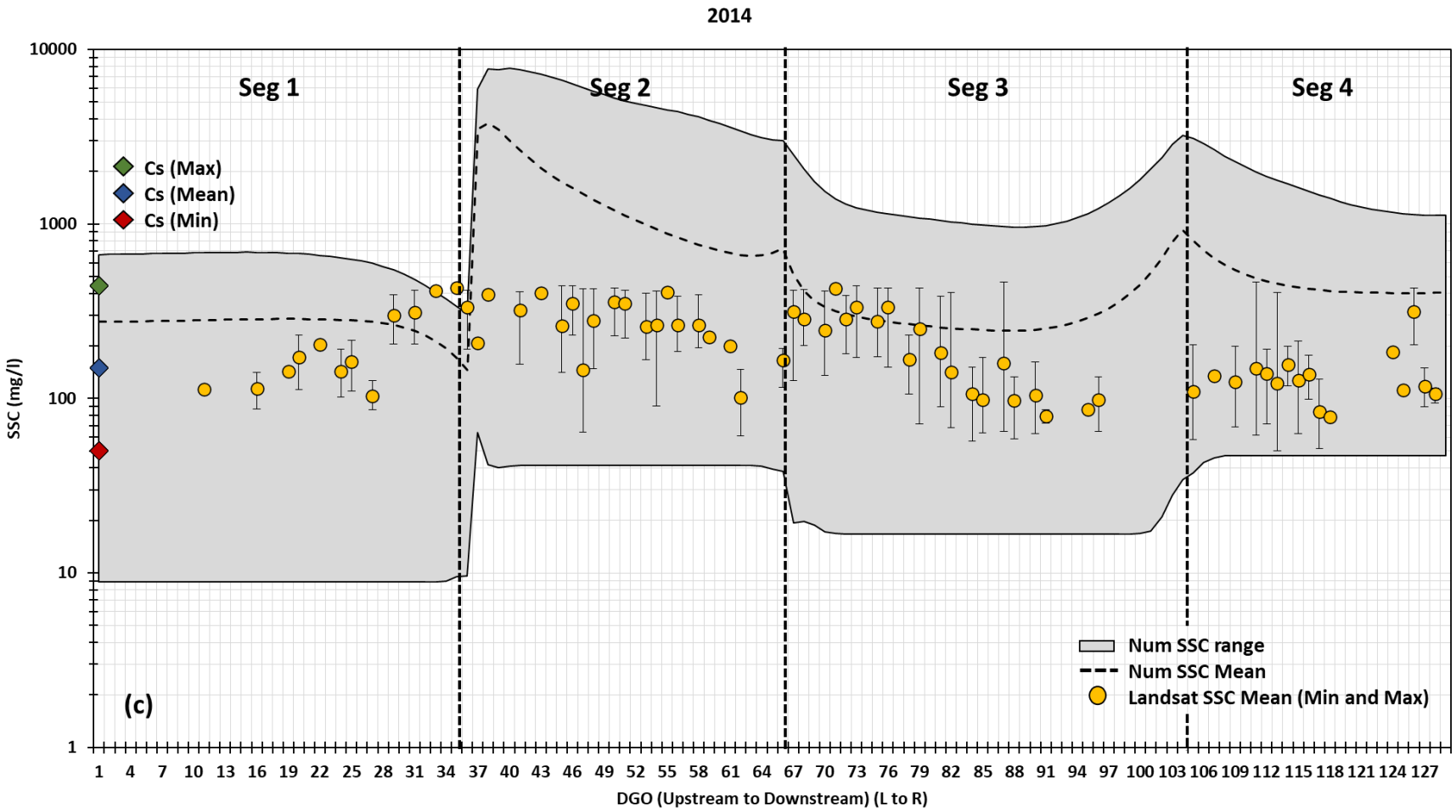
2014
Seg 1
Seg 2
Seg 3
Seg 4
Cs (Max)
Cs (Mean)
Cs (Min)
(c)
Num SSC range
Num SSC Mean
Landsat SSC Mean (Min and Max)
SSC (mg/l)
10000
1000
100
10
1
1 4 7 10 13 16 19 22 25 28 31 34 37 40 43 46 49 52 55 58 61 64 67 70 73 76 79 82 85 88 91 94 97 100 103 106 109 112 115 118 121 124 127
DGO (Upstream to Downstream) (L to R)

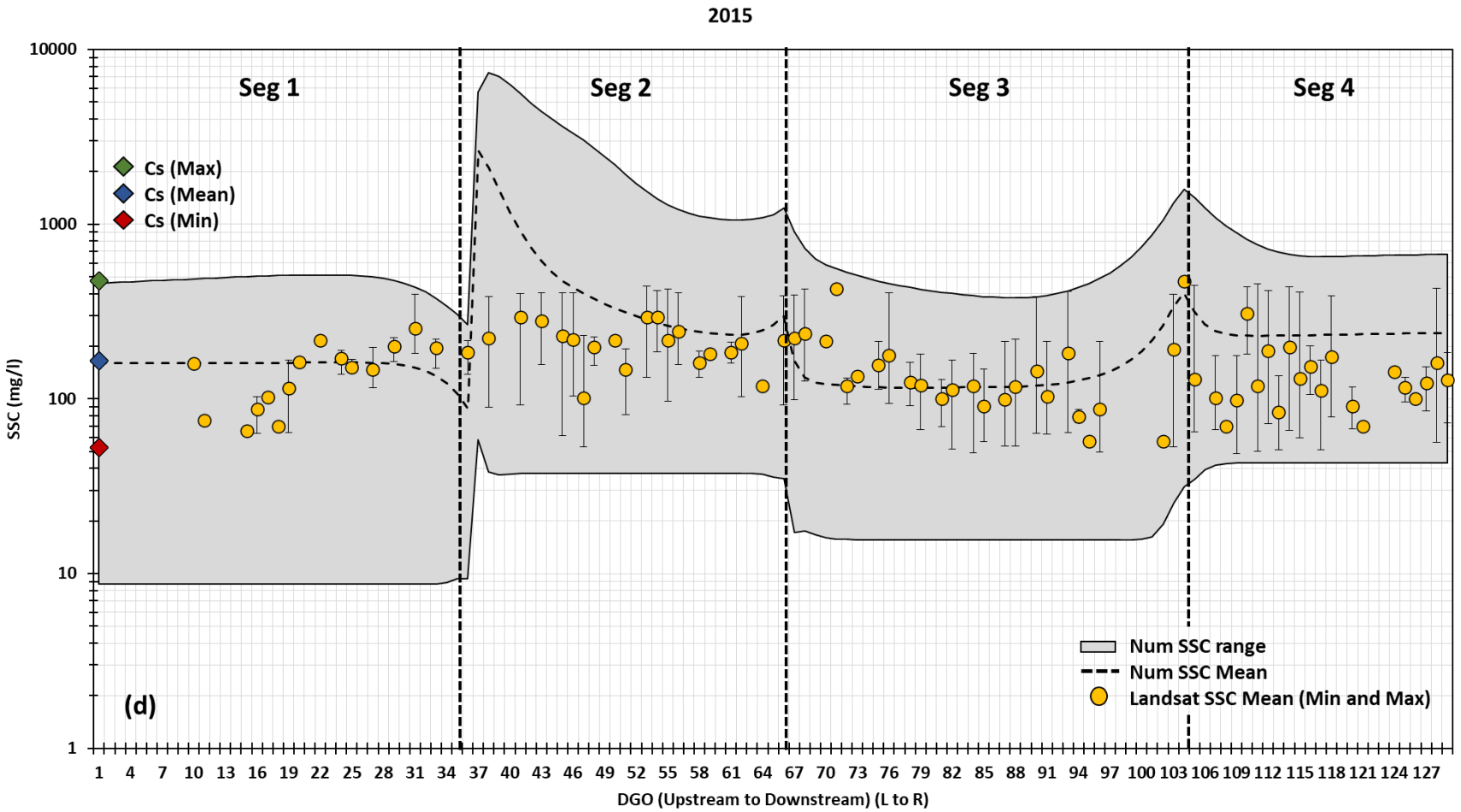
2015
Seg 1
Seg 2
Seg 3
Seg 4
Cs (Max)
Cs (Mean)
Cs (Min)
(d)
Num SSC range
Num SSC Mean
Landsat SSC Mean (Min and Max)
SSC (mg/l)
10000
1000
100
10
1
1 4 7 10 13 16 19 22 25 28 31 34 37 40 43 46 49 52 55 58 61 64 67 70 73 76 79 82 85 88 91 94 97 100 103 106 109 112 115 118 121 124 127
DGO (Upstream to Downstream) (L to R)

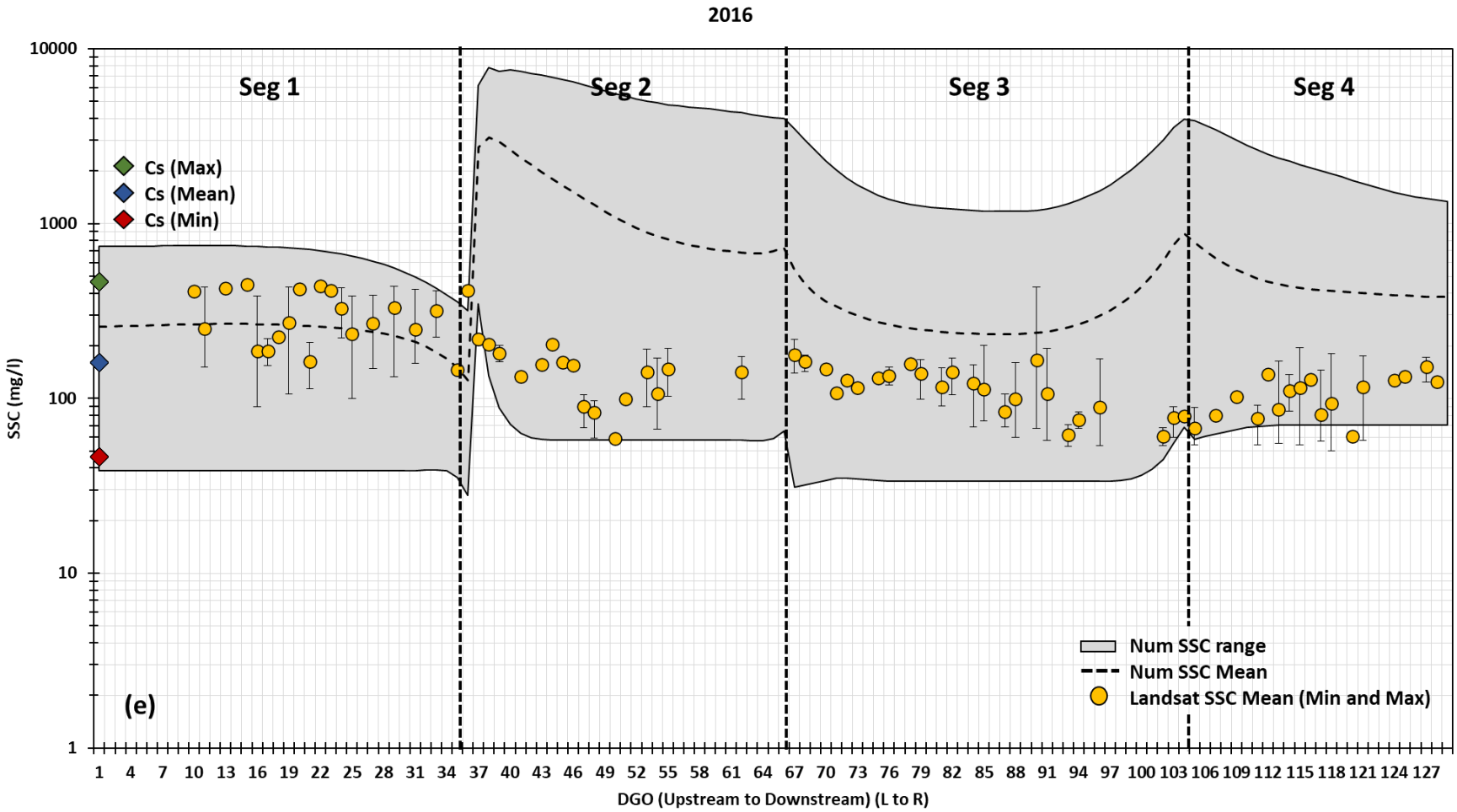
2016
Seg 1
Seg 2
Seg 3
Seg 4
Cs (Max)
Cs (Mean)
Cs (Min)
(e)
Num SSC range
Num SSC Mean
Landsat SSC Mean (Min and Max)
SSC (mg/l)
10000
1000
100
10
1
1 4 7 10 13 16 19 22 25 28 31 34 37 40 43 46 49 52 55 58 61 64 67 70 73 76 79 82 85 88 91 94 97 100 103 106 109 112 115 118 121 124 127
DGO (Upstream to Downstream) (L to R)

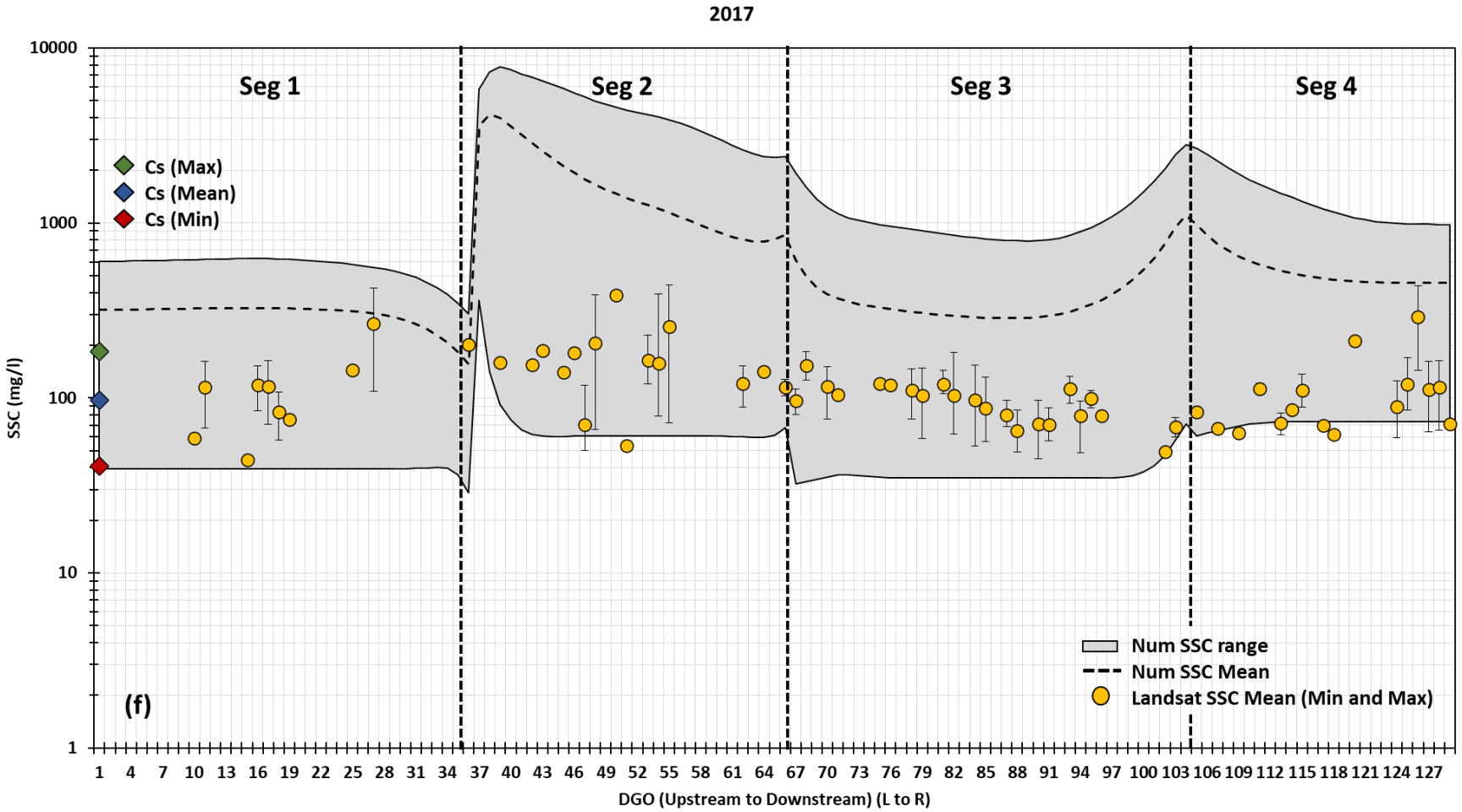
2017
Seg 1
Seg 2
Seg 3
Seg 4
Cs (Max)
Cs (Mean)
Cs (Min)
(f)
Num SSC range
Num SSC Mean
Landsat SSC Mean (Min and Max)
SSC (mg/l)
10000
1000
100
10
1
1 4 7 10 13 16 19 22 25 28 31 34 37 40 43 46 49 52 55 58 61 64 67 70 73 76 79 82 85 88 91 94 97 100 103 106 109 112 115 118 121 124 127
DGO (Upstream to Downstream) (L to R)

4.5.4 Implications of Spatial Calibration and Cloud-Free Scene Availability on Reconstructing the Sediment Pulse

An initial comparison between the two different sources of SSC data showed similarities between each other for the lower, mid, and higher end of the spectrum (Figure 4.8 a). However, for the peak high and peak low values predicted by Curran et al., (2018), Sharma (2023b) slightly underpredicted SSC, but matched the magnitude of the peak low SSC data through time. To gain a more comprehensive understanding of suspended sediment dynamics, the inclusion of minimum and maximum SSC ranges per segment was incorporated to compare with the turbidity-based SSC time series (Figure 4.8 a). This approach provided a more complete picture of the spatial variability in SSC, and also highlighted some of the limitations associated with point-to-point comparisons.

The numerical model used in the study was calibrated for SSC using the sediment transport equation by Ashida & Michiue, (1972). However, the spatial calibration was conducted at a coarser spatial resolution, that is for segment four by Sharma (2023b). Therefore, when comparing the numerical modeled results, it was essential to account for the statistical similarity between multiple cross sections encompassing segment four resulting from the changepoint analysis preceding a successful calibration process.

Next, results showed that the C_N values for the fourth segment were a close match to the turbidity generated SSC from Curran et al., (2018), from 2012 to 2014 (Figure 4.8 b, and c). Slight overprediction around the falling limb of the SSC graph was observed thereafter, hinting that the contribution of the channel bed generated SSC were overcompensated by the simplified numerical model. Overall, the goodness of fit coefficient (R^2) between C_N, and Curran et al., (2018) SSC data was around 0.27, showing moderate to low correlation between the two datasets, as compared to 0.1 for the Sharma (2023b) dataset, primarily attributing to extensive data coverage post 2016.

One of the limitations encountered during the study was the limited availability of cloud-free scenes, particularly during rising limb of the SSC hydrographs through time. However, the study successfully demonstrated the spatial and temporal variability in the response of the Elwha River to upstream sediment supply concentrations. The results emphasized the importance of considering the sphere of influence of process-based models when comparing them to point-based SSC estimates. By acknowledging these differences and considering the limitations

associated with a one to one point-based comparison, future researchers can work to enhance the reliability and applicability of process based numerical models. For practitioners and stakeholders involved in sediment management, river restoration, the methodology used has the potential to frame guiding principles for the development of best practices in scenarios involving a sediment disturbance or sediment management in general.

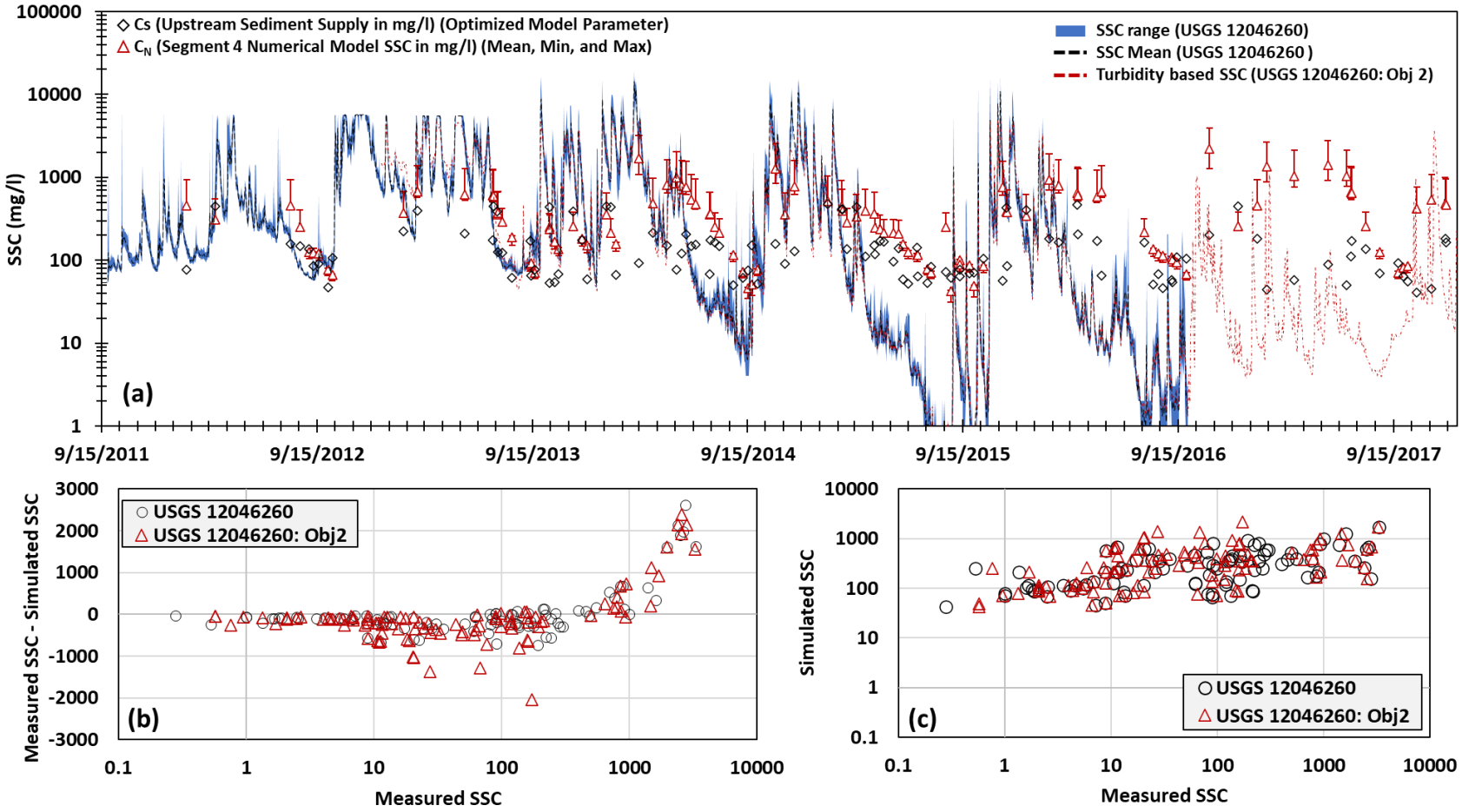

Figure 4.8 Comparing turbidity generated SSC time series (a) at the USGS gauge station location (USGS:12046260), with numerical model SSC simulations C_N (triangle) for the surrounding segment covering the mean, min, and max values for the segment through time, along with the optimized upstream concentration (diamond). Numerical SSC output comparison using a residual plot (b), and a 1:1 comparison with using two different reference datasets (c); hollow points representing SSC data by Curran et al., (2018), and hollow red triangle representing SSC data by Sharma (2023b)

4.6 Conclusions:

Despite the limitations and challenges encountered in the analysis of Landsat scenes for the Elwha River, this study provided valuable insights and introduced a novel approach to reconstructing the sediment pulse. By utilizing the available Landsat data, an initial range for the numerical model parameter, Cs, was established which is a significant contribution to sediment transport modeling. Furthermore, the study highlighted the importance of considering temporal resolution and cloud cover in satellite-based approaches. While the limited availability of scenes during specific months may pose challenges, it also opens up opportunities to capture sediment dynamics during other periods using Bayesian Regression or other similar extrapolation frameworks. This information can be valuable in understanding sediment transport processes and their implications for river ecosystems. The results highlighted the need for further investigation into the spatial variability of SSC, which was explored using the numerical model in later sections of the study.

The investigation of the relationship between Landsat SSC, the number of DGOs per scene, and flow rate provided insights into the interdependencies of these variables in sediment transport modeling. The high correlation between flow rate and Landsat SSC, coupled with the moderate correlation between Landsat SSC and the number of DGOs, highlighted the influence of flow dynamics and data availability on sediment concentration. The findings underscored the limitations associated with spatial discontinuity in data coverage, emphasizing the need for comprehensive data acquisition strategies for accurate sediment transport modeling using satellite imagery.

Further, the examination of post-optimization RMSE values shed light on the relationship between downstream concentration, flow rate, and the number of DGOs. Flow rate emerged as a significant contributor to the variability in RMSE, while the number of DGOs played a crucial role in capturing the spatial range of sediment concentration. Additionally, the influence of grain size distribution on RMSE values was acknowledged, although a detailed analysis of its temporal variations was beyond the scope of the study. Future researchers were encouraged to explore these factors further to enhance the accuracy and reliability of sediment transport models.

In summary, the evaluation of Cs and Landsat SSC revealed important patterns and trends. Cs demonstrated a decline after 2014, while the downstream concentration appeared to be independent of upstream supply. The spatial analysis of Landsat coverage highlighted the limited

data availability in the narrower first segment. Furthermore, the temporal analysis showed an increasing trend in Landsat SSC from upstream to downstream for specific years, followed by an overall declining trend after 2014. The concentration of sediment was highest at the upstream end and gradually decreased along each subsequent segment of the river.

One of the major advantages of this study was the introduction of a novel approach for reconstructing sediment pulse using Landsat data and numerical modeling. By establishing an optimized value for the numerical model parameter, Cs, based on Landsat-based SSC, the study introduced a method to quantify the upstream sediment supply time series post dam removals for the Elwha River. This integration of satellite imagery and numerical modeling provided a comprehensive and spatially explicit perspective on sediment transport processes, allowing for more informed decision-making in river management and restoration efforts. Additionally, the study highlighted the importance of considering the dynamic nature of sediment transport and the influence of various factors, such as channel shape and flow conditions, on sediment pulse propagation through time. Such insights contribute to advancing our knowledge of sediment transport processes and can be valuable for future research in this field. Despite limitations, such as cloud cover and data availability, valuable insights were gained regarding spatial variations in suspended sediment concentration and the influence of channel shape on sediment dynamics.

4.7 References:

Alber, A., & Piégay, H. (2011). Spatial disaggregation and aggregation procedures for characterizing fluvial features at the network-scale: Application to the Rhône basin (France). *Geomorphology*, *125*(3), 343–360.

Anderson, C. W., Wright, S. A., Schenk, L. N., Skalak, K., Curtis, J. A., East, A. E., & Benthem, A. (2019). Refining the Baseline Sediment Budget for the Klamath River, California. *SEDHYD 2019 Conference*, *5*.

Anderson, S. W., Keith, M. K., Magirl, C. S., Wallick, J. R., Mastin, M. C., & Foreman, J. R. (2017). *Geomorphic response of the North Fork Stillaguamish River to the State Route 530 landslide near Oso, Washington*. US Geological Survey.

Ashida, K., & Michiue, M. (1972). Study on hydraulic resistance and bed-load transport rate in alluvial streams. *Proceedings of the Japan Society of Civil Engineers*, *1972*(206), 59–69.

Benda, L. E. E., Poff, N. L., Miller, D., Dunne, T., Reeves, G., Pess, G., & Pollock, M. (2004). The network dynamics hypothesis: how channel networks structure riverine habitats. *BioScience*, *54*(5), 413–427.

Blumm, M. C., & Illowsky, D. (2022). The World's Largest Dam Removal Project: The Klamath River Dams. *Available at SSRN 4061159*.

Borselli, L., Cassi, P., & Torri, D. (2008). Prolegomena to sediment and flow connectivity in the landscape: a GIS and field numerical assessment. *Catena*, *75*(3), 268–277.

Brando, V. E., & Dekker, A. G. (2003). Satellite hyperspectral remote sensing for estimating estuarine and coastal water quality. *IEEE Transactions on Geoscience and Remote Sensing*, *41*(6), 1378–1387.

Breiman, L. (2001). Random forests. *Machine Learning*, *45*, 5–32.

Brice, J. C. (1964). *Channel patterns and terraces of the Loup Rivers in Nebraska*. US Government Printing Office.

Bright, C. E., & Mager, S. M. (2020). A national-scale study of spatial variability in the relationship between turbidity and suspended sediment concentration and sediment properties. *River Research and Applications*, *36*(8), 1449–1459.

Bright, C., Mager, S., & Horton, S. (2020). Response of nephelometric turbidity to hydrodynamic particle size of fine suspended sediment. *International Journal of Sediment Research*, *35*(5), 444–454.

Castro-Bolinaga, C. F., Diplas, P., & Bodnar, R. J. (2020). Modeling Hydro-Morphodynamic Processes During the Propagation of Fluvial Sediment Pulses: A Physics-Based Framework. *Journal of Geophysical Research: Earth Surface*, *125*(12), e2020JF005722.

Cavalli, M., Trevisani, S., Comiti, F., & Marchi, L. (2013). Geomorphometric assessment of spatial sediment connectivity in small Alpine catchments. *Geomorphology*, *188*, 31–41.

Chen, Z., Hu, C., & Muller-Karger, F. (2007). Monitoring turbidity in Tampa Bay using MODIS/Aqua 250-m imagery. *Remote Sensing of Environment*, *109*(2), 207–220.

Chib, S., & Greenberg, E. (1995). Understanding the metropolis-hastings algorithm. *The American Statistician*, *49*(4), 327–335.

Choubin, B., Solaimani, K., Rezanezhad, F., Roshan, M. H., Malekian, A., & Shamshirband, S. (2019). Streamflow regionalization using a similarity approach in ungauged basins: Application of the geo-environmental signatures in the Karkheh River Basin, Iran. *Catena*, *182*, 104128.

Cowan, W. L. (1956). Estimating hydraulic roughness coefficients. *Agricultural Engineering*, *37*(7), 473–475.

Crema, S., & Cavalli, M. (2018). SedInConnect: a stand-alone, free and open source tool for the assessment of sediment connectivity. *Computers & Geosciences*, *111*, 39–45.

Cui, Y., Dusterhoff, S. R., Wooster, J. K., & Downs, P. W. (2011). Practical considerations for modeling sediment transport dynamics in rivers. *Stream Restoration in Dynamic Fluvial Systems: Scientific Approaches, Analyses, and Tools"(Edited by Simon, A., Bennett, SJ, Castro, JM) American Geophysical Union, Washington DC*, 503–527.

Cui, Y., Parker, G., Braudrick, C., Dietrich, W. E., & Cluer, B. (2006). Dam removal express assessment models (DREAM). Part 1: model development and validation. *Journal of Hydraulic Research*, *44*(3), 291–307.

Cui, Y., & Wilcox, A. (2008). Development and application of numerical models of sediment transport associated with dam removal. *Chapter*, *23*, 995–1020.

D. N. Moriasi, J. G. Arnold, M. W. Van Liew, R. L. Bingner, R. D. Harmel, & T. L. Veith. (2007). Model Evaluation Guidelines for Systematic Quantification of Accuracy in Watershed Simulations. *Transactions of the ASABE*, *50*(3), 885–900. https://doi.org/10.13031/2013.23153

Davies, R. B. (2002). Hypothesis testing when a nuisance parameter is present only under the

alternative: linear model case. *Biometrika*, 484–489.

Dekker, A. G., & Peters, S. W. M. (1993). The use of the Thematic Mapper for the analysis of eutrophic lakes: a case study in the Netherlands. *International Journal of Remote Sensing*, *14*(5), 799–821.

Dethier, E. N., Renshaw, C. E., & Magilligan, F. J. (2020). Toward Improved Accuracy of Remote Sensing Approaches for Quantifying Suspended Sediment: Implications for Suspended-Sediment Monitoring. *Journal of Geophysical Research: Earth Surface*, *125*(7), e2019JF005033.

Ding, L., Chen, L., Ding, C., & Tao, J. (2019). Global trends in dam removal and related research: A systematic review based on associated datasets and bibliometric analysis. *Chinese Geographical Science*, *29*, 1–12.

dos Santos, A. L. M. R., Martinez, J. M., Filizola Jr, N. P., Armijos, E., & Alves, L. G. S. (2018). Purus River suspended sediment variability and contributions to the Amazon River from satellite data (2000–2015). *Comptes Rendus Geoscience*, *350*(1–2), 13–19.

Duda, J. J., & Bellmore, J. R. (2022). Dam Removal and River Restoration. *Encyclopedia of Inland Waters, Eds K. Tockner and T. Mehner (Oxford, UK: Elsevier Ltd). Doi*, *10*.

Duda, J. J., Freilich, J. E., & Schreiner, E. G. (2008). Baseline studies in the Elwha River ecosystem prior to dam removal: introduction to the special issue. *Northwest Science*, *82*(sp1), 1–12.

Duda, J. J., Warrick, J. A., & Magirl, C. S. (2011). Coastal and lower Elwha River, Washington, prior to dam removal—history, status, and defining characteristics. *Coastal Habitats of the Elwha River, Washington—Biological and Physical Patterns and Processes Prior to Dam Removal. US Geological Survey Scientific Investigations Report*, *5120*, 1–26.

East, A. E., Pess, G. R., Bountry, J. A., Magirl, C. S., Ritchie, A. C., Logan, J. B., Randle, T. J., Mastin, M. C., Minear, J. T., & Duda, J. J. (2015). Large-scale dam removal on the Elwha River, Washington, USA: River channel and floodplain geomorphic change. *Geomorphology*, *228*, 765–786.

Engelund, F., & Fredsøe, J. (1976). A sediment transport model for straight alluvial channels. *Hydrology Research*, *7*(5), 293–306.

Espinoza-Villar, R., Martinez, J.-M., Armijos, E., Espinoza, J.-C., Filizola, N., Dos Santos, A., Willems, B., Fraizy, P., Santini, W., & Vauchel, P. (2018). Spatio-temporal monitoring of

suspended sediments in the Solimões River (2000–2014). *Comptes Rendus Geoscience*, *350*(1–2), 4–12.

Ferguson, R. I., Church, M., Rennie, C. D., & Venditti, J. G. (2015). Reconstructing a sediment pulse: Modeling the effect of placer mining on Fraser River, Canada. *Journal of Geophysical Research: Earth Surface*, *120*(7), 1436–1454.

Feyisa, G. L., Meilby, H., Fensholt, R., & Proud, S. R. (2014). Automated Water Extraction Index: A new technique for surface water mapping using Landsat imagery. *Remote Sensing of Environment*, *140*, 23–35.

Foley, M. M., Bellmore, J. R., O'Connor, J. E., Duda, J. J., East, A. E., Grant, G. E., Anderson, C. W., Bountry, J. A., Collins, M. J., & Connolly, P. J. (2017). Dam removal: Listening in. *Water Resources Research*, *53*(7), 5229–5246.

Foley, M. M., Duda, J. J., Beirne, M. M., Paradis, R., Ritchie, A., & Warrick, J. A. (2015). Rapid water quality change in the E lwha R iver estuary complex during dam removal. *Limnology and Oceanography*, *60*(5), 1719–1732.

Fox, C. A., Reo, N. J., Fessell, B., & Dituri, F. (2022). Native American tribes and dam removal: restoring the Ottaway, Penobscot and Elwha Rivers. *Water Alternatives*, *15*(1), 31–55.

Francke, T., López-Tarazón, J. A., & Schröder, B. (2008). Estimation of suspended sediment concentration and yield using linear models, random forests and quantile regression forests. *Hydrological Processes: An International Journal*, *22*(25), 4892–4904.

Gao, B.-C. (1996). NDWI—A normalized difference water index for remote sensing of vegetation liquid water from space. *Remote Sensing of Environment*, *58*(3), 257–266.

Gao, P. (2008). Understanding watershed suspended sediment transport. *Progress in Physical Geography*, *32*(3), 243–263.

Gelfenbaum, G., Stevens, A. W., Miller, I., Warrick, J. A., Ogston, A. S., & Eidam, E. (2015). Large-scale dam removal on the Elwha River, Washington, USA: Coastal geomorphic change. *Geomorphology*, *246*, 649–668.

Gesch, D., Oimoen, M., Greenlee, S., Nelson, C., Steuck, M., & Tyler, D. (2002). The national elevation dataset. *Photogrammetric Engineering and Remote Sensing*, *68*(1), 5–32.

Gitelson, A. A., Dall'Olmo, G., Moses, W., Rundquist, D. C., Barrow, T., Fisher, T. R., Gurlin, D., & Holz, J. (2008). A simple semi-analytical model for remote estimation of chlorophyll-a in turbid waters: Validation. *Remote Sensing of Environment*, *112*(9), 3582–3593.

Graf, W. L. (1999). Dam nation: A geographic census of American dams and their large-scale hydrologic impacts. *Water Resources Research*, *35*(4), 1305–1311.

Gran, K. B., & Czuba, J. A. (2017). Sediment pulse evolution and the role of network structure. *Geomorphology*, *277*, 17–30. https://doi.org/https://doi.org/10.1016/j.geomorph.2015.12.015

Guarino, J. (2013). Tribal advocacy and the art of dam removal: The Lower Elwha Klallam and the Elwha Dams. *American Indian Law Journal*, *2*(1), 114–145.

Guertault, L., Camenen, B., Paquier, A., & Peteuil, C. (2018). A one-dimensional process-based approach to study reservoir sediment dynamics during management operations. *Earth Surface Processes and Landforms*, *43*(2), 373–386.

Guertault, L., Camenen, B., Peteuil, C., Paquier, A., & Faure, J. B. (2016). One-dimensional modeling of suspended sediment dynamics in dam reservoirs. *Journal of Hydraulic Engineering*, *142*(10), 4016033.

Guo, Y., Zhang, Y., Zhang, L., & Wang, Z. (2021). Regionalization of hydrological modeling for predicting streamflow in ungauged catchments: A comprehensive review. *Wiley Interdisciplinary Reviews: Water*, *8*(1), e1487.

Gupta, N., Atkinson, P. M., & Carling, P. A. (2013). Decadal length changes in the fluvial planform of the River Ganga: bringing a mega-river to life with Landsat archives. *Remote Sensing Letters*, *4*(1), 1–9.

Haefner, J. W. (2005). *Modeling biological systems:: principles and applications*. Springer Science & Business Media.

Hastings, W. K. (1970). *Monte Carlo sampling methods using Markov chains and their applications*.

Hearst, M. A., Dumais, S. T., Osuna, E., Platt, J., & Scholkopf, B. (1998). Support vector machines. *IEEE Intelligent Systems and Their Applications*, *13*(4), 18–28.

Hellweger, F. L., Schlosser, P., Lall, U., & Weissel, J. K. (2004). Use of satellite imagery for water quality studies in New York Harbor. *Estuarine, Coastal and Shelf Science*, *61*(3), 437–448.

Helsel, D. R., & Hirsch, R. M. (2002). Statistical methods in water resources. Hydrologic Analysis and Interpretation. *US Geological Survey Techniques of Water-Resources Investigations*, *510*.

Hilbert-Wolf, H. L., & Gerlak, A. K. (2022). The evolution of the modern dam conflict on the Snake River, USA. *Water International*, *47*(8), 1349–1369.

Hilldale, R. C., Carpenter, W. O., Goodwiller, B., Chambers, J. P., & Randle, T. J. (2015). Installation of impact plates to continuously measure bed load: Elwha River, Washington, USA. *Journal of Hydraulic Engineering*, *141*(3), 6014023.

Holliday, C. P., Rasmussen, T. C., & Miller, W. P. (2003). *Establishing the relationship between turbidity and total suspended sediment concentration*.

Hommes, L. (2022). The Ageing of Infrastructure and Ideologies: Contestations Around Dam Removal in Spain. *Water Alternatives*, *15*(3), 592–613.

Hsu, N.-S., & Huang, C.-J. (2017). Estimation of flow duration curve at ungauged locations in Taiwan. *Journal of Hydrologic Engineering*, *22*(8), 5017009.

Ibraheem, N. A., Hasan, M. M., Khan, R. Z., & Mishra, P. K. (2012). Understanding color models: a review. *ARPN Journal of Science and Technology*, *2*(3), 265–275.

Isikdogan, F., Bovik, A., & Passalacqua, P. (2017). RivaMap: An automated river analysis and mapping engine. *Remote Sensing of Environment*, *202*, 88–97.

Iverson, R. M. (2015). Scaling and design of landslide and debris-flow experiments. *Geomorphology*, *244*, 9–20.

Iverson, R. M., & George, D. L. (2016). Modelling landslide liquefaction, mobility bifurcation and the dynamics of the 2014 Oso disaster. *Géotechnique*, *66*(3), 175–187.

Iverson, R. M., George, D. L., Allstadt, K., Reid, M. E., Collins, B. D., Vallance, J. W., Schilling, S. P., Godt, J. W., Cannon, C. M., & Magirl, C. S. (2015). Landslide mobility and hazards: implications of the 2014 Oso disaster. *Earth and Planetary Science Letters*, *412*, 197–208.

James, N. A., & Matteson, D. S. (2013). ecp: An R package for nonparametric multiple change point analysis of multivariate data. *ArXiv Preprint ArXiv:1309.3295*.

Jastram, J. D., Zipper, C. E., Zelazny, L. W., & Hyer, K. E. (2010). Increasing precision of turbidity-based suspended sediment concentration and load estimates. *Journal of Environmental Quality*, *39*(4), 1306–1316.

Jensen, J. R. (2009). *Remote sensing of the environment: An earth resource perspective 2/e*. Pearson Education India.

Jiang, L., Westphal Christensen, S., & Bauer-Gottwein, P. (2021). Calibrating 1D hydrodynamic

river models in the absence of cross-section geometry using satellite observations of water surface elevation and river width. *Hydrology and Earth System Sciences*, *25*(12), 6359–6379.

Julien, P. Y. (2018). *River mechanics*. Cambridge University Press.

Kabir, S. M. I., & Ahmari, H. (2020). Evaluating the effect of sediment color on water radiance and suspended sediment concentration using digital imagery. *Journal of Hydrology*, *589*, 125189.

Karrasch, P., Henzen, D., Hunger, S., & Hörold, M. (2015). Determination of water body structures for small rivers using remote sensing data. *Remote Sensing for Agriculture, Ecosystems, and Hydrology XVII*, *9637*, 126–138.

Kellogg, K., Hoffman, P., Standley, S., Shaffer, S., Rosen, P., Edelstein, W., Dunn, C., Baker, C., Barela, P., & Shen, Y. (2020). NASA-ISRO synthetic aperture radar (NISAR) mission. *2020 IEEE Aerospace Conference*, 1–21.

Kendall, M. G. (1948). *Rank correlation methods.*

Khan, N. S., Roy, S. K., Mazumder, M. T. R., Talukdar, S., & Mallick, J. (2022). Assessing the long-term planform dynamics of Ganges–Jamuna confluence with the aid of remote sensing and GIS. *Natural Hazards*, *114*(1), 883–906.

Kirk, J. T. O. (1994). *Light and photosynthesis in aquatic ecosystems*. Cambridge university press.

Konrad, C. P. (2009). Simulating the recovery of suspended sediment transport and river-bed stability in response to dam removal on the Elwha River, Washington. *Ecological Engineering*, *35*(7), 1104–1115.

Lauer, D. T., Morain, S. A., & Salomonson, V. V. (1997). The Landsat program: Its origins, evolution, and impacts. *Photogrammetric Engineering and Remote Sensing*, *63*(7), 831–838.

Leisher, C., Hess, S., Dempsey, K., Payne Wynne, M. L., & Royte, J. (2022). Measuring the social changes from river restoration and dam removal. *Restoration Ecology*, *30*(1), e13500.

Leopold, L. B., Wolman, M. G., & Miller, J. P. (1964). Fluvial processes in geomorphology WH Freeman and Co. *San Francisco 522pp*.

Levins, R. (1966). The strategy of model building in population biology. *American Scientist*, *54*(4), 421–431.

Lindell, T., Pierson, D., & Premazzi, G. (1999). *Manual for monitoring European lakes using remote sensing techniques*.

Liu, C., He, B., Li, M., & Ren, X. (2006). Quantitative modeling of suspended sediment in middle Changjiang River from MODIS. *Chinese Geographical Science*, *16*, 79–82.

Long, C. M., & Pavelsky, T. M. (2013). Remote sensing of suspended sediment concentration and hydrologic connectivity in a complex wetland environment. *Remote Sensing of Environment*, *129*, 197–209.

Longbotham, N., Pacifici, F., Malitz, S., Baugh, W., & Camps-Valls, G. (2015). Measuring the spatial and spectral performance of WorldView-3. *Hyperspectral Imaging and Sounding of the Environment*, HW3B-2.

Ma, Y., & Huang, H. Q. (2016). Controls of channel morphology and sediment concentration on flow resistance in a large sand-bed river: A case study of the lower Yellow River. *Geomorphology*, *264*, 132–146.

Magirl, C. S., Hilldale, R. C., Curran, C. A., Duda, J. J., Straub, T. D., Domanski, M., & Foreman, J. R. (2015). Large-scale dam removal on the Elwha River, Washington, USA: Fluvial sediment load. *Geomorphology*, *246*, 669–686.

Mahoney, D. T., Fox, J. F., & Al Aamery, N. (2018). Watershed erosion modeling using the probability of sediment connectivity in a gently rolling system. *Journal of Hydrology*, *561*, 862–883.

Major, J. J. (2004). Posteruption suspended sediment transport at Mount St. Helens: Decadal-scale relationships with landscape adjustments and river discharges. *Journal of Geophysical Research: Earth Surface*, *109*(F1).

Major, J. J., Bertin, D., Pierson, T. C., Amigo, Á., Iroumé, A., Ulloa, H., & Castro, J. (2016). Extraordinary sediment delivery and rapid geomorphic response following the 2008–2009 eruption of Chaitén Volcano, Chile. *Water Resources Research*, *52*(7), 5075–5094.

Major, J. J., Pierson, T. C., Dinehart, R. L., & Costa, J. E. (2000). Sediment yield following severe volcanic disturbance—a two-decade perspective from Mount St. Helens. *Geology*, *28*(9), 819–822.

Mangiarotti, S., Martinez, J.-M., Bonnet, M.-P., Buarque, D. C., Filizola, N., & Mazzega, P. (2013). Discharge and suspended sediment flux estimated along the mainstream of the Amazon and the Madeira Rivers (from in situ and MODIS Satellite Data). *International*

Journal of Applied Earth Observation and Geoinformation, *21*, 341–355.

Mann, H. B. (1945). Non-parametric test against trend. Econometrika 13, 245–259. *Search In*.

Matteson, D. S., & James, N. A. (2014). A nonparametric approach for multiple change point analysis of multivariate data. *Journal of the American Statistical Association*, *109*(505), 334–345.

Mauer, K. W. (2020). Monopoly's winners and losers: Elwha River Dam construction as social closure. *Journal of Environmental Studies and Sciences*, *10*(2), 137–147.

McCulloch, W. S., & Pitts, W. (1943). A logical calculus of the ideas immanent in nervous activity. *The Bulletin of Mathematical Biophysics*, *5*, 115–133.

McElreath, R. (2020). *Statistical rethinking: A Bayesian course with examples in R and Stan*. CRC press.

Metropolis, N., Rosenbluth, A., Rosenbluth, M., Teller, A., & Teller, E. (1953). Introduction of the metropolis algorithm for molecular-dynamics simulation. *J. Chem. Phys*, *21*, 1987.

Milliman, J. D., & Syvitski, J. P. M. (1992). Geomorphic/tectonic control of sediment discharge to the ocean: the importance of small mountainous rivers. *The Journal of Geology*, *100*(5), 525–544.

Mostafa, Y., & Abdelhafiz, A. (2017). Shadow identification in high resolution satellite images in the presence of water regions. *Photogrammetric Engineering & Remote Sensing*, *83*(2), 87–94.

Murphy, B. P., Czuba, J. A., & Belmont, P. (2019). Post-wildfire sediment cascades: A modeling framework linking debris flow generation and network-scale sediment routing. *Earth Surface Processes and Landforms*, *44*(11), 2126–2140.

Nash, J. E., & Sutcliffe, J. V. (1970). River flow forecasting through conceptual models part I—A discussion of principles. *Journal of Hydrology*, *10*(3), 282–290.

Nelson, A., & Dubé, K. (2016). Channel response to an extreme flood and sediment pulse in a mixed bedrock and gravel-bed river. *Earth Surface Processes and Landforms*, *41*(2), 178–195.

Nelson, P. A., Brew, A. K., & Morgan, J. A. (2015). Morphodynamic response of a variable-width channel to changes in sediment supply. *Water Resources Research*, *51*(7), 5717–5734.

O'CALLAGHAN, J., ROBERTSON, P., & Fraser, D. (1982). *Colour image display: it's not that*

simple.

O'Hanley, J. R., Pompeu, P. S., Louzada, M., Zambaldi, L. P., & Kemp, P. S. (2020). Optimizing hydropower dam location and removal in the São Francisco river basin, Brazil to balance hydropower and river biodiversity tradeoffs. *Landscape and Urban Planning*, *195*, 103725.

Olden, J. D., Lawler, J. J., & Poff, N. L. (2008). Machine learning methods without tears: a primer for ecologists. *The Quarterly Review of Biology*, *83*(2), 171–193.

Palu, M. C., & Julien, P. Y. (2019). Modeling the sediment load of the Doce River after the Fundão tailings dam collapse, Brazil. *Journal of Hydraulic Engineering*, *145*(5), 5019002.

Pettitt, A. N. (1979). A non-parametric approach to the change-point problem. *Journal of the Royal Statistical Society: Series C (Applied Statistics)*, *28*(2), 126–135.

Piman, T., & Babel, M. S. (2013). Prediction of rainfall-runoff in an ungauged basin: case study in the mountainous region of Northern Thailand. *Journal of Hydrologic Engineering*, *18*(2), 285–296.

Popović, P., Devauchelle, O., Abramian, A., & Lajeunesse, E. (2021). Sediment load determines the shape of rivers. *Proceedings of the National Academy of Sciences*, *118*(49), e2111215118.

Pugliese, A., Farmer, W. H., Castellarin, A., Archfield, S. A., & Vogel, R. M. (2016). Regional flow duration curves: Geostatistical techniques versus multivariate regression. *Advances in Water Resources*, *96*, 11–22.

Rand, W. M. (1971). Objective criteria for the evaluation of clustering methods. *Journal of the American Statistical Association*, *66*(336), 846–850.

Randle, T. J., Bountry, J. A., Ritchie, A., & Wille, K. (2015). Large-scale dam removal on the Elwha River, Washington, USA: Erosion of reservoir sediment. *Geomorphology*, *246*, 709–728.

Rasmussen, P. P., Gray, J. R., Glysson, G. D., & Ziegler, A. C. (2009). Guidelines and procedures for computing time-series suspended-sediment concentrations and loads from in-stream turbidity-sensor and streamflow data. *US Geological Survey Techniques and Methods, Book*, *3*, 52.

Razavi, T., & Coulibaly, P. (2016). Improving streamflow estimation in ungauged basins using a multi-modelling approach. *Hydrological Sciences Journal*, *61*(15), 2668–2679.

Reneau, S. L., Katzman, D., Kuyumjian, G. A., Lavine, A., & Malmon, D. V. (2007). Sediment delivery after a wildfire. *Geology*, *35*(2), 151–154.

Ritchie, A. C., Warrick, J. A., East, A. E., Magirl, C. S., Stevens, A. W., Bountry, J. A., Randle, T. J., Curran, C. A., Hilldale, R. C., & Duda, J. J. (2018). Morphodynamic evolution following sediment release from the world's largest dam removal. *Scientific Reports*, *8*(1), 13279.

Robert, E., Grippa, M., Kergoat, L., Pinet, S., Gal, L., Cochonneau, G., & Martinez, J.-M. (2016). Monitoring water turbidity and surface suspended sediment concentration of the Bagre Reservoir (Burkina Faso) using MODIS and field reflectance data. *International Journal of Applied Earth Observation and Geoinformation*, *52*, 243–251.

Robertson, P. K., & O'Callaghan, J. F. (1988). The application of perceptual color spaces to the display of remotely sensed imagery. *IEEE Transactions on Geoscience and Remote Sensing*, *26*(1), 49–59.

Rojas, R. (2013). *Neural networks: a systematic introduction*. Springer Science & Business Media.

Roux, C., Alber, A., Bertrand, M., Vaudor, L., & Piégay, H. (2015). "FluvialCorridor": A new ArcGIS toolbox package for multiscale riverscape exploration. *Geomorphology*, *242*, 29–37.

Ryan Bellmore, J., Duda, J. J., Craig, L. S., Greene, S. L., Torgersen, C. E., Collins, M. J., & Vittum, K. (2017). Status and trends of dam removal research in the United States. *WIREs Water* , *4*(2), e1164. https://doi.org/https://doi.org/10.1002/wat2.1164

Rymszewicz, A., O'sullivan, J. J., Bruen, M., Turner, J. N., Lawler, D. M., Conroy, E., & Kelly-Quinn, M. (2017). Measurement differences between turbidity instruments, and their implications for suspended sediment concentration and load calculations: A sensor inter-comparison study. *Journal of Environmental Management*, *199*, 99–108.

Schermerhorn, V. P. (1967). Relations between topography and annual precipitation in western Oregon and Washington. *Water Resources Research*, *3*(3), 707–711.

Schwarz, G. E., & Alexander, R. B. (1995). *State soil geographic (STATSGO) data base for the conterminous United States*.

Sehgal, D., Martinez-Carreras, N., Hissler, C., Bense, V., & Hoitink, T. A. J. F. (2022). *Influence of riverine suspended sediment carbon content and particle size on turbidity*. Copernicus

Meetings.

Sharma, A., Castro-Bolinaga, C., & Nelson, N. (2022). An integrated modeling approach to evaluate the propagation of fluvial sediment pulses following dam removals: A case study from the Elwha River, Washington, USA. *Proceedings of the 39th IAHR World Congress*, 938–945. https://doi.org/10.3850/iahr-39wc252171192022365

Sharma, S., Waldman, J., Afshari, S., & Fekete, B. (2019). Status, trends and significance of American hydropower in the changing energy landscape. *Renewable and Sustainable Energy Reviews*, *101*, 112–122.

Simmons, S. M., Parsons, D. R., Best, J. L., Oberg, K. A., Czuba, J. A., & Keevil, G. M. (2017). An evaluation of the use of a multibeam echo-sounder for observations of suspended sediment. *Applied Acoustics*, *126*, 81–90.

Simmons, S. M., Parsons, D. R., Best, J. L., Orfeo, O., Lane, S. N., Kostaschuk, R., Hardy, R. J., West, G., Malzone, C., & Marcus, J. (2010). Monitoring suspended sediment dynamics using MBES. *Journal of Hydraulic Engineering*, *136*(1), 45–49.

Smith, D., & Davis-Colley, R. (2001). Turbidity suspended sediment and water clarity. *J Am Water Resour Assoc*, *37*, 1085–1101.

Smith, T., Marshall, L., & Sharma, A. (2014). Predicting hydrologic response through a hierarchical catchment knowledgebase: A Bayes empirical Bayes approach. *Water Resources Research*, *50*(2), 1189–1204.

Song, K., Wang, Z., Blackwell, J., Zhang, B., Li, F., Zhang, Y., & Jiang, G. (2011). Water quality monitoring using Landsat Themate Mapper data with empirical algorithms in Chagan Lake, China. *Journal of Applied Remote Sensing*, *5*(1), 53506.

Sousa, J., García-Sánchez, C., & Gorlé, C. (2018). Improving urban flow predictions through data assimilation. *Building and Environment*, *132*, 282–290.

Sousa, J., & Gorlé, C. (2019). Computational urban flow predictions with Bayesian inference: Validation with field data. *Building and Environment*, *154*, 13–22.

Steinschneider, S., Yang, Y.-C. E., & Brown, C. (2015). Combining regression and spatial proximity for catchment model regionalization: a comparative study. *Hydrological Sciences Journal*, *60*(6), 1026–1043.

Strick, R. J. P., Ashworth, P. J., Sambrook Smith, G. H., Nicholas, A. P., Best, J. L., Lane, S. N., Parsons, D. R., Simpson, C. J., Unsworth, C. A., & Dale, J. (2019). Quantification of

bedform dynamics and bedload sediment flux in sandy braided rivers from airborne and satellite imagery. *Earth Surface Processes and Landforms*, *44*(4), 953–972.

Swain, J. B., & Patra, K. C. (2017). Streamflow estimation in ungauged catchments using regional flow duration curve: comparative study. *Journal of Hydrologic Engineering*, *22*(7), 4017010.

Syvitski, J., Ángel, J. R., Saito, Y., Overeem, I., Vörösmarty, C. J., Wang, H., & Olago, D. (2022). Earth's sediment cycle during the Anthropocene. *Nature Reviews Earth & Environment*, *3*(3), 179–196.

Syvitski, J. P. M., & Kettner, A. (2011). Sediment flux and the Anthropocene. *Philosophical Transactions of the Royal Society A: Mathematical, Physical and Engineering Sciences*, *369*(1938), 957–975.

Syvitski, J. P., Morehead, M. D., Bahr, D. B., & Mulder, T. (2000). Estimating fluvial sediment transport: the rating parameters. *Water Resources Research*, *36*(9), 2747–2760.

Tarolli, P., & Mudd, S. M. (2020). *Remote Sensing of Geomorphology* (Vol. 23). Elsevier.

Tegegne, G., & Kim, Y.-O. (2018). Modelling ungauged catchments using the catchment runoff response similarity. *Journal of Hydrology*, *564*, 452–466.

Umar, M., Rhoads, B. L., & Greenberg, J. A. (2018). Use of multispectral satellite remote sensing to assess mixing of suspended sediment downstream of large river confluences. *Journal of Hydrology*, *556*, 325–338.

Vahedifard, F., Madani, K., AghaKouchak, A., & Thota, S. K. (2021). Are we ready for more dam removals in the United States? *Environmental Research: Infrastructure and Sustainability*, *1*(1), 13001.

Van Liew, M. W., & Mittelstet, A. R. (2018). *Comparison of three regionalization techniques for predicting streamflow in ungaged watersheds in Nebraska, USA using SWAT model*.

Vercruysse, K., Grabowski, R. C., & Rickson, R. J. (2017). Suspended sediment transport dynamics in rivers: Multi-scale drivers of temporal variation. *Earth-Science Reviews*, *166*, 38–52.

Vermote, E., Justice, C., Claverie, M., & Franch, B. (2016). Preliminary analysis of the performance of the Landsat 8/OLI land surface reflectance product. *Remote Sensing of Environment*, *185*, 46–56.

Vogel, R. M., & Fennessey, N. M. (1995). Flow duration curves II: A review of applications in

water resources planning 1. *JAWRA Journal of the American Water Resources Association*, *31*(6), 1029–1039.

Wang, J.-J., & Lu, X. X. (2010). Estimation of suspended sediment concentrations using Terra MODIS: An example from the Lower Yangtze River, China. *Science of the Total Environment*, *408*(5), 1131–1138.

Wang, J., Lu, X. X., Liew, S. C., & Zhou, Y. (2009). Retrieval of suspended sediment concentrations in large turbid rivers using Landsat ETM+: an example from the Yangtze River, China. *Earth Surface Processes and Landforms*, *34*(8), 1082–1092.

Warrick, J. A., Bountry, J. A., East, A. E., Magirl, C. S., Randle, T. J., Gelfenbaum, G., Ritchie, A. C., Pess, G. R., Leung, V., & Duda, J. J. (2015). Large-scale dam removal on the Elwha River, Washington, USA: Source-to-sink sediment budget and synthesis. *Geomorphology*, *246*, 729–750.

Wen, C.-Y., & Chou, C.-M. (2004). Color image models and its applications to document examination. *Forensic Science Journal*, *3*(1), 23–32.

Wilcox, A. C., O'Connor, J. E., & Major, J. J. (2014). Rapid reservoir erosion, hyperconcentrated flow, and downstream deposition triggered by breaching of 38 m tall Condit Dam, White Salmon River, Washington. *Journal of Geophysical Research: Earth Surface*, *119*(6), 1376–1394.

Wohl, E., Bledsoe, B. P., Jacobson, R. B., Poff, N. L., Rathburn, S. L., Walters, D. M., & Wilcox, A. C. (2015). The natural sediment regime in rivers: Broadening the foundation for ecosystem management. *BioScience*, *65*(4), 358–371.

Wohl, E., Brierley, G., Cadol, D., Coulthard, T. J., Covino, T., Fryirs, K. A., Grant, G., Hilton, R. G., Lane, S. N., & Magilligan, F. J. (2019). Connectivity as an emergent property of geomorphic systems. *Earth Surface Processes and Landforms*, *44*(1), 4–26.

Xu, H. (2005). A study on information extraction of water body with the modified normalized difference water index (MNDWI). *JOURNAL OF REMOTE SENSING-BEIJING-*, *9*(5), 595.

Zhang, M., Dong, Q., Cui, T., Xue, C., & Zhang, S. (2014). Suspended sediment monitoring and assessment for Yellow River estuary from Landsat TM and ETM+ imagery. *Remote Sensing of Environment*, *146*, 136–147.

Zhang, Y., Chiew, F. H. S., Li, M., & Post, D. (2018). Predicting runoff signatures using

regression and hydrological modeling approaches. *Water Resources Research*, *54*(10), 7859–7878.

5 CONCLUSIONS

5.1 Findings

5.1.1 Data-driven Modeling of Sediment Pulse Propagation Dynamics.

A reflectance-turbidity modeling framework was developed using machine learning, reflectance from satellite imagery, and physically informed predictors for predicting turbidity in data-rich and data-scarce regions. The modeling framework was tested using 20 locations in Washington State, out of which three experienced sediment pulses in the past. The key findings are summarized as follows:

- The Random Forest algorithm utilizing band ratios and Sediment Delivery Index as predictor variables was the most accurate combination in predicting turbidity across Washington for the data rich scenario. This highlighted the impact of training algorithms and nature of predictor variables on prediction accuracy for the reflectance-turbidity modeling framework.
- Inclusion of Sediment Delivery Index to drive the training and testing data split for a data limited scenario suggested that the physically informed predictor was successful in identification of a donor catchment for another test catchment within the study area. It was critical to understand the role of predictor variables on model transferability of the reflectance-turbidity modeling framework.
- The accuracy and transferability of a data-based model in predicting sediment pulses was dependent on availability of data from locations with similar experience and similar structural sediment connectivity.

5.1.2 Construction, Calibration, and Validation of a hydro-morphodynamic process-based numerical models using remote sensing.

Publicly available remote sensing data were used to extract different channel attributes such as width, sinuosity, and slope to setup a simplified numerical model. The inclusion of aerial imagery enabled model setup for data scarce regions. The overall methodology was novel in terms of extracting river mask using supervised classification, simplifying numerical model setup using a non-parametric multivariate changepoint approach, and calibrating the hydraulic and sediment transport components of the numerical model. Testing the methodology for Elwha River provided key insights as follows:

- Classification of shadows using supervised learning minimized noise in the river mask creation, and eventually extraction of channel attributes such as width and sinuosity. Overall,

this showed the potential to implement aerial imagery in constructing channel geometry for a process based numerical model.

- Multivariate changepoint analysis was effective as compared to univariate Hubert's test and successful in simplifying channel geometry for the 1D numerical model. It highlighted the potential of simplification of channel geometry using a single test, as opposed to running multiple tests for each channel attribute.
- 1D numerical model performed satisfactorily during the calibration of the hydraulics (NSE = 0.9, PBIAS = 12, RSR = 0.43), and validation of the aggradation-degradation patterns for the Elwha River. This indicated that model constructed using publicly available hydrological data, and remote sensing data was successful in accurately representing the hydromorphodynamic processes in the fluvial domain. This integration of remote sensing and numerical modeling approaches showed the potential to construct numerical models for data scarce regions.

5.1.3 Coupled Data-Driven and Process-Based Modeling of Sediment Pulse Propagation Dynamics.

A framework was developed to inverse model the upstream sediment supply, one of the drivers behind a river's response to dam removal. The method utilized MCMC sampling to inverse model the upstream sediment supply concentration (Cs), an input parameter to the 1D numerical model using Landsat derived SSC as measured data. Testing the method using the Elwha River dam removals offered the required critical assessment. Key findings from the study are presented as follows:

- Performance of parameter optimization minimizing RMSE was dependent on Landsat based SSC data availability, the pulse propagation phase of the sediment pulse under construction, and the upstream flow rate.
- The optimized model successfully simulated SSC during the initial sediment pulse propagation phase (2012 to 2014), whereas the Landsat based SSC data consistently under predicted the peak high values during the same phase. It highlighted the importance of enhancing the performance of numerical models using remote sensing and machine learning derived SSC data.
- Downstream Landsat SSC response throughout the evaluation period was explained by a dynamic influence of flow rate and upstream sediment supply concentration through time.

Inclusion of numerical modeling helped in understanding the interaction of different hydrodynamics variables through space and time that resulted in the observed response. This led to the identification of different driving factors behind a river's response to a sediment pulse.

- Variability in channel geometry in terms of width, slope, and roughness explained spatial trends observed in Landsat SSC data across the four segments of the study reach. The results highlighted the importance of spatial detail in measured data used for optimization, and the unintended consequences of segmentation on model accuracy of the optimized model.

5.2 Broader Impacts

The method developed as part of the dissertation has broader impacts on various aspects of simulating sediment dynamics across the fluvial domain of river systems. The key points outlined below highlight the potential contributions and implications of this work:

- Predicting turbidity for data scarce regions: The inclusion of SDI as a predictor variable to denote physical similarity between multiple locations facilitates turbidity prediction using remote sensing-based reflectance data. This research offered a novel approach to simulate water turbidity, providing valuable insights into water quality dynamics and enabling targeted management strategies.
- Multi site estimation of turbidity using remote sensing-based prediction models: The utilization of remote sensing data at a larger spatial scale for prediction modeling has wide-ranging implications. The development of robust models based on remote sensing information can enhance our understanding of hydrological processes, facilitate early warning systems for extreme events, and support decision-making processes for water resource management and environmental planning.
- Constructing numerical models and simulating channel processes for an ungauged reach: In many regions, water quality data may be limited or unavailable for ungauged reaches, making it challenging to understand and represent channel processes via modeling accurately. This research proposes an innovative approach that leverages remote sensing-based data as an alternative source of information to construct and simulate channel processes using Numerical modeling. The method enabled simulation of flow and sediment dynamics across river corridors for data scarce reach, which may be used by researchers and practitioners associated with river sediment management, and restoration efforts.

- Simulating sediment pulses generated in the past using remote sensing and numerical modeling: The dynamics in sediment transport plays a crucial role in various environmental processes, such as river morphology, nutrient cycling, and aquatic ecosystem health. By using satellite and aerial imagery, this research developed and tested a method to simulate sediment pulses generated after dam removals. However, the methodology has the potential to be tested to reconstruct sediment pulses generated after other natural or anthropogenic sources of disturbances such as wildfires, volcanic eruptions, floods, mining related activities, and landslides.
- Quantification of upstream sediment supply conditions using downstream response: Understanding the relationship between upstream conditions and downstream response is vital for effective water resources management. This research proposes an inverse modeling framework that quantifies the upstream sediment supply concentration based on Landsat based downstream response. However, the application of the approach is not limited to dam removals, but can be used for wider applications focused on sediment management.

5.3 Limitations

While the methodologies employed in this study have shown promise, it is important to acknowledge certain limitations that may impact the results and interpretation. The following key points outline the limitations of this research:

- Inclusion of satellite imagery dependent upon cloud-free days: The estimation of suspended sediment concentration (SSC) using satellite imagery relies on the availability of cloud-free data. Cloud cover can hinder the accurate retrieval of SSC values, limiting the estimation to clear days only. Consequently, the SSC estimation may not capture variations and dynamics that occur during cloudy periods, potentially introducing bias and limiting the overall temporal coverage of the study.
- Numerical model efficiency for SSC estimation dependent upon empirical equations: The estimation of SSC using numerical models often relies on empirical equations. These equations introduce a level of uncertainty into the simulations, as the accuracy of the estimations is contingent upon the validity of the chosen equations. The reliance on empirical equations can lead to inherent limitations in capturing the complex interactions between sediment transport processes and environmental factors. Addressing this uncertainty requires

the consideration of a Bayesian framework to account for the inherent limitations of the empirical equations and improve the reliability of the simulation results.

- Spatial and temporal resolution limitation associated with remote sensing data: The resolution of satellite imagery may present limitations in capturing fine-scale variations in suspended sediment dynamics. The coarse spatial resolution of satellite imagery and the simplifications within the numerical models may overlook local variations and intricacies in sediment transport processes. These limitations may result in a loss of detail and potential underestimation or overestimation of sediment concentrations and dynamics at smaller spatial scales.
- Assumptions and simplifications in the numerical model: Like any modeling study, this research made simplifications to the dimensionality and channel geometry of the numerical representing an otherwise complex real-world process. These assumptions and simplifications are a source of uncertainty, and their impact needs to be evaluated on the results to ensure that any conclusions drawn in the study are not overly influenced by these simplifications.
- Data availability and quality: The accuracy of the data based prediction model relies heavily on the availability and quality of input data, including satellite imagery, ground measurements, and model parameters. Limited data availability or low-quality data can introduce uncertainties and affect the reliability of the findings. Careful consideration and validation of the input data sources are essential to ensure the robustness of the analysis.

5.4 Recommendations for future research

The findings of this study lay the groundwork for several future research directions that can advance the understanding and application of the methodology proposed. The following key points provide recommendations for future work:

- Testing novel remote sensing sensors: To further improve the capabilities of the proposed methodologies, it is recommended to test and validate the techniques developed in the dissertation using newer satellite sensors such as Sentinel, Planet, and SWOT. These sensors offer enhanced spatial and temporal resolutions, as well as advanced imaging capabilities. By incorporating data from these sensors, future research can refine the simulation models and prediction algorithms, leading to more accurate and reliable results.

- Testing SDI on a larger spatial scale: The application of SDI in this study demonstrates its potential for improving data integration and accessibility. Future work should focus on testing SDI on a larger spatial scale, such as regional or national scales. By implementing SDI on a broader scope, researchers and stakeholders can benefit from improved data sharing, collaboration, and decision-making processes. This expansion would facilitate the integration of multiple data sources and enable a more comprehensive understanding of hydrological processes and water resource management.
- Including additional model parameters in the inverse modeling framework: The inverse modeling framework presented in this study can be further enhanced by including additional relevant model parameters under a Bayesian framework. Consideration of factors such as soil characteristics, land cover, and vegetation dynamics can improve the accuracy and reliability of the inverse modeling approach. By expanding the range of parameters, future research can capture a more comprehensive representation of the system behavior and enable more robust predictions and estimations.
- Estimating the probability density function (pdf) for Cs: Instead of relying on discrete values for the upstream sediment supply concentration (Cs), future work can focus on estimating a probability density function. This approach would account for the uncertainty associated with sediment transport processes and provide a probabilistic representation of Cs through the evaluation period for the Elwha Dam removals. Estimating a pdf would enhance the predictive capabilities of the inverse modeling framework, enabling more accurate and reliable quantification of upstream conditions and their impact on downstream responses for different sediment disturbance scenarios.

6 APPENDIX

6.1 MCMC based inverse modeling code (R code)

```
library(mcmc)
# MCMC-based optimization using Metropolis-Hastings algorithm with adaptive scaling
mcmc_optimization <- function(Num_model, param_range, n_iter, initial_proposal_sd,
scaling_factor) {
 # Function to calculate acceptance probability
 acceptance_prob <- function(curr_rmse, new_rmse) {
  return(min(1, exp(curr_rmse - new_rmse)))
 }

 # Initialize optimization variables
 best_param <- 0
 best_rmse <- Inf
 curr_param <- SSC[1]
 curr_rmse <- best_rmse

 proposal_sd <- initial_proposal_sd

 # Generate initial parameter value within the specified range
 curr_param <- runif(1, param_range[1], param_range[2])

 # Perform MCMC iterations
 for (i in 1:n_iter) {
  # Generate proposal parameter
  proposal_param <- rnorm(1, mean = curr_param, sd = proposal_sd)

  # Ensure proposal parameter is within the specified range
  proposal_param <- pmax(proposal_param, param_range[1])
  proposal_param <- pmin(proposal_param, param_range[2])
```

```
    # Calculate RMSE for the proposal parameter
    proposal_rmse <- Num_model(proposal_param)

    # Accept or reject proposal based on acceptance probability
    if (runif(1) < acceptance_prob(curr_rmse, proposal_rmse)) {
      curr_param <- proposal_param
      curr_rmse <- proposal_rmse
    }

    # Update best parameter and RMSE
    if (curr_rmse < best_rmse) {
      best_param <- curr_param
      best_rmse <- curr_rmse
    }

    # Adaptively adjust proposal_sd based on acceptance rate
    acceptance_rate <- i / (i + 1)
    proposal_sd <- proposal_sd * (1 + scaling_factor * (acceptance_rate - 0.25))
  }

  # Return best parameter and RMSE
  return(list("best_param" = best_param, "best_rmse" = best_rmse))
}

# Define parameter range (min and max values)
param_range <- range(SSC)  # Range for the parameter that comes from Landsat SSC

# Set number of iterations, initial proposal standard deviation, and scaling factor
n_iter <- 50          # Number of iterations
initial_proposal_sd <- 0.0005   # Initial proposal standard deviation
scaling_factor <- 0.1   # Scaling factor for adaptive scaling
```

```
# Run MCMC-based optimization with adaptive scaling
tic()
result <- mcmc_optimization(Num_model, param_range, n_iter, initial_proposal_sd,
scaling_factor)
toc()
# Print the best parameter and RMSE
par <- result$best_param
rmse <- result$best_rmse
```